AFCRL-68-0651

INVESTIGATION OF SEMICONDUCTOR SCHOTTKY BARRIERS FOR OPTICAL DETECTION AND CATHODIC EMISSION

by

Jerome Cohen

Jüri Vilms, Robert J. Archer

HEWLETT hp PACKARD

1501 Page Mill Road Palo Alto, California 94304

Contract No. F19628-68-C-0090

Project No. 5621, 5638
Task No. 562107, 563801
Work Unit No. 56210701, 56380101

FINAL REPORT

15 November 1967 14 November 1968
18 December 1968

Contract Monitor: A.C. Yang
Solid State Sciences Laboratory

Prepared
for

Air Force Cambridge Research Laboratories
Office of Aerospace Research
United States Air Force
Bedford, Massachusetts 01730

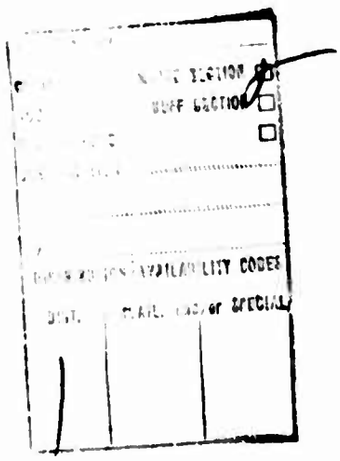

AFCRL-68-0651

INVESTIGATION OF SEMICONDUCTOR SCHOTTKY BARRIERS FOR OPTICAL DETECTION AND CATHODIC EMISSION

by
Jerome Cohen, Jüri Vilms, Robert J. Archer

Hewlett-Packard Company
1501 Page Mill Road
Palo Alto, California 94304

Contract No. F19628-68-C-0090

Project No. 5621, 5638
Task No. 562107, 563801
Work Unit No. 56210701, 56380101

FINAL REPORT
15 November, 1967 - 14 November, 1968

18 December, 1968

Contract Monitor: A. C. Yang
Solid State Sciences Laboratory

Prepared
for

AIR FORCE CAMBRIDGE RESEARCH LABORATORIES
OFFICE OF AEROSPACE RESEARCH
UNITED STATES AIR FORCE
BEDFORD, MASSACHUSETTS 01730

ABSTRACT

The yield in percent for photoemission of either electrons or holes into Si from Au contacts approximately obeys

$$y = \frac{(h\nu - h\nu_o)^2}{h\nu}$$

for thick Au films and incidence from the Si side of the contact. For p- and n-type Si $h\nu_o$ is, respectively, 0.3 eV and 0.8 eV. By optical impedance matching the yields can be increased by at least 10-fold over narrow wavelength ranges. Au films thinner than 100Å also exhibit nearly an order of magnitude greater yield. This latter fact leads to enhanced yields at the edges of Au pads evaporated through loosely fitting masks. Very low barriers are obtained on p-type Ge. For Au, Ag and Ni, the values are < 0.03 eV, 0.11 eV and 0.9 eV - 0.1 eV, respectively.

Rectifying Ag contacts to etch-polished GaP, ZnSe and ZnS can be made with nearly ideal I-V characteristics. The Schottky barrier heights are about 1.5 eV for the former two contacts and 1.8 eV for the latter. The efficiency of cathodic emission into vacuum for diodes with barrier heights equal to or less than 1.5 eV and with cesiated Ag films 300Å thick having work functions of about 1.5 eV obeys a theory which assumes isotropic scattering of electrons on transmission through the interface.

The maximum measured efficiency is nearly 10^{-4} for Ag-ZnSe. At least 0.02 is expected for Ag-ZnS but has not yet been measured. Under the cathodic emission conditions, the diodes have so far not had ideal electrical properties and there is a serious problem in achieving stable, chemically inert contacts to the II-VI materials.

FOREWORD

The work reported on in this report has been authorized by the Contracting Officer, Joseph F. McNally, Air Force Cambridge Research Laboratories, Office of Aerospace Research, United States Air Force, Bedford, Massachusetts, under Contract No. F19628-68-C-0090 and titled, "Investigation of Semiconductor Schottky Barriers for Optical Detection and Cathodic Emission."

The work has been performed at Hewlett-Packard Laboratories under the general supervision of Dr. M. M. Atalla and under the direct supervision of Dr. R. J. Archer. The report has been prepared by R. J. Archer, J. Cohen, and J. Vilms.

Previous and related contracts are Contract No. AF 19(628)-5046, Contract No. F33615-68-C-1054, and Contract No. Da 44-009-AMC-1250(T).

TABLE OF CONTENTS

I. INTRODUCTION

This is the final report of a one-year project to explore two new applications of metal-semiconductor diodes. The phenomena investigated are cathodic emission into vacuum and photoemission into semiconductors. They are intended, respectively, to be the basis of the development of cold cathodes and infrared photo-detectors.

The report covers the results of the entire project with emphasis on the details of the final quarter. The project was sub-divided into two separate programs and is so reported here. Our overall effort on the cold cathode included besides this program a parallel HP-sponsored project. This program's effort was concerned mainly with diode development and some aspects of the emission measurements. The HP project involved the development of vacuum technology, the study of the lowering of metal work functions, and most of the emission studies. Our report on the cold cathode covers all of the diode development and summarizes the important results of the emission measurements.

The feasibility of both mechanisms for the respective device developments has been demonstrated. The final section outlines our conclusions and indicates the unanswered questions and the course required for further work.

II. PHOTOEMISSION IN METAL-SEMICONDUCTOR CONTACTS FOR OPTICAL DETECTION

II. 1. Introduction

Photoemission at rectifying metal-semiconductor contacts affords a mechanism for optical detection. We established theoretically before the beginning of this project that such a diode can have a greater D* than an equivalent pn junction under the operating conditions of the pn junction. Generally, this superiority is most important in the infrared, e.g., 1μ to 10μ, and requires photoemissive yields of the order of one percent. An important feature of the device is that the threshold for optical response can be adjusted through control of the Schottky barrier height. Our effort has centered on establishing the absolute magnitude and the wavelength dependence of yield, on investigating the influence on yield of the structural properties of the contacts, on developing contacts with a wide range of barrier heights, and on optical impedance matching to increase the absorption of incident radiant energy in the metal.

A simple physical embodiment of the diode and a representation of the photoemission mechanism is shown in Figures II-1 and II-2. As represented, radiant energy is incident from the semiconductor side of the contact in our experimental studies, and our concern is always with $h\nu < E_g$.

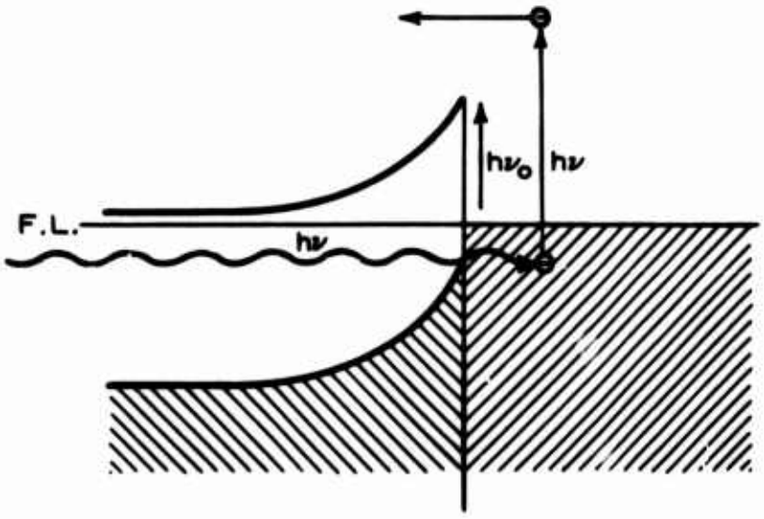

FIGURE II-1: Photoemission in the metal-semiconductor contact.

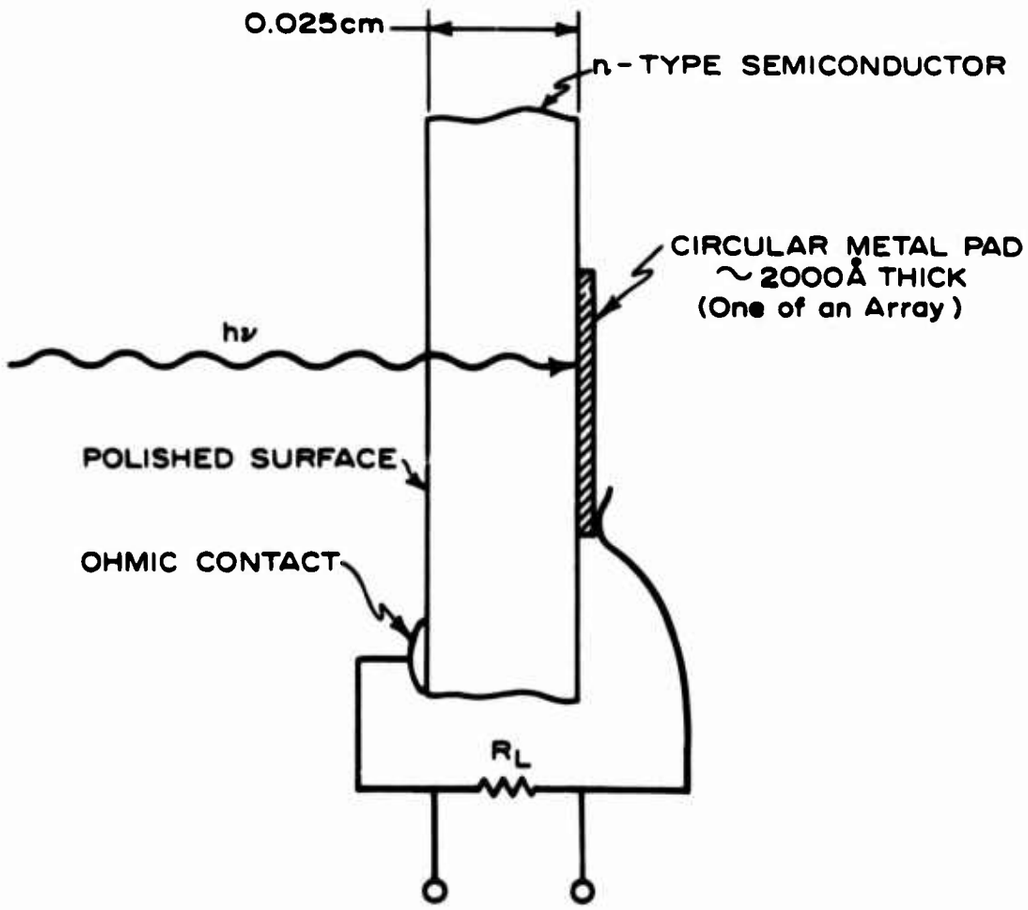

FIGURE II-2 : Metal-semiconductor photoemissive optical detector.

As a guide to studying and interpreting the dependence of yield on photon energy, we use the following simple theory of photoemission. The derivation is based on the picture given by Figure II-3 and on the following assumptions:

1. The probability of excitation is independent of the energy of the initial and final states.
2. The lifetime of an excited electron is independent of energy and the rate of thermalization from any excited state is fast compared to the loss by photoemission.
3. There is an abrupt transition from filled to empty states at equilibrium at the Fermi level E_F.
4. $E_F >> h\nu$, which is tantamount to assuming that the density of states (dN/dE) is nearly constant over the energy range, $h\nu$, of interest.
5. An electron is photoemitted if, and only if, excited to a state for which the component of velocity normal to the interface corresponds to a kinetic energy equal to or greater than the barrier ($E_F + h\nu_o$).

From assumptions (1) through (4), it follows that the distribution of photoexcited electrons is constant in energy from E_F up to $E_F + h\nu$ where the distribution cuts off abruptly. The total number of possible excited states is

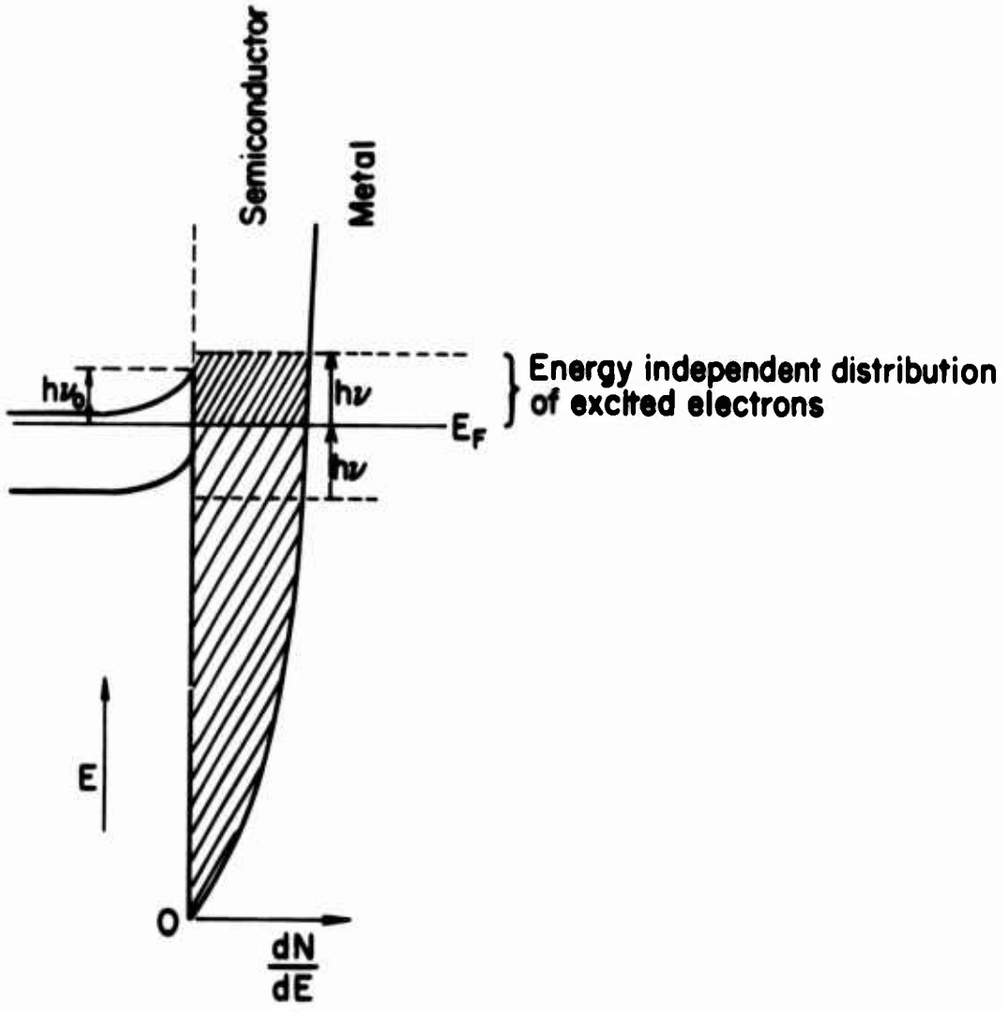

FIGURE II-3: Representation of a simple model of photoemission.

$$N_T = \int_{E_F}^{E_F + h\nu} \left(\frac{dN}{dE}\right) dE = \left(\frac{dN}{dE}\right) h\nu \, . \qquad (1)$$

The number of states which meet the momentum criterion, assumption (5), is

$$N_E = \int_{E_F + h\nu_o}^{E_F + h\nu} \tfrac{1}{2}\left(\frac{dN}{dE}\right)\left(1 - \sqrt{\frac{E_F + h\nu}{E}}\right) dE$$

$$= \left(\frac{dN}{dE}\right) \frac{(h\nu - h\nu_o)^2}{8E_F} \, . \qquad (2)$$

It follows that the yield, defined as the ratio of photoemitted electron flux to the absorbed photon flux is

$$y_o = \frac{N_E}{N_T} = \frac{(h\nu - h\nu_o)^2}{8h\nu \, E_F} \, . \qquad (3)$$

This relationship differs from the usual Fowler equation[1]

$$y_o = \text{const.} \, (h\nu - h\nu_o)^2 \qquad (4)$$

in the specification of the constant and in the dependence on photon energy. It is the $h\nu$ term in the denominator that we deem of importance since it implies greater yield at long wavelengths than Eq. (4), and since it is supported by our experimental results, as discussed below.

Much of our effort involves contacts to p-type semiconductors. The photoemission of holes can be shown to obey a relationship with the same dependence on photon energy as Eq. (3).

II. 2. The Measurement of Photoemissive Yield

Relative to incident rather than absorbed radiant energy, the absolute quantum yield of a photodiode is given by

$$y = \frac{(I/q)}{(PA/h\nu)} \tag{5}$$

where I = short circuit photocurrent

q = charge of an electron

P = incident power density

A = effective area of photodiode.

To determine yield, we used the following experimental setups to measure the short circuit photocurrent and the incident power density. Figure II-4 shows the apparatus used in the near infrared measurements on n-type Si diodes. In this wavelength region, 1.2μ - 1.5μ, we use standard optical components such as glass lenses and a tungsten source in a glass bulb. A Bausch and Lomb 250mm grating monochrometer is used with a Si filter to remove higher order energy and stray light.

The monochromatic light beam of 100Å bandwidth is focused by means of an achromatic condenser lens onto either the photodiode or a

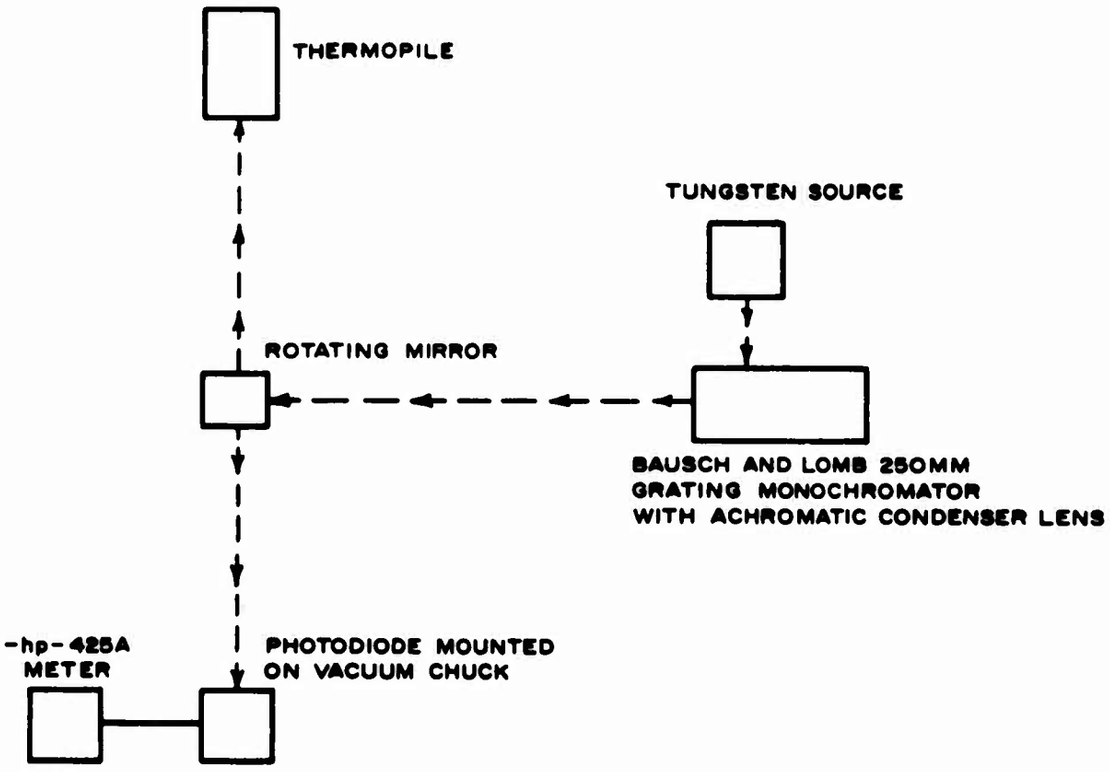

FIGURE II-4: Experimental setup used to obtain spectral response of Au n-type Si photodiodes.

calibrated thermopile by means of a front surface mirror which can be rotated. The size of the image is about 0.5 cm wide by about 5 cm high. After measuring illumination flux, the short circuit photocurrent is obtained with an HP 425a meter. An estimate of system accuracy is ±10% for absolute measurements and ±5% for relative measurements.

Figure II-5 shows the setup used to obtain measurements on the p-type Si diodes in the region 1.2μ - 4.5μ. For this wavelength range an Infrared Industries Nernst Glower is used as a radiation source with first surface mirrors for entrance and exit optics to a Bausch and Lomb 500mm monochrometer. The monochrometer bandwidth is set at 264Å. The energy leaving the monochrometer passes through an appropriate optical filter and is then imaged as a 0.2 by 2 cm rectangular beam onto the sample in the dewar (the dewar windows are u. v. grade sapphire). The short circuit photocurrent is measured with a Brower Model 131 lock-in voltmeter system which chops the incident energy at 13Hz. A synchronous detection system is required for this case due to the low level signal and the need to distinguish between the response of the photodiode to background blackbody radiation and the desired signal. To calibrate the energy flux, the sample is replaced by an HP thermopile with an u. v. grade sapphire window. We estimate the absolute system accuracy to be ±30% and the relative system accuracy to be ±20%.

All the yield measurements were performed on unbiased diodes. Therefore, to permit accurate low-level measurements of short circuit

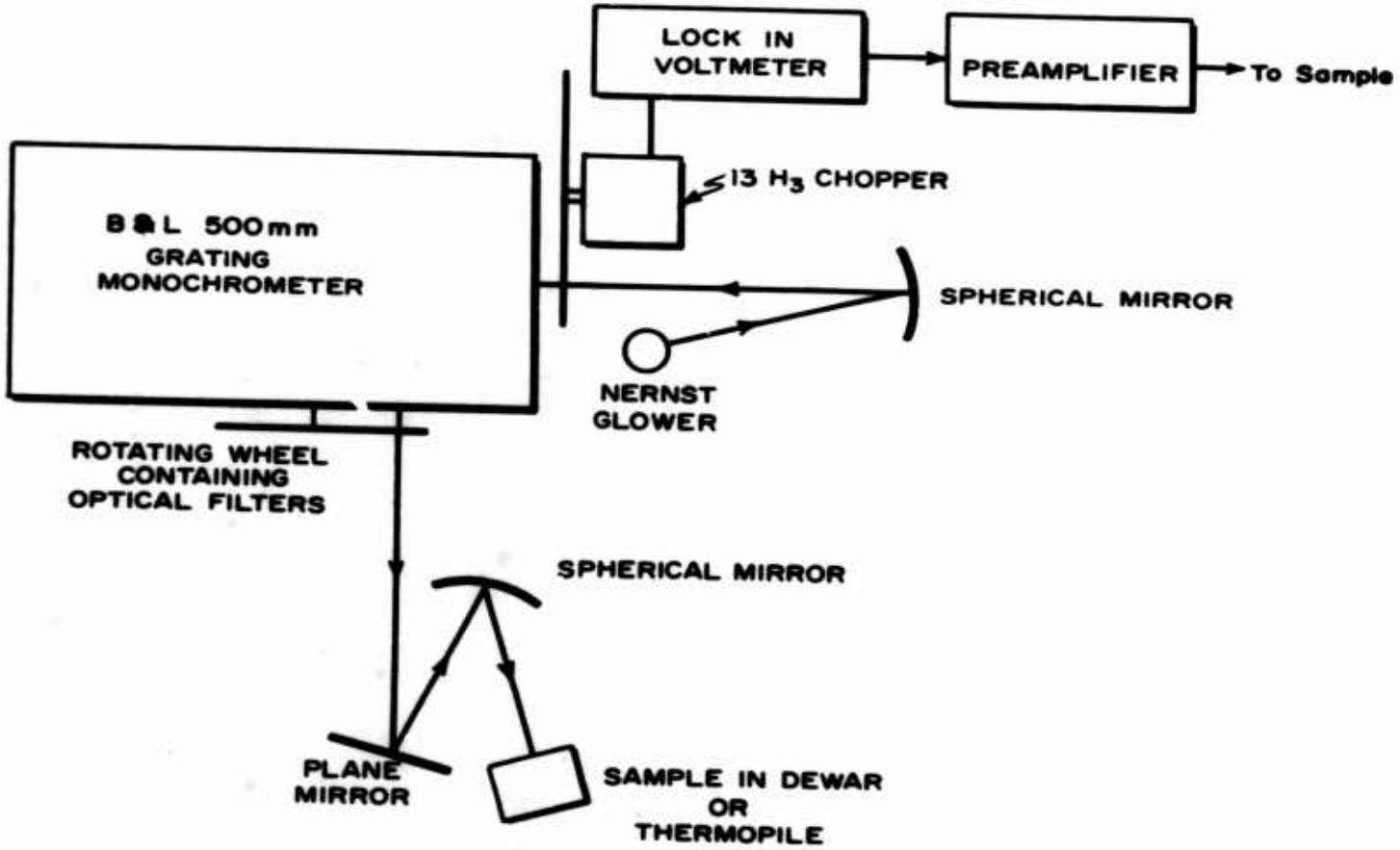

FIGURE II-5: Setup for absolute photoemission measurements in the far infrared.

photocurrent, the zero-bias impedance of the diodes must be much larger than the load resistance. In order to accomplish this condition for the Au p-type Si contacts, they were cooled to 77°K. For some high leakage cases of Au n-type Si samples, this condition could not be met and, thus, suitable corrections were included.

II. 3. The Yield of Au Contacts to n-type Si: Edge Effect, Influence of Au Film Thickness

We have reported earlier on a survey of the yields for a number of metals to n-type Si.[2] Our studies of the yields of Au n-type Si contacts during the present program mainly involved the observation of pad-diameter dependence of yield and its elucidation.

We observed that the yields of diodes with 0.017 in. diameter Au pads on n-type Si were greater than the yields for diodes with 0.051 in. diameter pads. At a photon energy of 1.0 eV this difference is about a factor of three, approximately 0.2% versus 0.06%, for thick gold pads. This was determined by evaporating both size pads onto the same wafer, utilizing both 1 and 10 ohm-cm materials. By utilizing a selective etching procedure, whereby we etched away either a central region or an edge region of a Au pad, we determined by comparing the yield of the resulting diode to the yield of the original that the efficiency of the edge region was greater than that of the central region and concluded that the influence of pad diameter on yield is caused by the increase in the perimeter to area

ratio with decreasing pad diameter and the resultant increase in the contribution of the edge response to the total response. Only the initially evaporated edge region and not an etch-generated edge region shows the enhanced yield.

II.3.1. Small Light Beam Scanning Experiments

To ascertain quantitatively the distribution of yield across a diode diameter, a 0.001 in. diameter light beam (λ = 1.3μ) was used to scan across the diode while the short circuit photocurrent was recorded. The block diagram for this experiment is shown in Figure II-6.

Data from these scanning experiments are plotted in Figure II-7, II-8, and II-9 for diodes having diameters of 0.0525 in., 0.0169 in., and 0.008 in., respectively. The ratio of the largest of the two edge peaks to that of the central region is 18 for the 0.0525 in. diode, 12 for the 0.0169 in. diodes, and 6 for the 0.008 in. diode.

A scanned response on a diode whose initial perimeter was etched away showed that the characteristically observed edge response was now absent, as expected from the results of the selective etching experiment.

Using this same small light beam, we obtained Fowler plots for the central region and the edge region of a diode. A typical Fowler plot is shown in Figure II-10. The barrier heights for the two regions differ by no more than 0.01 eV. Thus, the enhanced yield is not due to differences in barrier height for the two regions.

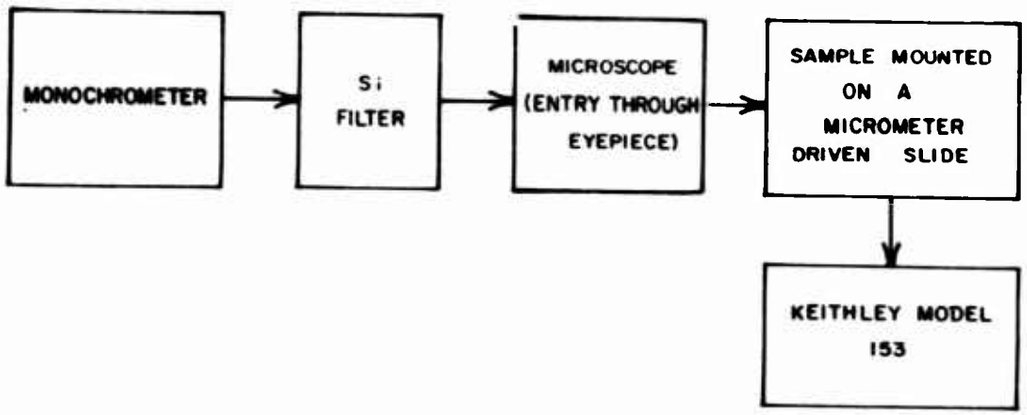

FIGURE II-6: Block diagram of the experimental set-up used to scan the diode with a small beam.

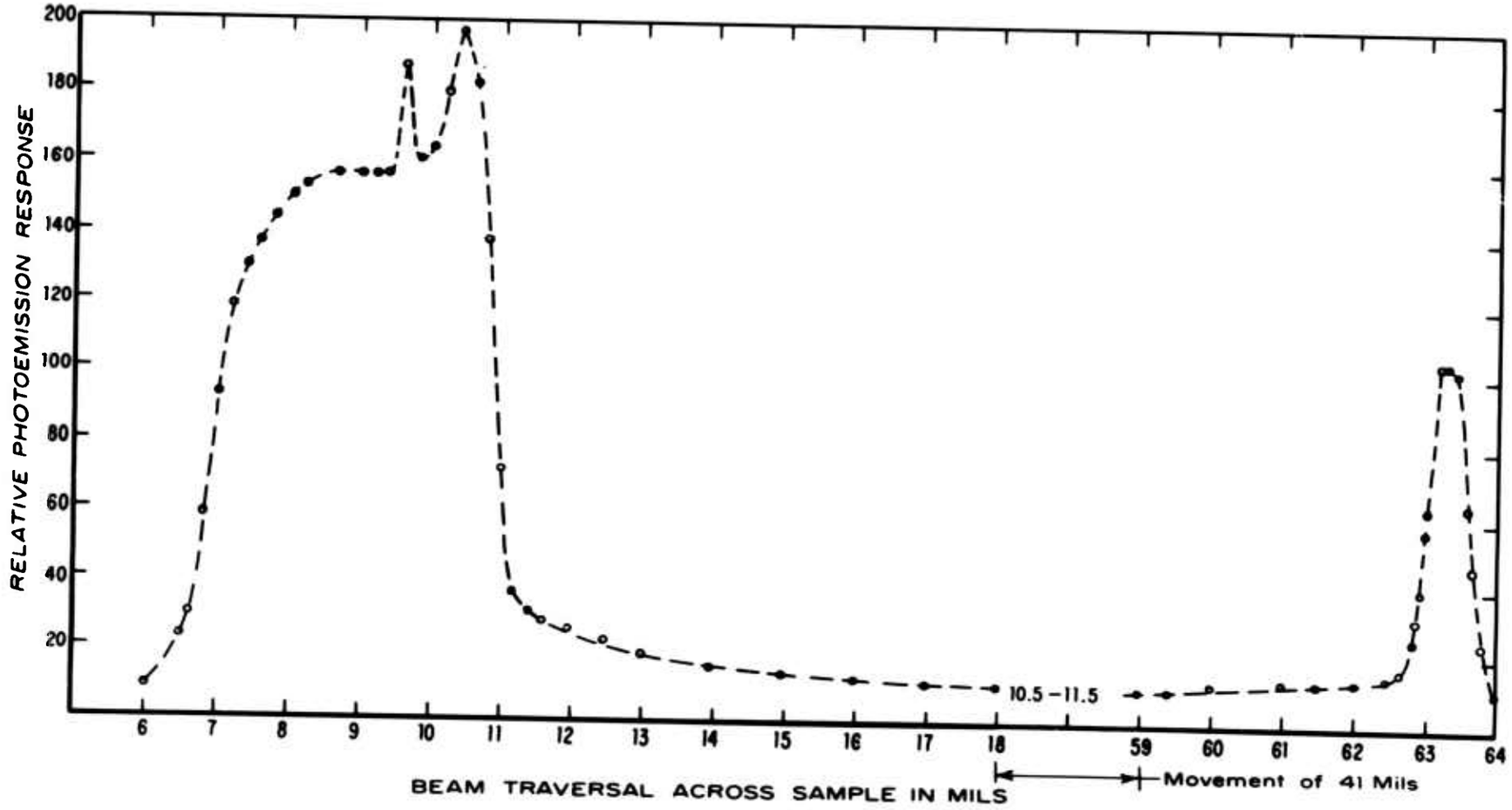

FIGURE II-7: Relative photoemission response of a 0.0525 in. diameter Au-n-type Si diode as a small light beam traverses across a diameter.

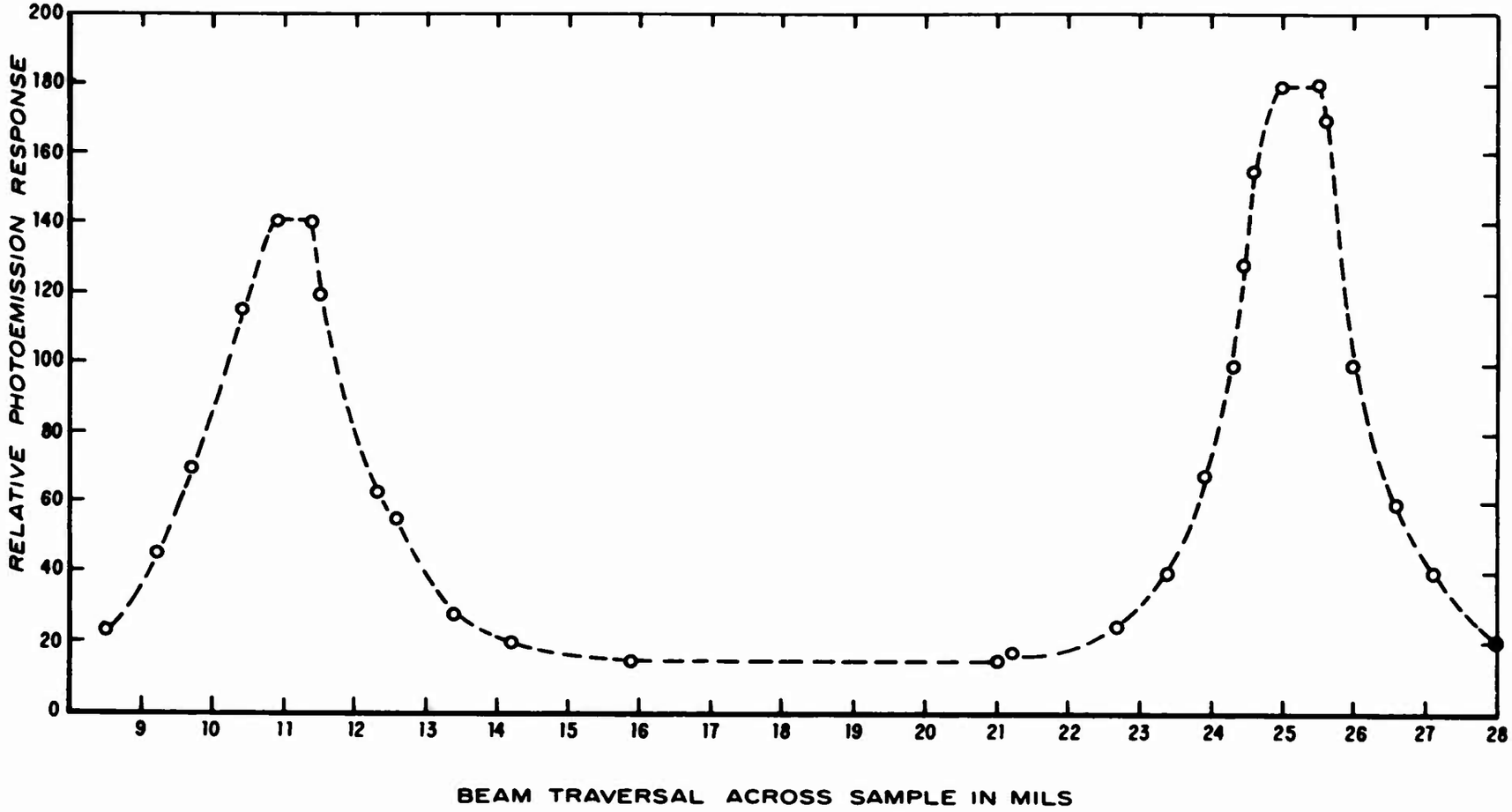

FIGURE II-8: Relative photoemission response of a 0.0169 in. diameter Au-n-type Si diode as a small light beam traverses across a diameter.

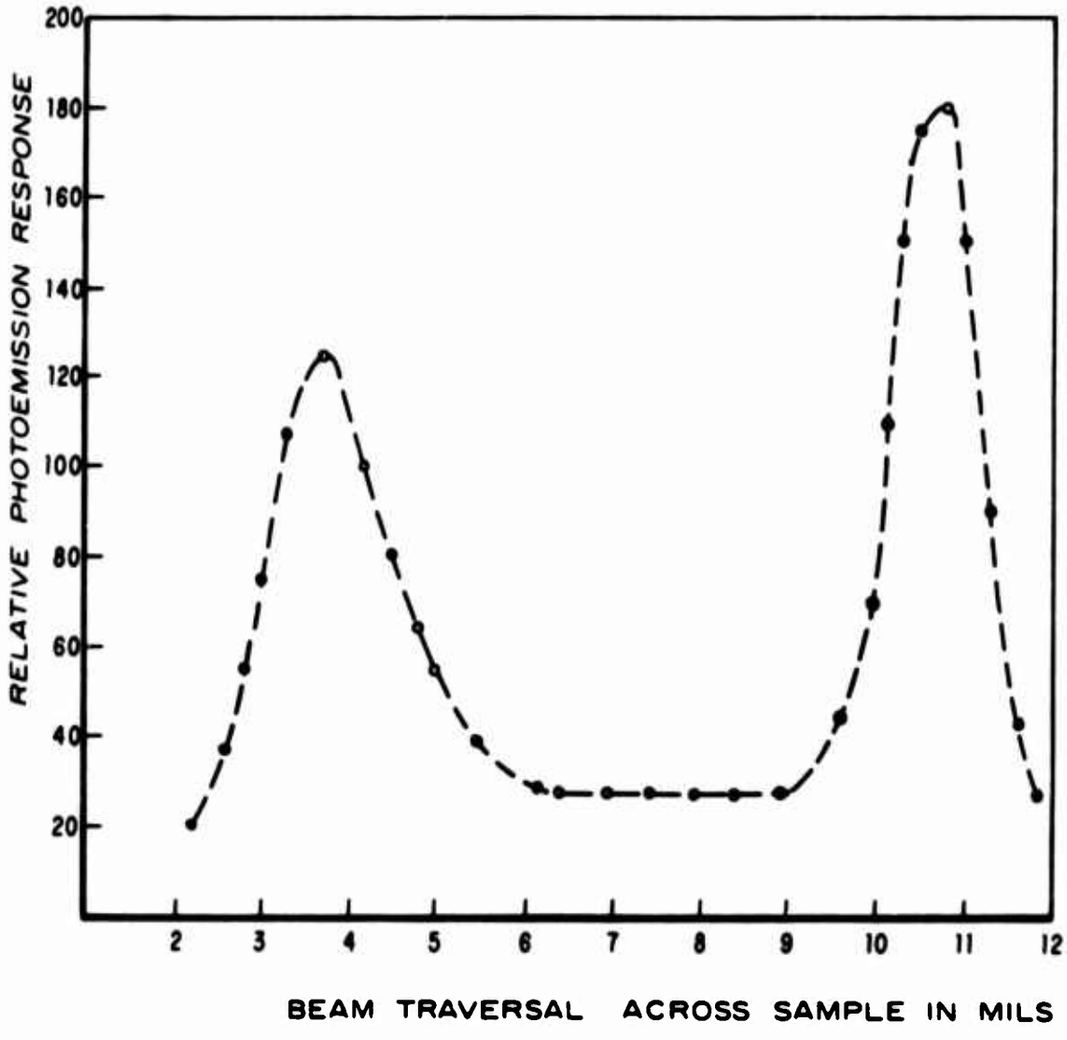

Figure II-9: Relative photoemission response of a 0.008 in. diameter Au-p-type Si diode as a small light beam traverses across a diameter.

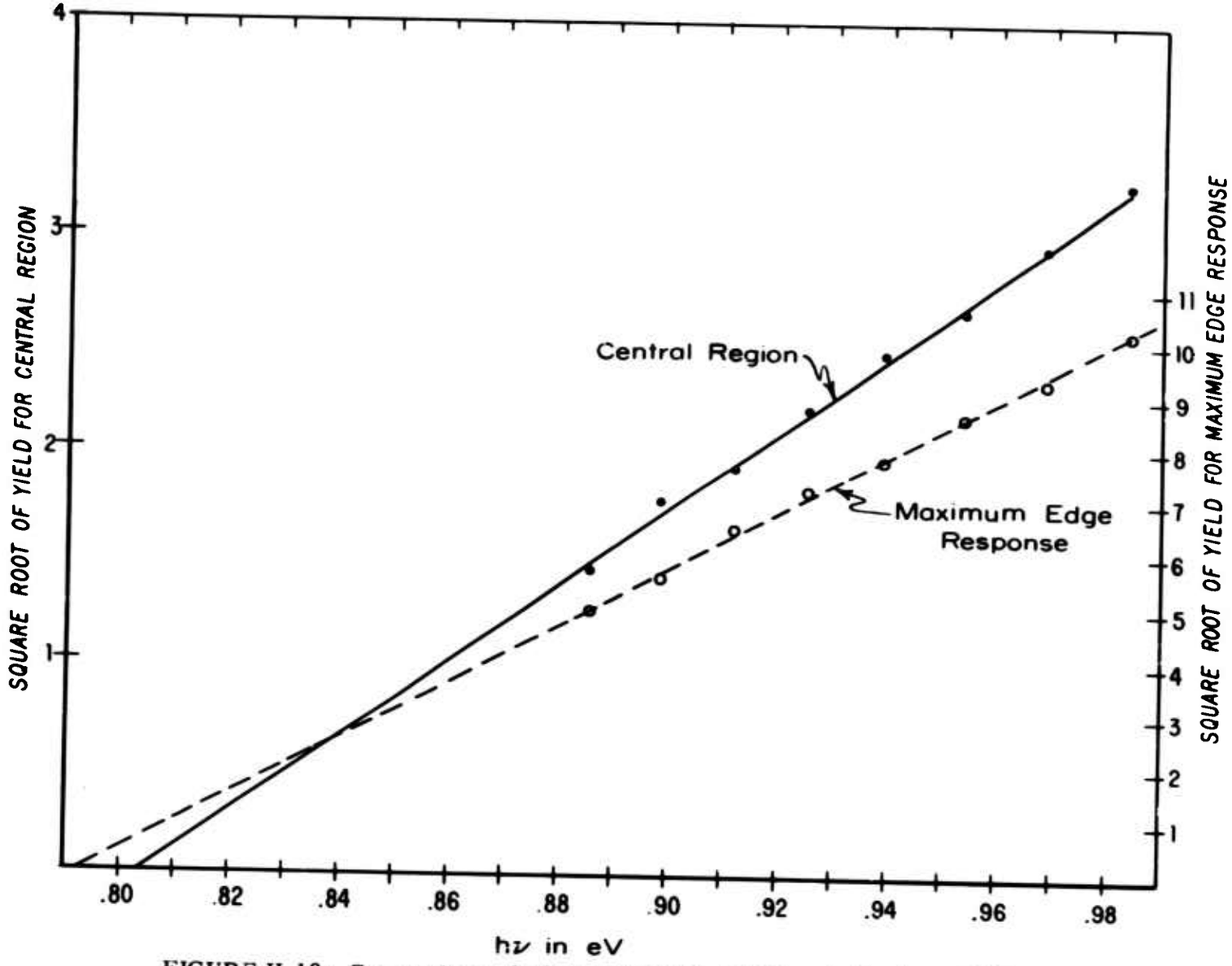

FIGURE II-10: Comparison of edge and center relative yields for a 2000A 0.05 in. diode.

II. 3. 2. Effects of Evaporation Rate and Heating

Initially, we suspected that the "edge effect" was due to structural differences in the Au pad regions caused by heating during evaporation of the Au contact. Heating by either radiation or condensation causes the center to be hotter than the edge.

The evaporation procedure was varied from the extremes of a very fast 1-second evaporation to a very slow 9-minute evaporation. No essential differences between the resulting diodes and those formed by our usual 40-second evaporation was observed.

Diodes were heated in an oven to 275°C, 325°C and 400°C. The yields were measured before and after each heat treatment. After the 275°C heat treatment the yields for a 0.052 in. pad and a 0.017 in. pad increased by 30% and 65%, respectively. After the higher temperature heat treatments, however, yields approached the pre heat-treatment values.

We conclude that the "edge effect" is not caused by heating or by any effects related to rates of evaporation.

II. 3. 3. Dependence of Yield on Au Film Thickness

Another possible explanation for the "edge effect" is a gradation of Au film thickness at the edge of a diode due to the shadowing effect of a loosely fitting evaporation mask. If either absorption or some other aspect of the photoemission process were enhanced for thinner films, increased edge yield would result. To test this hypothesis a mask having very good

edge definition was prepared. This mask had arrays of 0.050, 0.030, 0.015, and 0.007 in. diameter holes. For the evaporation we placed the sample and mask into a special holder which insured good contact between the mask and the wafer surface.

The average yields at 1.0 eV for 2000Å thick Au films of different pad size made with the improved mask are shown in Table II-1 under the column labeled 2000Å. The efficiencies are nearly independent of pad diameter and are all smaller than those obtained for pads evaporated with the loose fitting mask, e.g., the 0.015 in. diode is a factor of 5 less efficient. There is an absence of a size effect except for the 0.007 in. pads. The 0.001 in. diameter light beam mentioned previously was used to scan these diodes. The increased edge response (Figure II-11) was still present but it was confined to a very narrow region, thus minimizing its effect.

We now used this new evaporation technique and varied the evaporated Au film thickness. Table II-1 shows the average yields at 1.0 eV for samples having thickness of 100Å, 75Å, and 40Å. These thin film thicknesses were measured using an ellipsometer. Note now the following results: the yields for the 100Å samples were increased on the average by over a factor of 2 from the 2000Å case; the yields for the 75Å and 40Å samples were increased by a factor of 6. Note also that any difference in yield for the different sizes on a single wafer is almost fully explained by the relative experimental error of ±5%. Furthermore, the "edge effect" was not observed for several scanned diodes with the 75Å thick Au pad.

TABLE II-1

Yield at 1.0 eV for Au Pads of Different Diameters and Thicknesses Made with Tight Mask

Au Thickness / Pad Diameter	(2000Å)	(100Å)	(75Å)	(40Å)
0.050 in.	0.039%	0.094%	0.228%	0.240%
0.030 in.	0.044%	0.107%	0.231%	
0.015 in.	0.039%	0.105%	0.231%	0.253%
0.007 in.	0.055%	0.100%	0.243%	

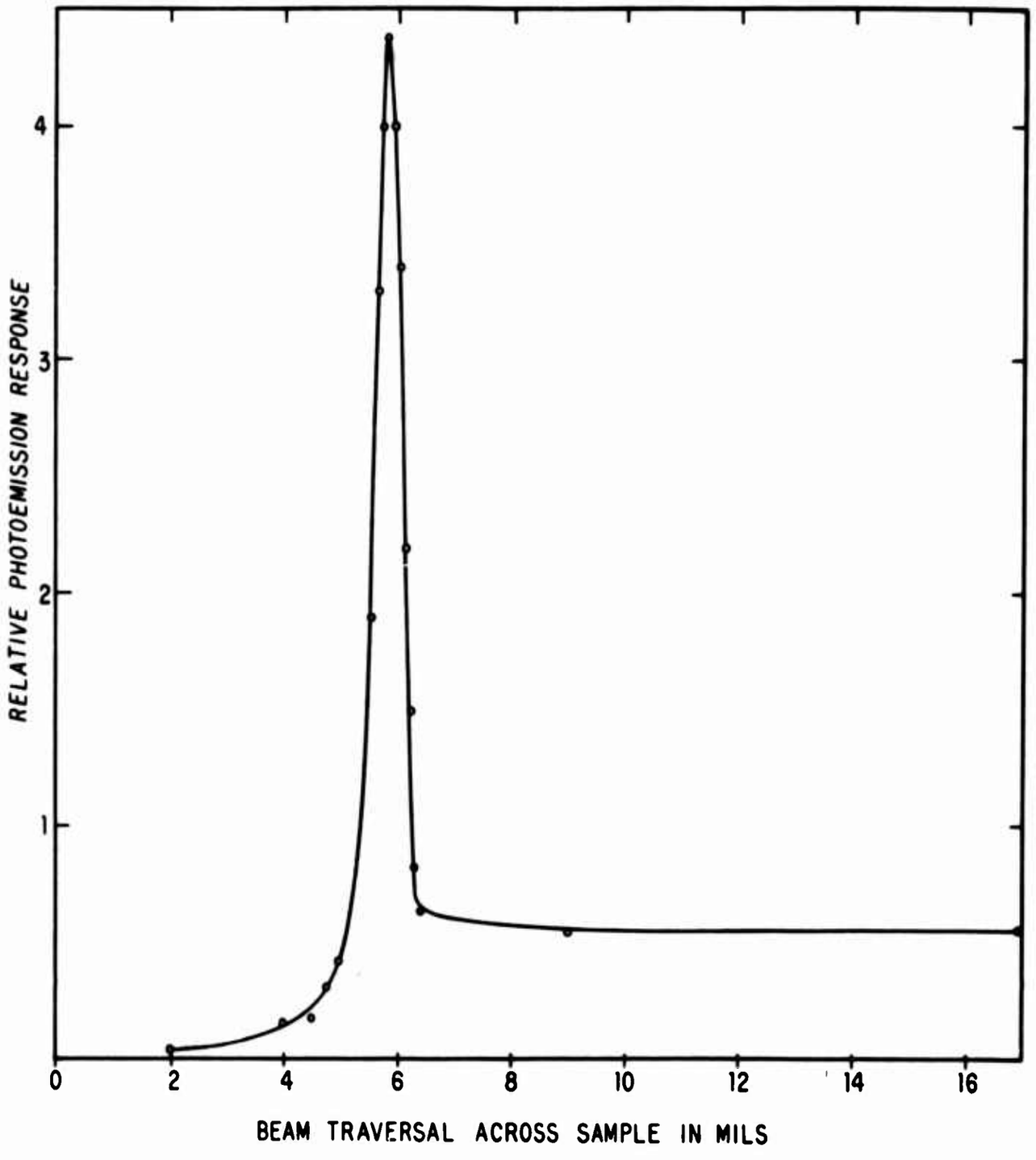

FIGURE II-11: Scanning profile for a 0.05 in. diode made with tight evaporation mask.

On the basis of these results we conclude that the yield is greater for very thin films and that the "edge effect" is caused by the film being thinner at the perimeter because of shadowing resulting from a poorly fitting evaporation mask.

The major cause of increased yield in very thin films is believed to be increased optical absorption. Sennett and Scott[3] found that large absorption maxima occur for absorption versus thickness for various metal films. Their measurements do not extend into the infrared but at 7000Å their Au films showed a maximum at 140Å where the absorption was 30% or about 9 times larger than expected for thick films. For Ag films, a similar maximum occurs at 100Å. The effect is explained on the basis of the particulate structure of the thin films and the resulting variation of the optical constants with thickness using the theory of Garnett.[4] The theory stipulates that this increase is an increase in free carrier or Drude absorption. This is an important fact since this kind of absorption leads to the excitation that we expect to contribute to photoemission whereas other mechanisms of absorption such as those involving bound states and interband transitions may not lead to photoemission.

A similar but smaller enhancement of absorption for our diode structure can be predicted from thin film theory[5] for films of constant optical properties (i.e., films with the bulk, continuous structure). Such a calculation is presented in Figure II-12.

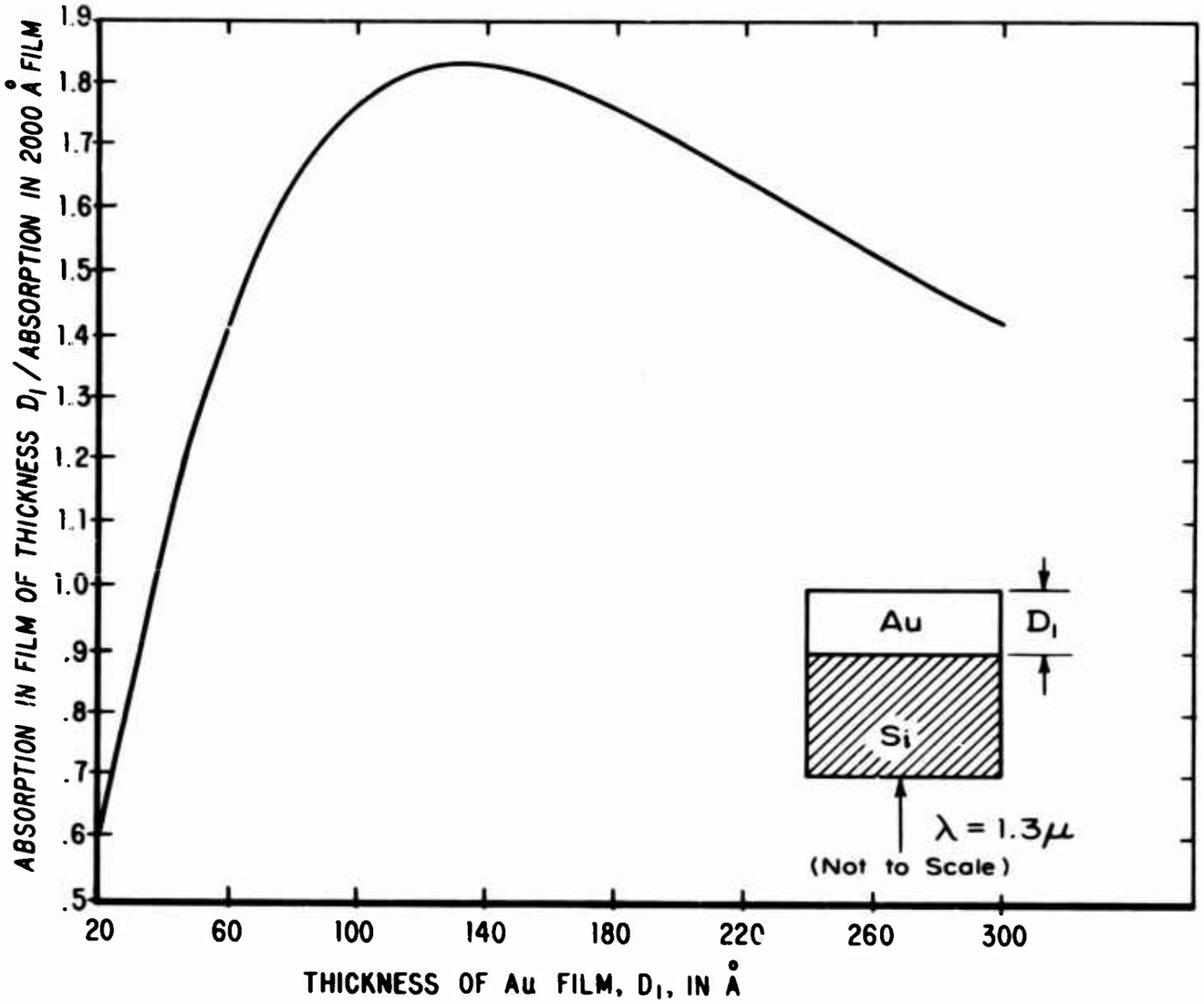

FIGURE II-12: The ratio of the absorption in very thin Au films to that in a very thick film assuming thickness independent optical constants.

As an experimental check we determined the absorption of 2000Å 100Å, and 50Å thick Au films on Si with the light incident from the Si side by measuring reflection and transmission with a Beckman DK40 spectrophotometer using A = 1 - R - T. The results at 1.3μ are given in Table II-2. The uncertainties in the values are in all cases not less than ±2% (i.e., a typical entry should be (17 ± 2)%). Further, we believe that the correct value for the absorption for the 2000Å case should be 5% on the basis of the optical properties of Au films[6, 7] and Si (n = 3.6). We conclude that this experimental check reveals as much as a factor of 4 difference in the absorption of the two thin films compared to the thick film.

Another factor which might contribute to enhanced photoemission from very thin films is the possibility of the emission of electrons that are reflected and even multiply reflected from the metal surfaces. Such an effect would be expected for films thinner than the mean free path of the excited electrons. For electrons about 1 eV above the Fermi level in Au films, nearly elastic phonon scattering has a mean free path of about 300Å and electron-electron scattering, with large energy loss, has a mean free path of about 1000Å.

In view of the practical importance for optical detection of the large increase in yield for thin films shown in Table II-1, a detailed study of the influence of thickness and evaporation conditions on yield is indicated to find what maximum values can be obtained.

TABLE II-2

Optical Absorption at 1.3μ
in Au Films on Si

Thickness of Au	Sample #1 Absorption	Sample #2 Absorption	Average Absorption
2000Å	7.5%	5.5%	6.5%
100Å	17%	19%	18%
50Å	17.5%	17%	17.3%

II. 4. Low Barriers - Low Temperatures

In order to further our understanding of the photoemission process--especially of the functional relationship between yield and photon energy--and more particularly to develop and characterize contacts for far infrared optical detection, we have studied contacts with low barrier heights to both p-type Si and p-type Ge. The barrier heights are of the order of 0.3 eV and 0.1 eV, respectively, for the two materials and since the values are small compared to the bandgaps, they permit the study of yield over a photon energy range that is several times the barrier height which is important for deciding between the two relationships of Eq. (3) and Eq. (4). We would have preferred to study low barriers on n-type semiconductors and electron rather than hole emission so that the results could be unambiguously compared to n-type Si barriers whose properties we now understand well, but there are no known metal-n-type semiconductor contacts with barrier heights less than 0.3 eV for semiconductors with bandgaps that are large compared to the barrier heights.

Since yield is determined from a measurement of the short-circuit photo-current at zero bias, it is required that the impedance of the diode at zero bias, R_0, be large compared to that of the measuring instrument which for precise, accurate measurement must be of the order of 10^5 - 10^6 ohms because of the relatively low signals involved. Capacitance and forward bias current-voltage measurements roughly require $R_0 > 10^5$ ohms.

For an ideal diode, the zero bias impedance is

$$R_0 = \frac{kT\, e^{\phi_{MS}/kT}}{q\, 120T^2\, m^* A} \qquad (6)$$

where m^* is carrier effective mass and A is diode area. It follows from Eq. (6) that for typical diodes a 0.3 eV barrier requires measurement near or below 100°K and a 0.1 eV barrier near or below 40°K.

II.4.1. Cryostat

The cryogenic system used for the diodes with low barriers is the Andonian dewar shown in Figures II-13 and II-14. This apparatus was mounted on a hydraulic elevator for the manipulations required in filling with refrigerants, sample mounting and adjustment in the optical measurement setup. Cooling is accomplished either by a flow of cold gas adjusted with the throttling valve or by immersion. Cooling to below 4°K is practical.

II.4.2. Au Contacts to p-type Si

II.4.2.1. Diode Fabrication

The p-type substrate is prepared in a standard manner that includes the diffusion of boron to form a thin p^+ skin on part of the back surface of the wafer. The front surface and most of the back surface is etch-polished and as a final cleaning step thermally oxidized. The thermal oxide is removed in HF; an array of Au pads 2000Å thick is evaporated on

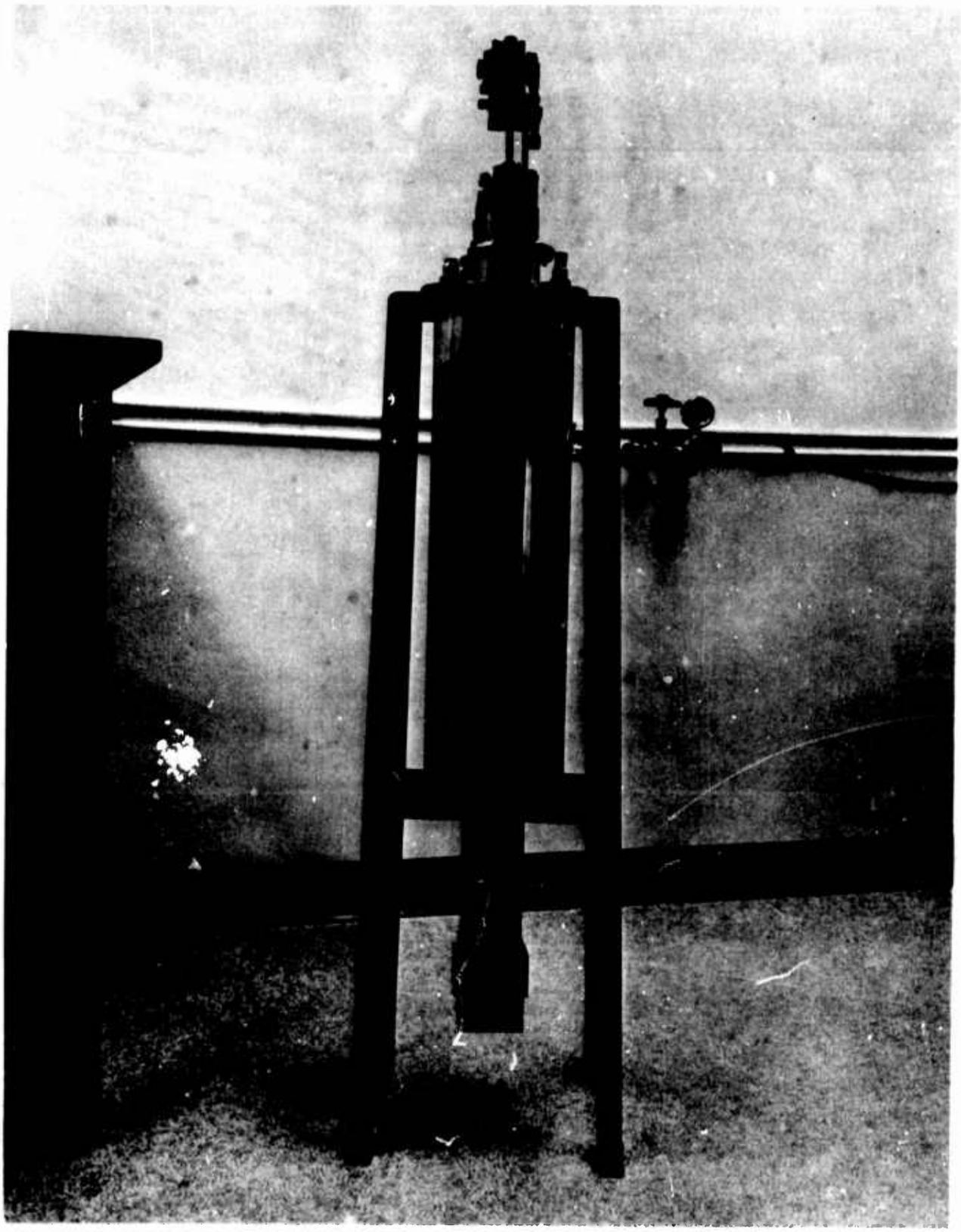

FIGURE II-13: Andonian cryogenic system.

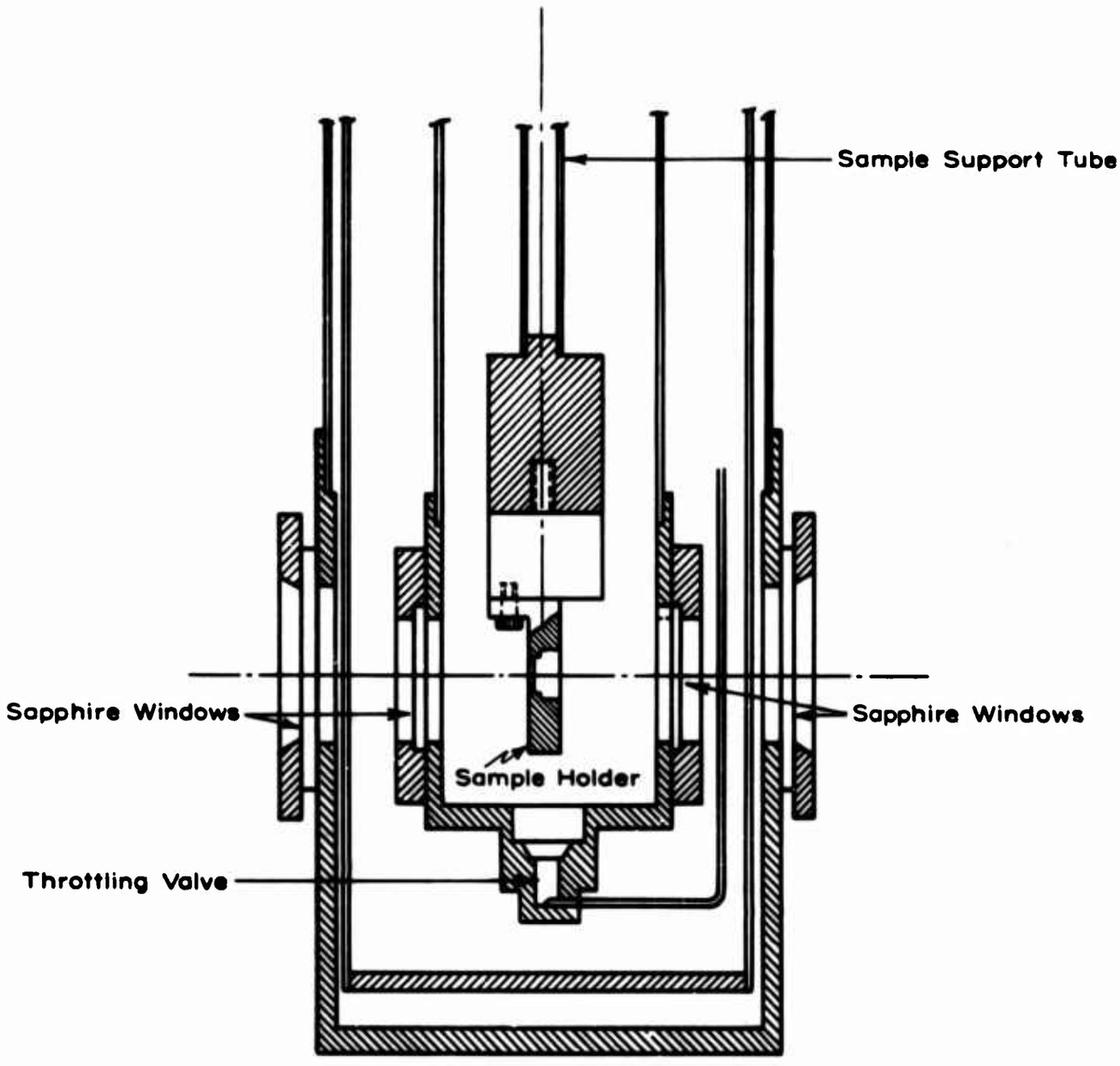

FIGURE II-14 : Tail section of Andonian cryogenic system.

the front surface, and a Au film is evaporated on that part of the back surface with the p^+ layer for ohmic contacting.

II.4.2.2. Forward Current-Voltage Characteristics

Figure II-15 gives representative I-V characteristics for two different sized diodes at 77°K. The slope

$$\frac{d \ln I}{dV} = \frac{q}{1.04\ kT} \tag{7}$$

indicates essentially ideal diode behavior and from the relationship

$$J_S = 120T^2\ m^*\ e^{-\phi_{MS}/kT} \tag{8}$$

we calculate from the saturation currents, using $m^* = 0.5$, $\phi_{MS} = 0.28$ eV. Taking into account image force lowering, the corrected value is about 0.29 eV.

II.4.2.3 Capacitance

Figure II-16 is a representative plot of $1/C^2$ vs. applied reverse bias at 77°. The slope gives $N_A = 2.0 \times 10^{15}$ in agreement with the resistivity, and the voltage intercept, 0.27 V, gives for the barrier height 0.31 eV which is about 0.02 eV greater than the value calculated from the saturation current.

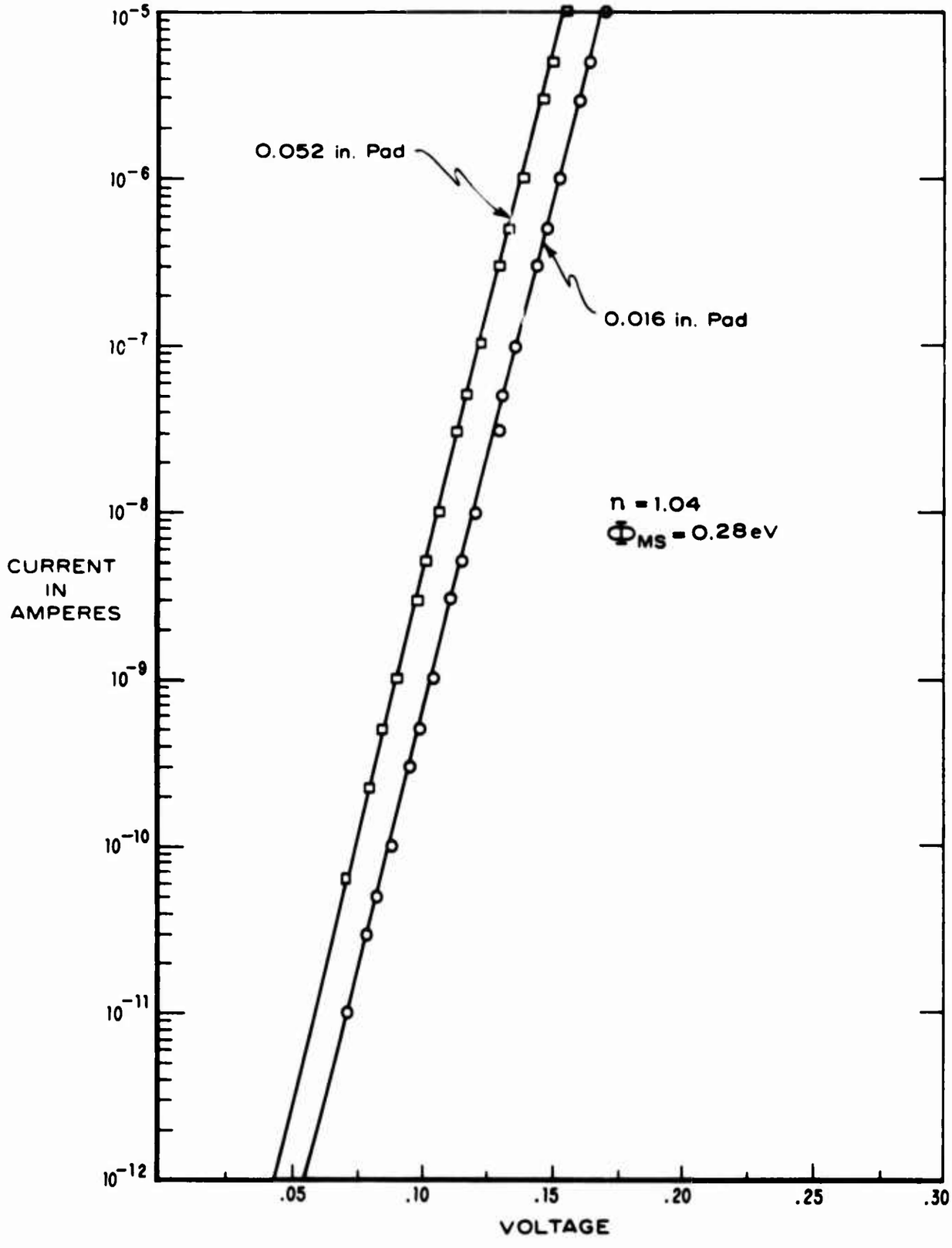

FIGURE II-15: Forward V-I characteristics of 0.016 in. and 0.052 in. Au-p-type Si diodes at 77°K.

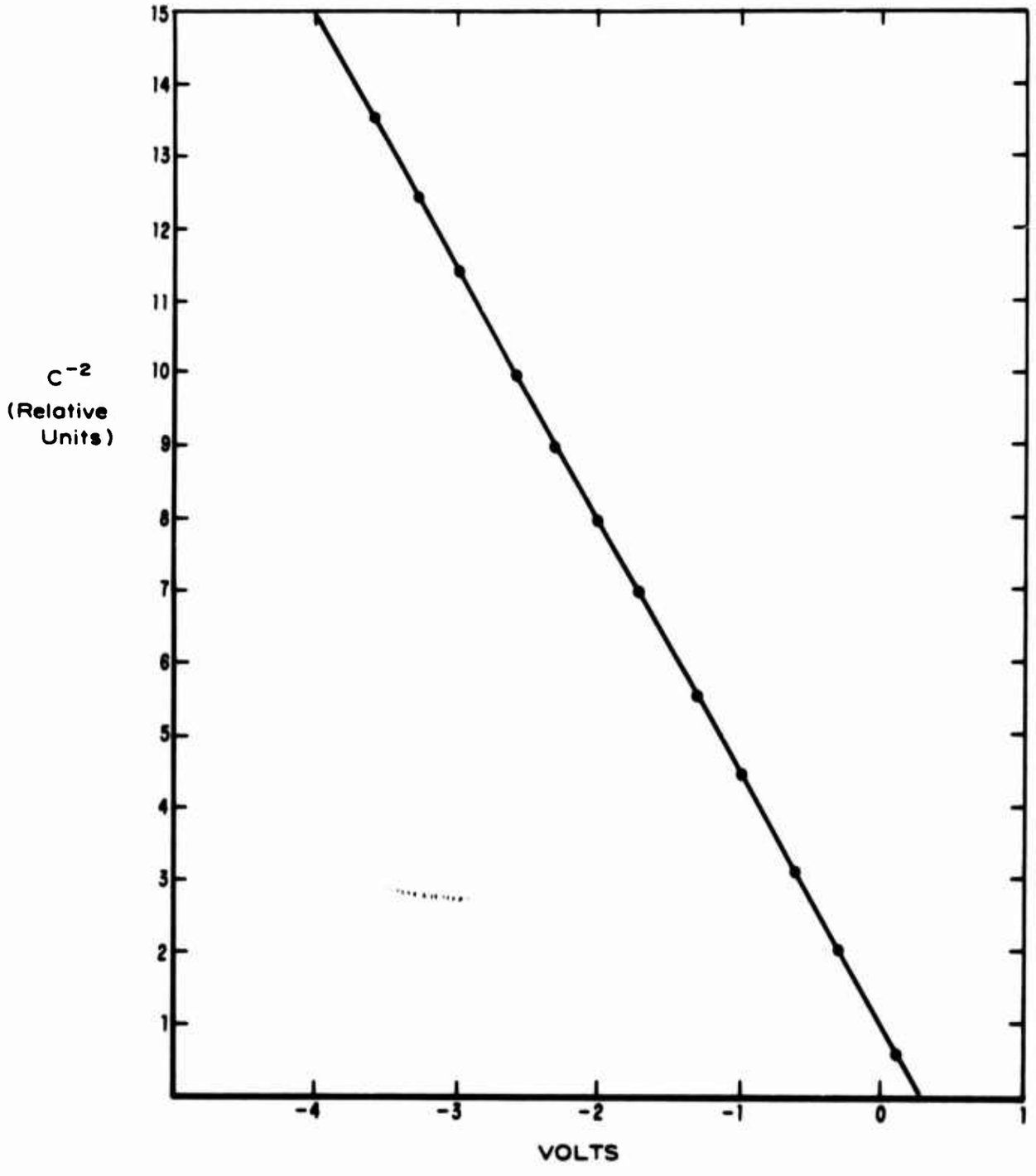

FIGURE II-16: Capacitance-voltage characteristics of a 0.052 in. Au-p-type Si diode at 77°K.

II.4.2.4. Photoemissive Yield

Representative absolute photoemissive yields are plotted in Figures II-17 and II-18 for 0.016 in. and 0.052 in. diameter diodes, respectively, immersed in liquid nitrogen. From these and similar data, we conclude the following:

1. The intercepts of the Fowler plots of six different diodes give

$$h\nu_o = 0.288 \pm 0.002 \text{ eV}$$

and taking into account image force lowering we conclude that the barrier height is 0.30 eV in good agreement with the I-V and capacitance values.

2. The yields for a number of diodes on the same wafers for both size pads agree within about 20%. However, a second array of 0.05 in. diameter diodes has yields that are a factor of 3 to 4 greater than for diodes on the wafer represented by Figure II-18.

3. There is therefore a 3- to 12-fold greater yield for the 0.016 in. diodes compared to the 0.015 in. diodes which indicates an edge effect for hole emission like that observed for electron emission (the loosely fitting mask was used to evaporate these contacts).

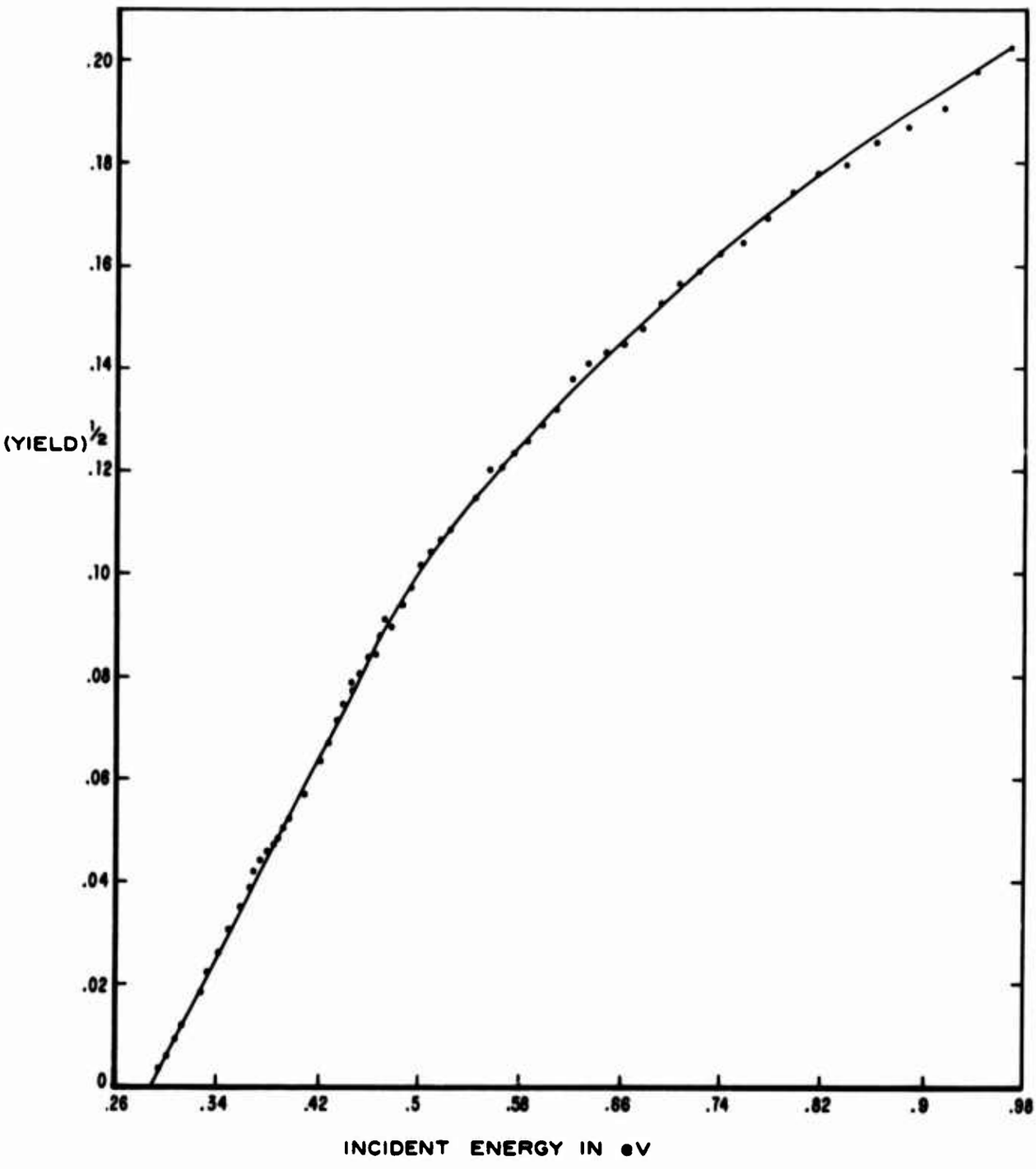

FIGURE II-17: The dependence of absolute yield on photon energy for a 0.016 in. Au p-type Si diode of wafer A.

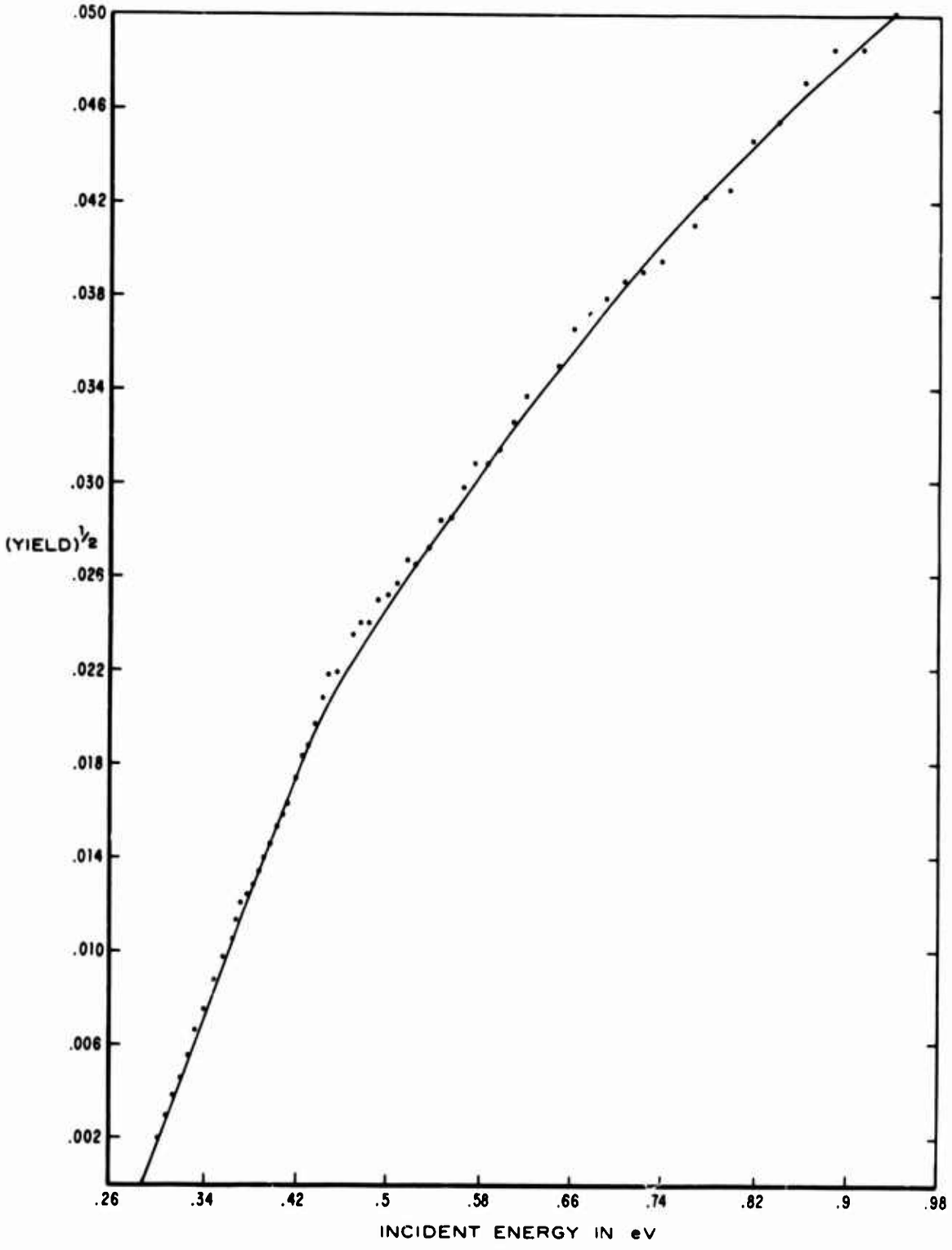

FIGURE II-18: The dependence of absolute yield on photon energy for a 0.052 in. Au p-type Si diode of wafer B.

4. The deviation from linearity of the Fowler plots is a characteristic of all of the data and is consistent with the dependence of yield on photon energy given by Eq. (3) as is demonstrated by the re-plotting of the data of Figure II-18 in Figure II-19 which shows that $\sqrt{y h\nu}$ vs. $h\nu$ is more nearly linear than the Fowler representation. This treatment assumes that the fraction of the incident power which is absorbed in the Au film is constant and independent of photon energy. However, the reflectivity changes over the range of Figure II-19, but the change is attributed[6] to interband transitions which may not contribute to photoemission and the free-carrier or Drude absorption should be nearly constant over the range.[6]

II. 4. 3. Au, Ag, and Ni Contacts to p-type Ge

We have studied the electrical properties of contacts to p-type Ge to obtain barrier heights but have not yet measured photoemission.

II. 4. 3. 1. Diode Fabrication

The procedure for etch-polishing and cleaning Ge surfaces was established using the criterion of the thickness of the residual surface film as measured with an ellipsometer. The procedure adopted results in a residual surface film of about 13Å thick. On the basis of our experience with ellipsometer measurements on Si, we judge this to be an unusually

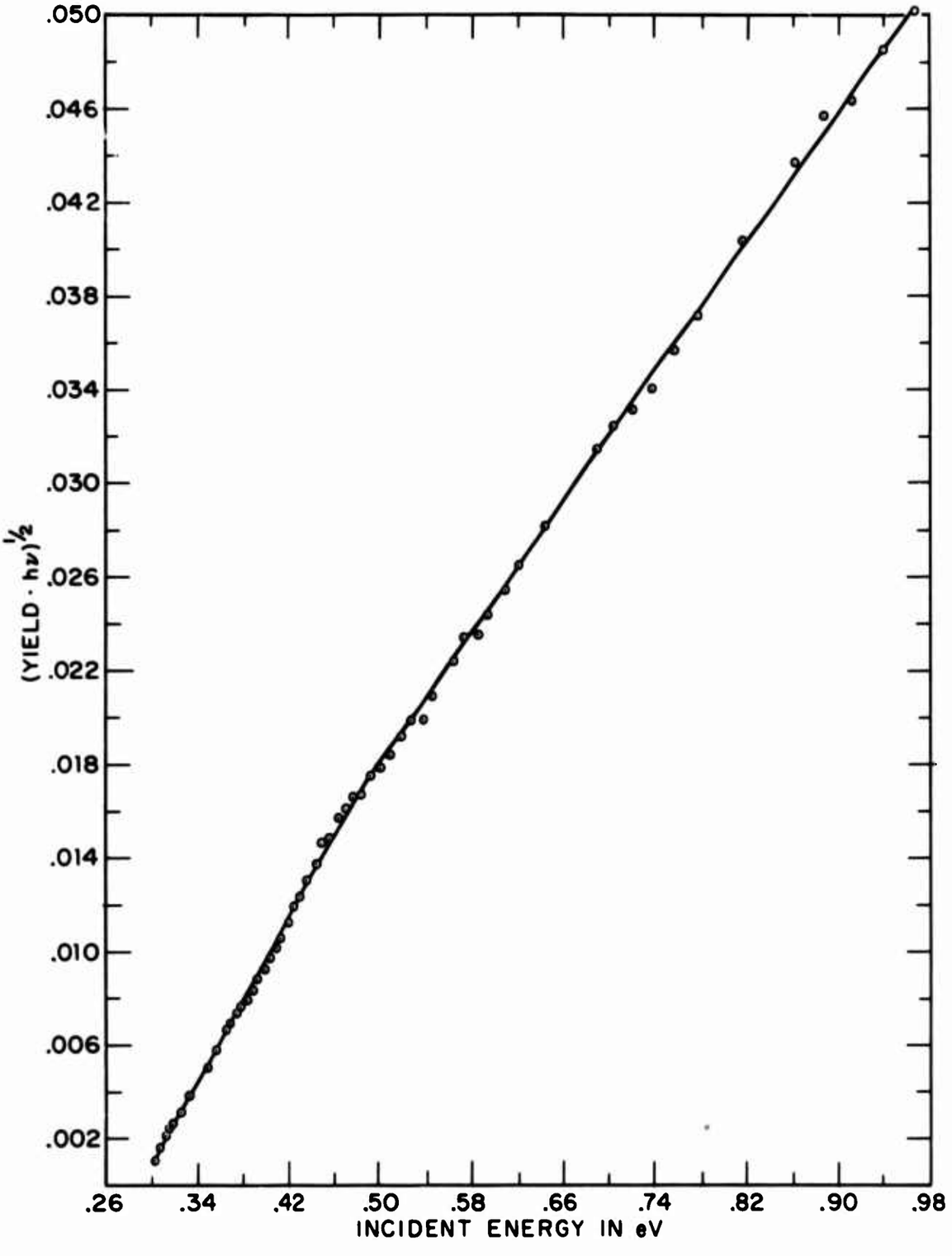

FIGURE II-19: Re-plotting of the data of Figure II-18 showing the better fit to Eq. (3) than Eq. (4).

clean etch-polished surface. The diodes are fabricated as follows from <100> oriented, 1 ohm-cm p-type Ge slices:

1. Mechanically polish both surfaces.
2. Alloy an Al film that covers a portion of the back surface for ohmic contact.
3. Rotary etch front surface in 1:2:6 hydrofluoric, acetic and nitric acids.
4. Clean in boiling TCE, acetone and methanol.
5. Boil for 10 minutes in double-distilled water.
6. Rinse in HF using a technique that prevents immersion of the Al ohmic contact.
7. Evaporate metal pads 2000Å thick.

II.4.3.2. Au-Ge Contacts

Au contacts are ohmic down to somewhere near or below 10°K, where carrier freeze-out occurs and the I-V characteristic is essentially that of an insulator but shows breakdown for both polarities at about 6V bias presumably owing to impact ionization of shallow impurities. We conclude that the barrier height must be less than about 0.03 eV. Thus the Au-Ge contact is not suitable for photoemission studies except in the frozen out state, assuming the barrier height is finite, where photoemission and photo-excitation of shallow impurities could compete and obscure the interpretation of data.

II. 4. 3. 3. Ag-Ge Contacts

Figure II-20 plots the forward I-V characteristics of a Ag p-type Ge diode (0.016 in. in diameter) at several temperatures between 23°K and 55°K. The increase in the slope constant

$$n = \frac{q}{kT}\left(\frac{dV}{d \ln I}\right) \tag{9}$$

with decreasing temperature is consistent with the expectation for thermionic-field emission of holes. From the theory for this process[8] we expect, for the present case,

$$\frac{d \ln I_S}{d\left(\frac{1}{nkT}\right)} = \frac{1}{\phi_{MS}} \tag{10}$$

where I_S is the extrapolated current intercept of the I-V characteristic. The plot based on Eq. (10) is given in Figure II-21. The slope gives for the barrier height

$$\phi_{MS} = 0.10 \text{ eV}.$$

At the highest temperature, 54.6°K, the near unity magnitude, n = 1.13, indicates that the current is approaching the thermionic limit. For this case, a calculation of the barrier height from the ideal thermionic diode

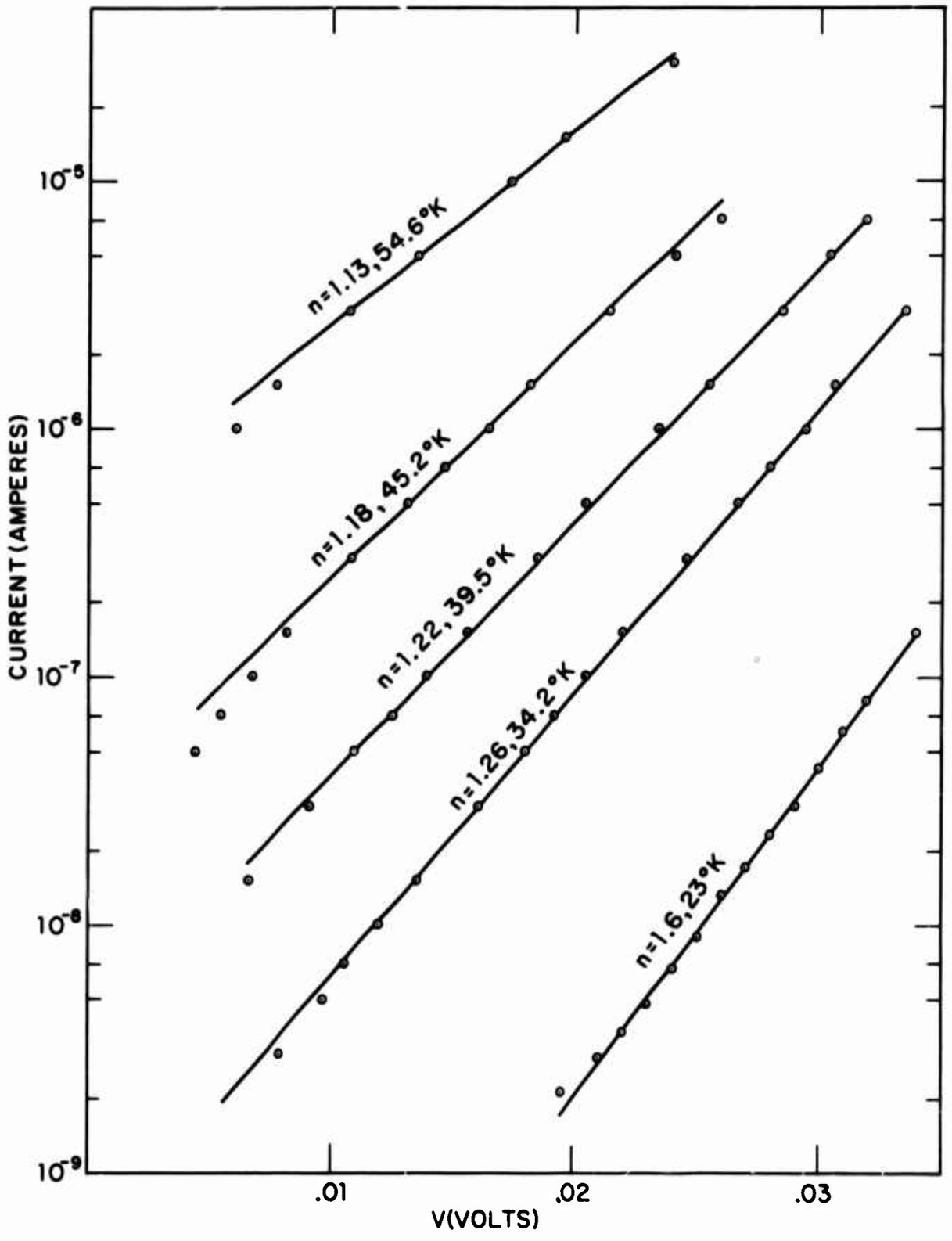

FIGURE II-20: Ag contacts to p-type Ge at various temperatures.

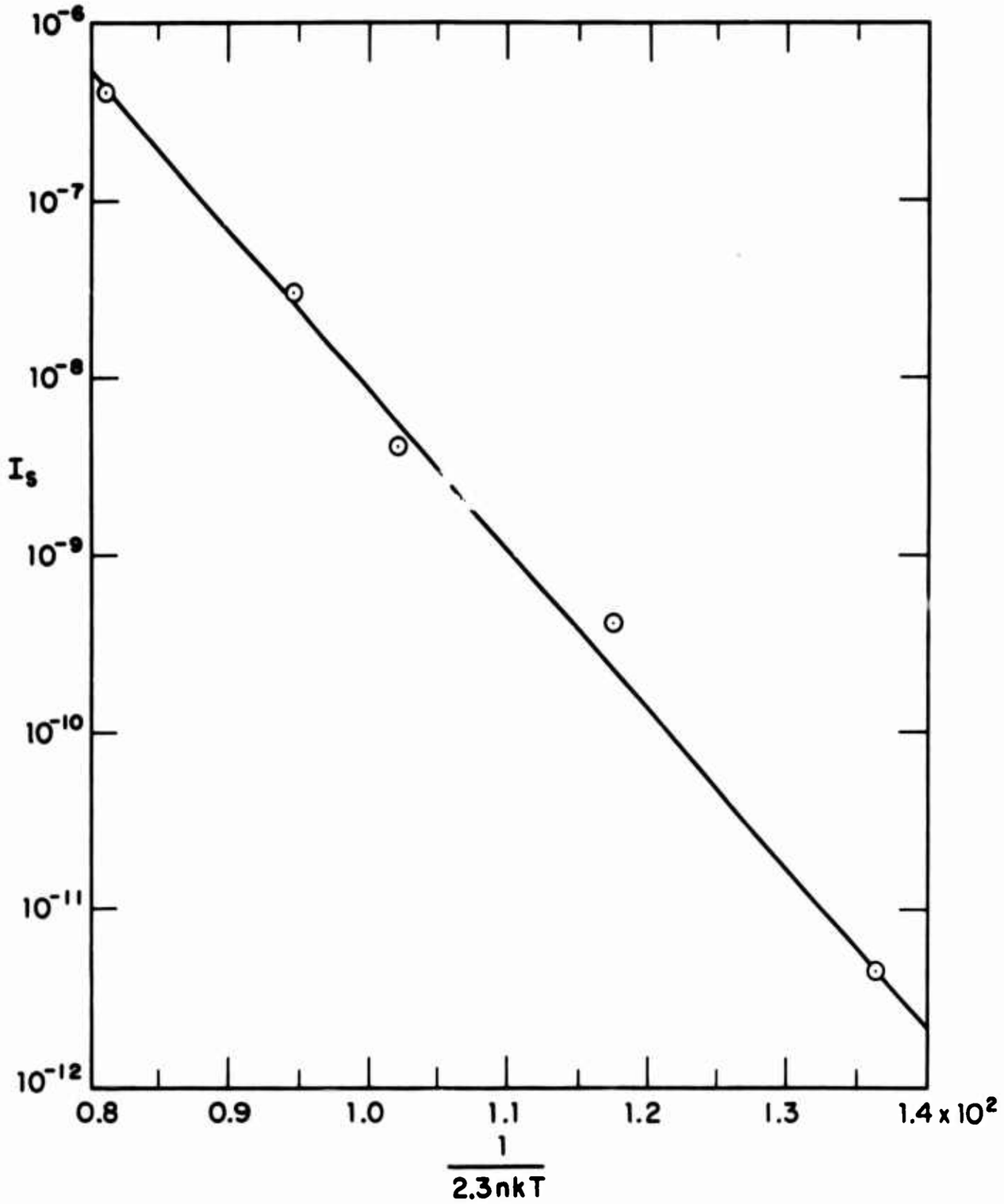

FIGURE II-21: Plot of data from Figure II-20 according to Eq. (10) to obtain barrier height of Ag on p-type Ge.

Eq. (8), gives ϕ_{MS} = 0.093 eV which substantiates the value deduced from thermionic-field emission theory. Taking into account image force lowering of the barrier we conclude that the barrier height for the Ag p-type Ge contact is 0.11 eV.

This conclusion is in good agreement with the capacitance-voltage data of Figure II-22 taken at 24°K which gives 0.12 eV for the barrier height.

II.4.3.4. Ni-Ge Contacts

The I-V characteristic for a Ni p-type Ge contact at two temperatures is given in Figure II-23. Again the slope constant decrease with temperature indicates thermionic-field emission. By comparison with Ag-Ge data, we conclude that the barrier height is 10 - 20 meV lower for the Ni diodes or about 0.09 - 0.10 eV. For the higher temperature data, Eq. (8) gives ϕ_{MS} = 0.07 eV.

II.5. Increasing the External Yield of Photoemission at Metal-Semiconductor Contacts by Optical Impedance Matching

II.5.1. Introduction

The external yield for photoemission at metal-semiconductor contacts is expected to be approximately proportional to the fraction of the incident optical power which is absorbed in the metal. For the simple structure shown in Figure II-2 this fraction (symbolized L here) is small

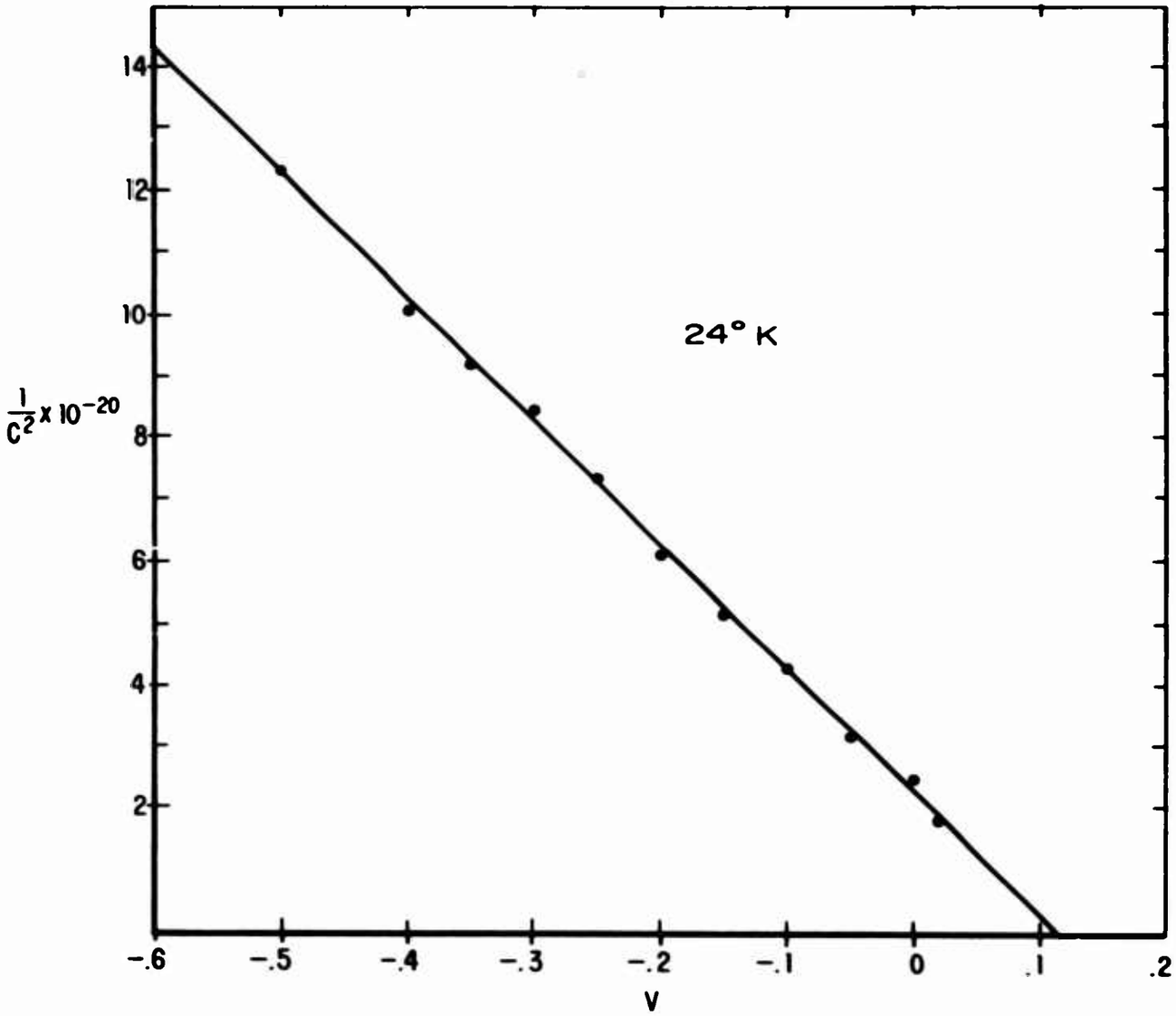

FIGURE II-22: Capacitance-voltage data for Ag p-type Ge diode at 24°K.

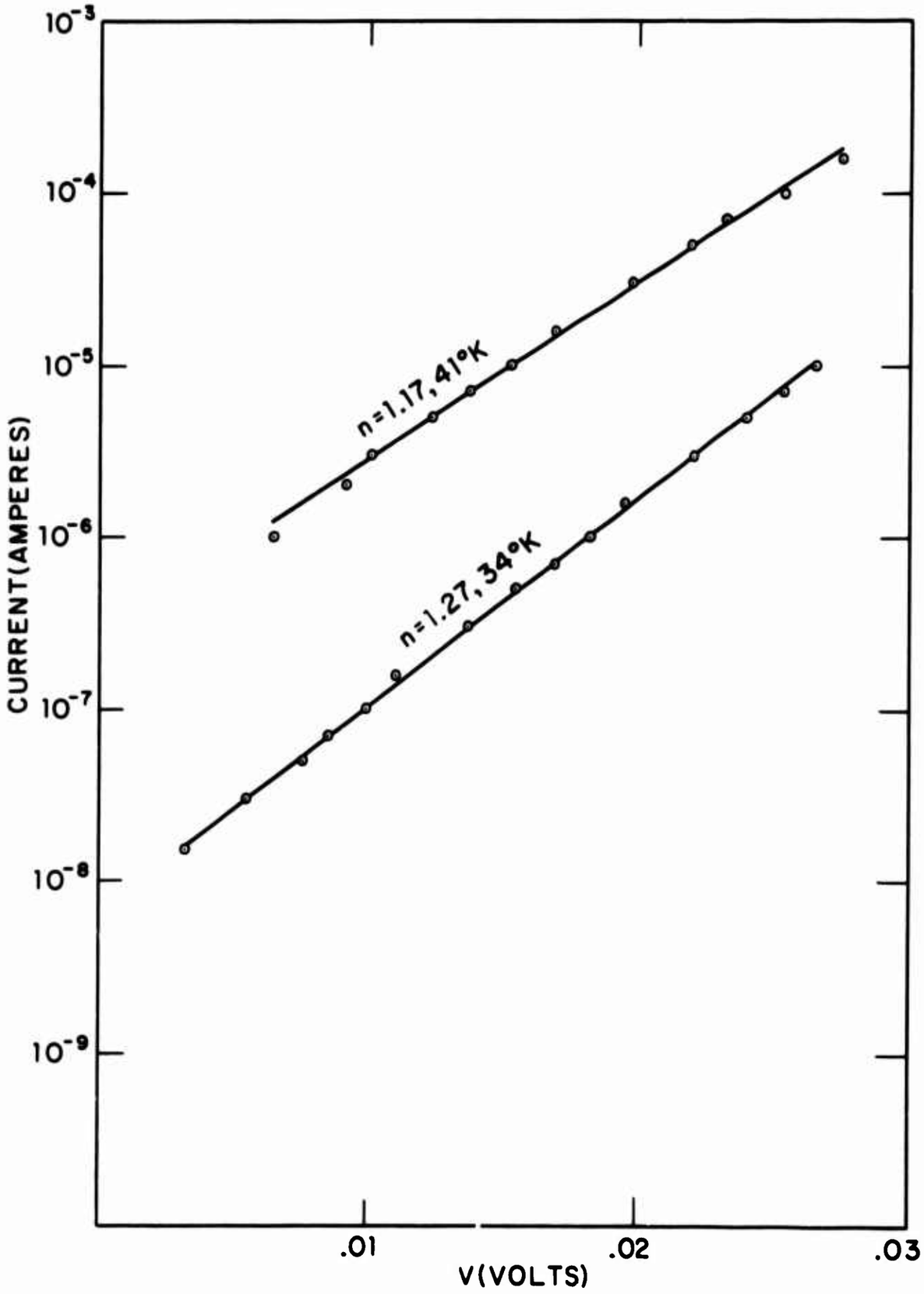

FIGURE II-23: Ni conta s to p-type Ge.

because of the high reflectivity of the metal-semiconductor interface. To overcome this limitation on yield we have conceived* and analyzed the impedance matching structure shown in Figure II-24. As we will show below, this structure leads to a many-fold increase in the fraction L of the incident power that is absorbed in the thin metal layer.

Our concept of the matching structure is based on the narrow band reflection interference filter as analyzed and developed by Hadley and Dennison.[10, 11] This structure is represented in Figure II-25. They calculate and measure reflectivities of nearly 100% at energies $2qh\nu_1$ and nearly 0 percent at $(2q + 1)h\nu_1$ where q is an integer and ν_1 is the frequency of the incident light for which the effective optical thickness of the dielectric layer is a quarter-wavelength. The nearly ideal reflectivities only obtain for the far infrared where the mirror is nearly perfect and the approximation

$$n = k = (\sigma/2\omega\epsilon_o)^{\frac{1}{2}} \tag{11}$$

is valid for the complex index of refraction (n - ik) of the metal where σ is the conductivity of the metal film, ω is the angular frequency and ϵ_o is the permittivity of free space.

It is implicit in the assumptions for the properties of the structure that for the case of zero reflectance <u>all</u> of the incident power is absorbed

*The idea and some initial work on matching occurred before the beginning of the present project. See Ref. 9, for example.

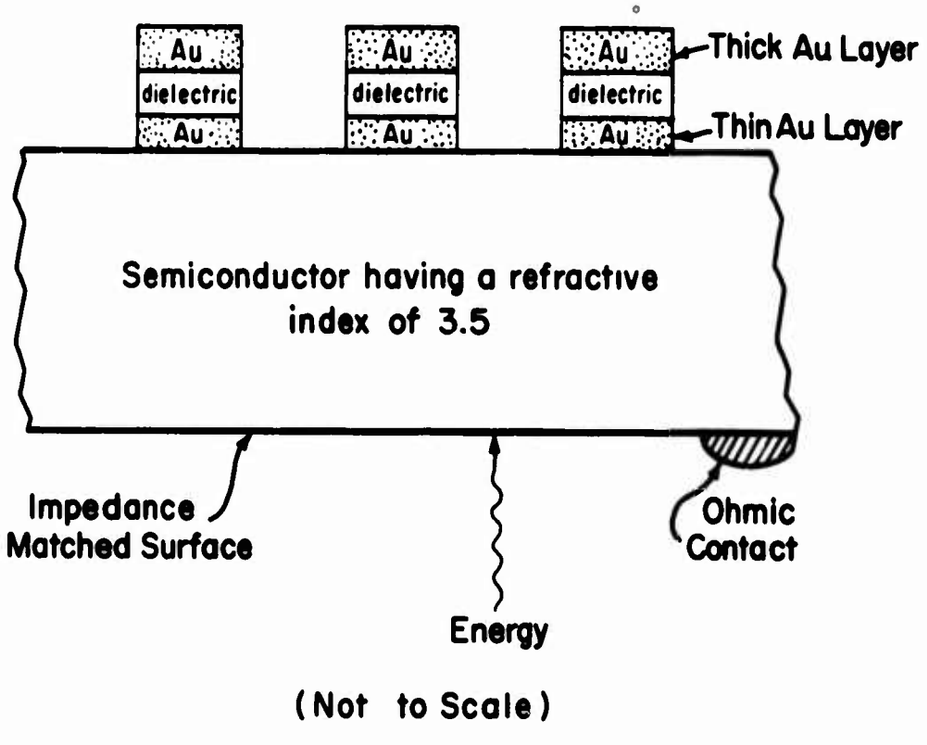

FIGURE II-24: Matching structure to obtain increased external yield.

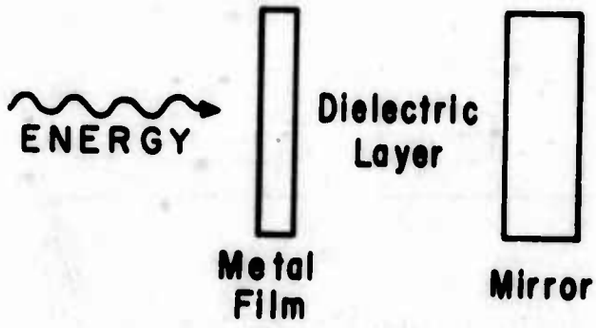

FIGURE II-25: Hadley and Dennison's reflection filter.

in the thin metal film. This fact inspired our investigation of the structure for our application.

The assumption of a nearly perfect mirror and of Eq. (11) for the metal film are the basis of the analysis used by Hadley and Dennison to determine the conditions of zero reflectance. These assumptions are invalid for the infrared range of wavelengths with which we are concerned. Therefore, we use perfectly general multilayer thin film optical theory to analyze the structure of Figure II-22. Our concern is to find the absorption L in the thin metal film as a function of the thicknesses and optical constants of the structure. Figure II-26 shows the basic form of the matching structure expressed in terms of the physical properties necessary for the formulation of the problem. The material of index $n_3 - ik_3$ corresponds to the thick Au layer; as all of the energy entering it is absorbed, it is, therefore, not necessary to specify its thickness. We will thus interpret the transmittance of the system, T, as the energy absorbed in the thick Au layer. Furthermore, as we will utilize a lossless dielectric for the material of index $n_2 - ik_2$ ($\therefore k_2 = 0$), we can express the absorption in the thin Au film, L, as

$$L = 1 - R - T \tag{12}$$

where R is the reflectance of the system. A general multilayer thin film optical theory[5] was employed to calculate R and T. Utilizing this technique

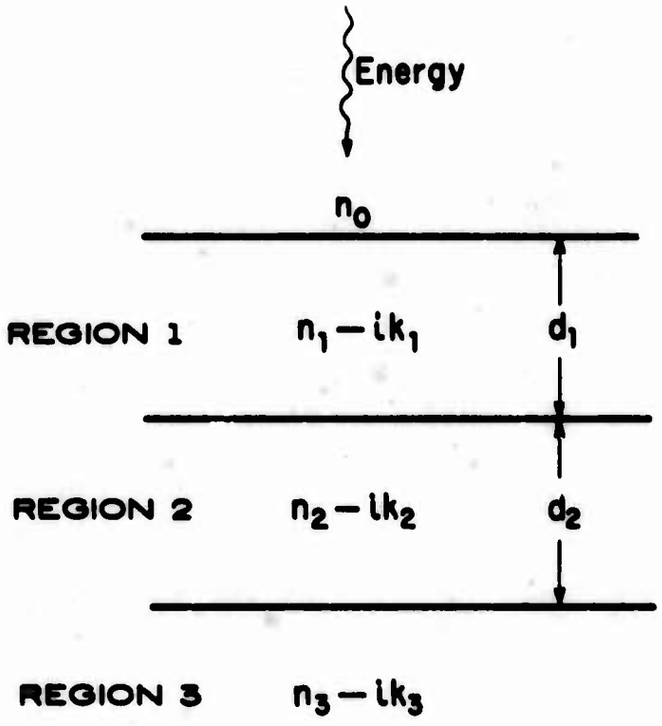

FIGURE II-26: Two absorbing films on an absorbing substrate.

which expresses the relations between the electric vectors in successive layers in terms of Fresnel coefficients, R and T can be expressed as:

$$R = \frac{t_{13}^2 + u_{13}^2}{p_{13}^2 + q_{13}^2} \tag{13}$$

and

$$T = \frac{n_3}{n_o} \frac{l_{13}^2 + m_{13}^2}{p_{13}^2 + q_{13}^2} \; * \tag{14}$$

R and T are evaluated through the use of the following relations:

$$m_{13} = h_1 (1+g_2)(1+g_3) + h_2 (1+g_3)(1+g_1) + h_3 (1+g_1)(1+g_2) - h_1 h_2 h_3$$

$$l_{13} = (1+g_1)(1+g_2)(1+g_3) - h_2 h_3 (1+g_1) - h_3 h_1 (1+g_2) - h_1 h_2 (1+g_3)$$

$$u_{13} = u_{12} p_3 + t_{12} q_3 + w_{12} t_3 + v_{12} u_3$$

$$t_{13} = t_{12} p_3 - u_{12} q_3 + v_{12} t_3 - w_{12} u_3$$

$$q_{13} = q_{12} p_3 + p_{12} q_3 + s_{12} t_3 + r_{12} u_3$$

$$p_{13} = p_{12} p_3 - q_{12} q_3 + r_{12} t_3 - s_{12} u_3$$

$$w_{12} = w_2 + h_1 r_2 + g_1 s_2$$

$$v_{12} = v_2 + g_1 r_2 - h_1 s_2$$

$$s_{12} = s_2 + h_1 v_2 + g_1 w_2$$

$$r_{12} = r_2 + g_1 v_2 - h_1 w_2$$

$$u_{12} = u_2 + h_1 p_2 + g_1 q_2$$

*In normalizing this expression, it will be observed that only the real part of the complex refractive index of region 3 was necessary.[12] This is proper if one interprets T as the energy absorbed in region 3.

$$t_{12} = t_2 + g_1 p_2 - h_1 q_2$$

$$q_{12} = q_2 + h_1 t_2 + g_1 u_2$$

$$p_{12} = p_2 + g_1 t_2 - h_1 u_2$$

$$u_3 = e^{-\alpha_2} (h_3 \cos \gamma_2 - g_3 \sin \gamma_2)$$

$$t_3 = e^{-\alpha_2} (g_3 \cos \gamma_2 + h_3 \sin \gamma_2)$$

$$q_3 = e^{\alpha_2} \sin \gamma_2$$

$$p_3 = e^{\alpha_2} \cos \gamma_2$$

$$h_3 = 2(n_2 k_3 - n_3 k_2) / \left[(n_2 + n_3)^2 + (k_2 + k_3)^2\right]$$

$$g_3 = \left[n_2^2 - n_3^2 + k_2^2 - k_3^2\right] / \left[(n_2 + n_3)^2 + (k_2 + k_3)^2\right]$$

$$w_2 = -e^{-\alpha_1} \sin \gamma_1$$

$$v_2 = e^{-\alpha_1} \cos \gamma_1$$

$$s_2 = e^{\alpha_1} (h_2 \cos \gamma_1 + g_2 \sin \gamma_1)$$

$$r_2 = e^{\alpha_1} (g_2 \cos \gamma_1 - h_2 \sin \gamma_1)$$

$$u_2 = e^{-\alpha_1} (h_2 \cos \gamma_1 - g_2 \sin \gamma_1)$$

$$t_2 = e^{-\alpha_1} (g_2 \cos \gamma_1 + h_2 \sin \gamma_1)$$

$$q_2 = e^{\alpha_1} \sin \gamma_1$$

$$p_2 = e^{\alpha_1} \cos \gamma_1$$

$$h_2 = 2(n_1 k_2 - n_2 k_1) / \left[(n_1 + n_2)^2 + (k_1 + k_2)^2\right]$$

$$g_2 = \left[n_1^2 - n_2^2 + k_1^2 - k_2^2\right] / \left[(n_1 + n_2)^2 + (k_1 + k_2)^2\right]$$

$$\gamma_2 = (2\pi/\lambda)\, n_2 d_2 \text{ (radians)}$$

$$\alpha_2 = (2\pi/\lambda)\, k_2 d_2 \text{ (radians)}$$

$$h_1 = 2n_o k_1 / \left[(n_0 + n_1)^2 + k_1^2\right]$$

$$g_1 = \left[n_o^2 - n_1^2 - k_1^2\right] / \left[(n_0 + n_1)^2 + k_1^2\right]$$

$$\gamma_1 = (2\pi/\lambda)\, n_1 d_1 \text{ (radians)}$$

$$\alpha_1 = (2\pi/\lambda)\, k_1 d_1 \text{ (radians)}$$

II. 5. 2. Calculated Matching for Au-Si Contacts

The index of refraction of Si is taken to be 3. 5 at all wavelengths, and the complex index of refraction of Au* as a function of wavelength is obtained by interpolating the data of Ref. 7. Also we did calculations using values of 1. 5, 2. 5, and 4 for the index of refraction of the dielectric layer and found, as expected, that only effective optical thicknesses (including interfacial phase changes) mattered and that the value for the dielectric index of refraction was otherwise irrelevant.

Using a computer, we evaluated Eq. (12) to find the following:

1. For each of a number of closely spaced values for the thin Au film thickness we programmed the computer to select the value for the dielectric film thickness that leads to a maximum in L. Maximum values of L versus the thin Au film thickness are plotted in Figure II-27 for L = 1. 3μ and in Figure II-28 for L = 4. 0μ. The broken curves plot the optimum thickness of the dielectric film having an index of refraction of 2. 5.

*The index of refraction of an evaporated Au film depends upon many different factors, e.g., the film thickness and the method of deposition. Due to these variables, large differences in the values of optical constants have been reported by different observers. We have chosen the values from Ref. 7 to form a consistent set which we feel will reveal the essential properties of the matching structure.

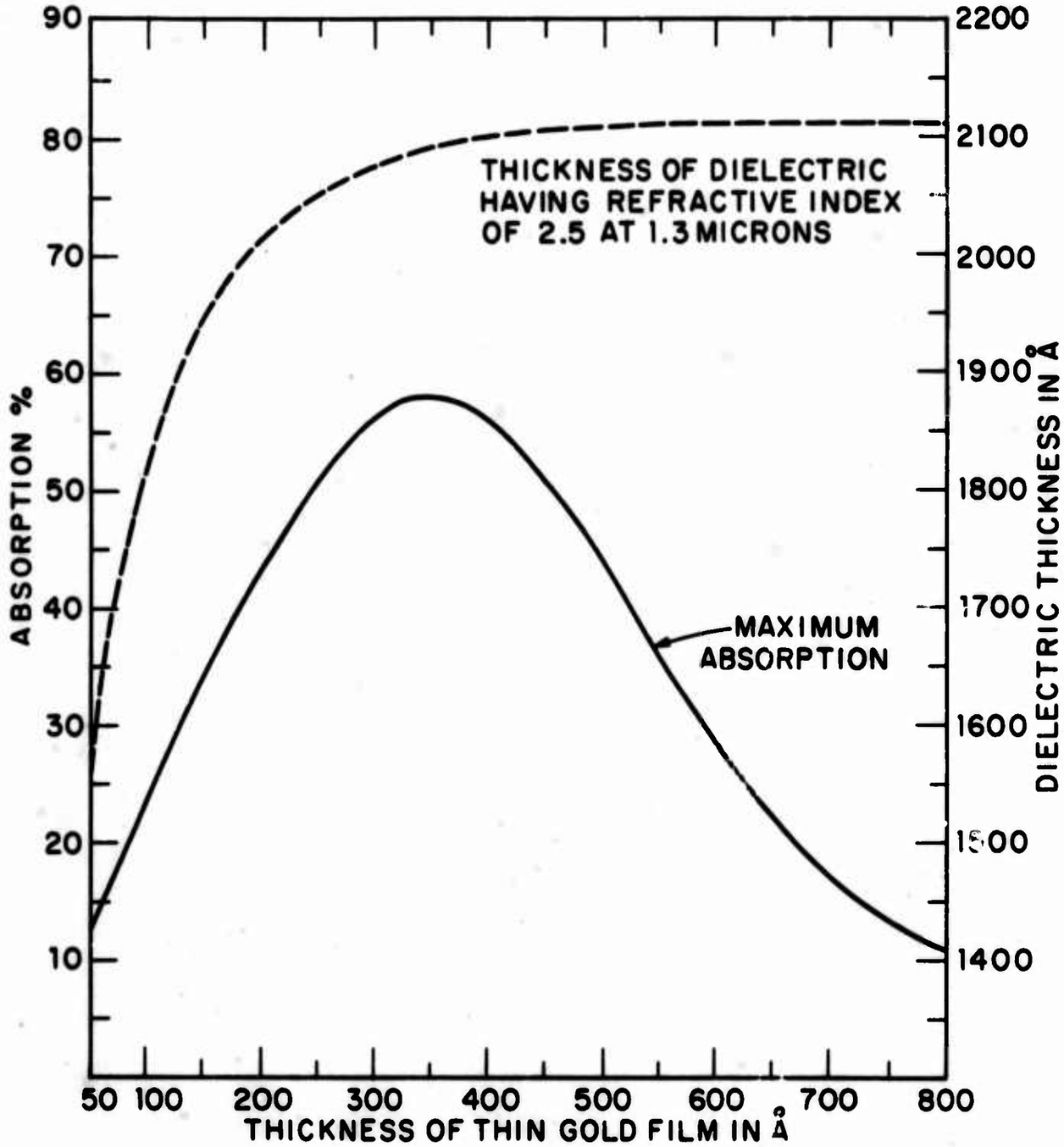

FIGURE II-27: Maximum in absorption at 1.3μ for the matching structure on Si and the thickness of the dielectric layer required for maximum absorption as functions of the thickness of the thin Au film.

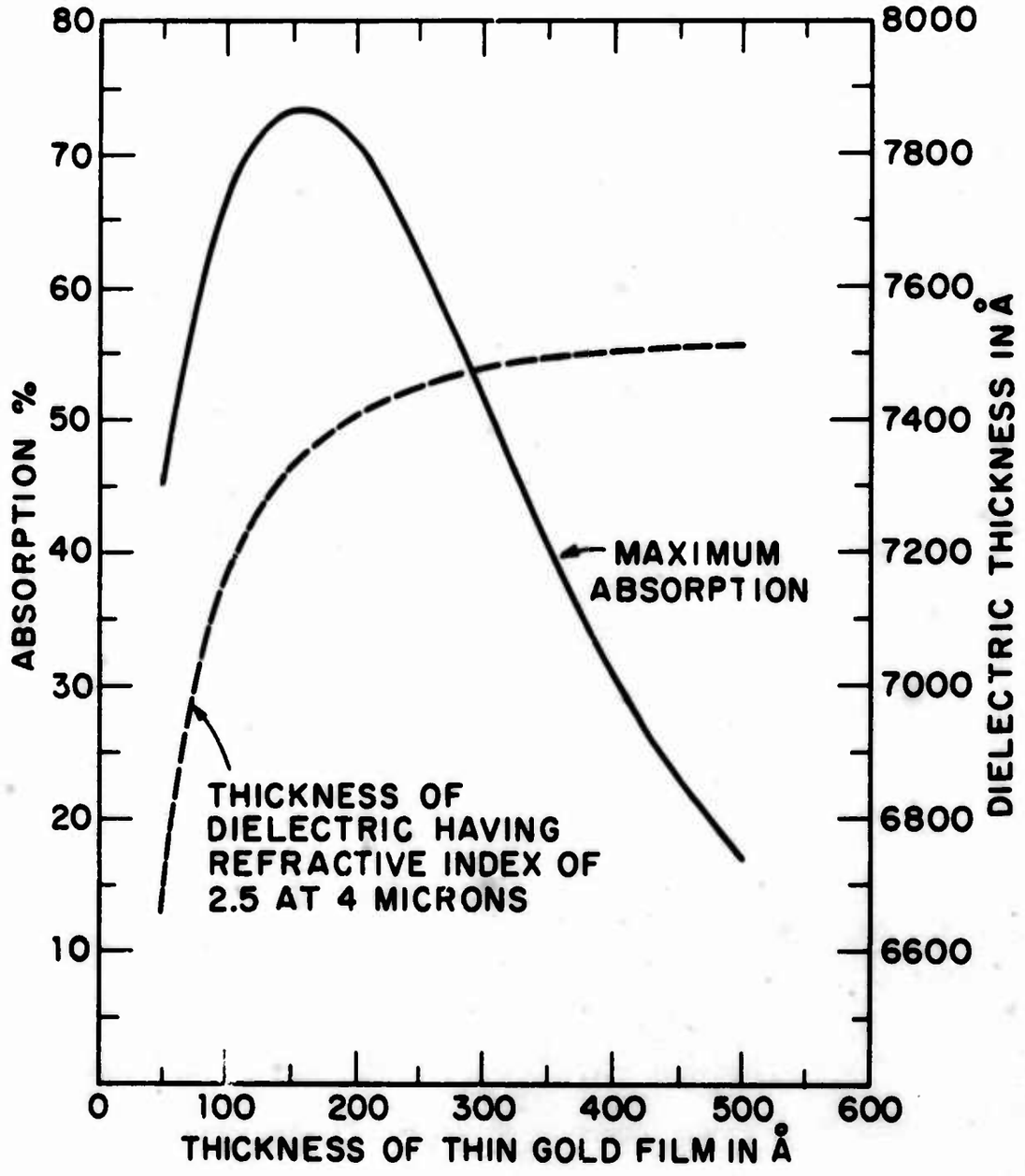

FIGURE II-28: Maximum in absorption at 4.0μ for the matching structure on Si and the thickness of the dielectric layer required for maximum absorption as functions of the thickness of the thin Au film.

2. We computed the optimum matching structures shown in Figures II-29 and II-30 for 1.385μ and 4μ, respectively, and the dependence of L on λ in a range centered on the matched wavelength. For 4μ we also plot L vs. λ for a value of the thin Au film thickness, 50Å, rather far from the optimum value, 150Å. For this latter case the dielectric film thickness is the optimum value for a 50Å Au film.

From the above results we conclude the following:

1. L $\overline{vs}$ Au film thickness, Figures II-27 and II-28, has a fairly broad maximum so that near optimum matching does not require a precise value for the Au film thickness. Roughly, within ±50Å of the optimum value is satisfactory.
2. The unmatched Au-Si interface has a reflectivity of 95% at 1.3μ and 97.5% of 4μ. We conclude that the matched structures lead to a 12-fold increase in absorption at 1.3μ and a 29-fold increase at 4μ.
3. A comparison of the curves in Figure II-30 leads to the conclusion that by adjusting the thin Au film thickness for which the dielectric film thickness is optimized there can be a trade-off between the value L at the matched wavelength and the breadth of the wavelength range over which enhancement in L is effected.

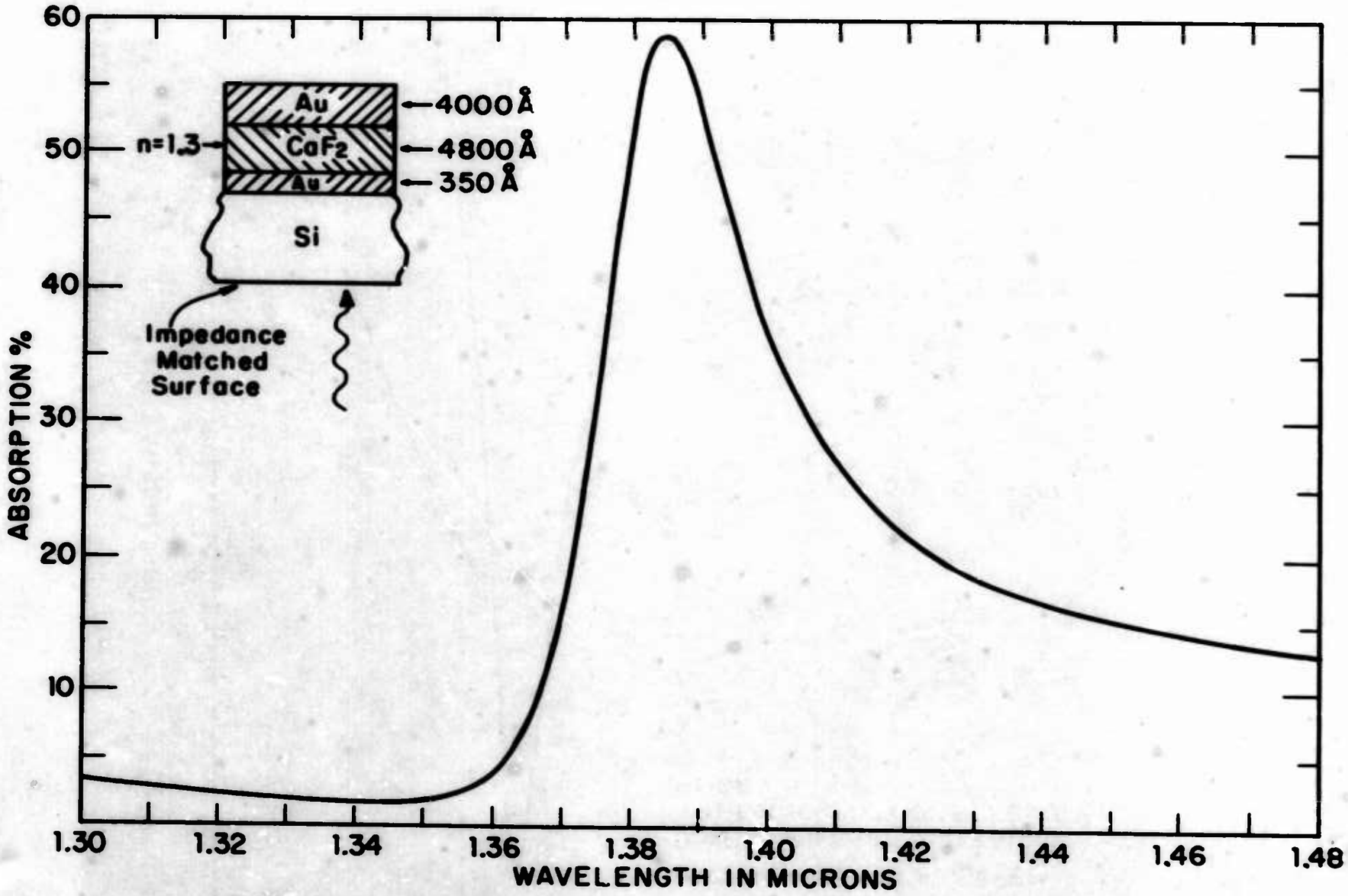

FIGURE II-29: Absorption in thin Au layers as a function of wavelength for the inset structure.

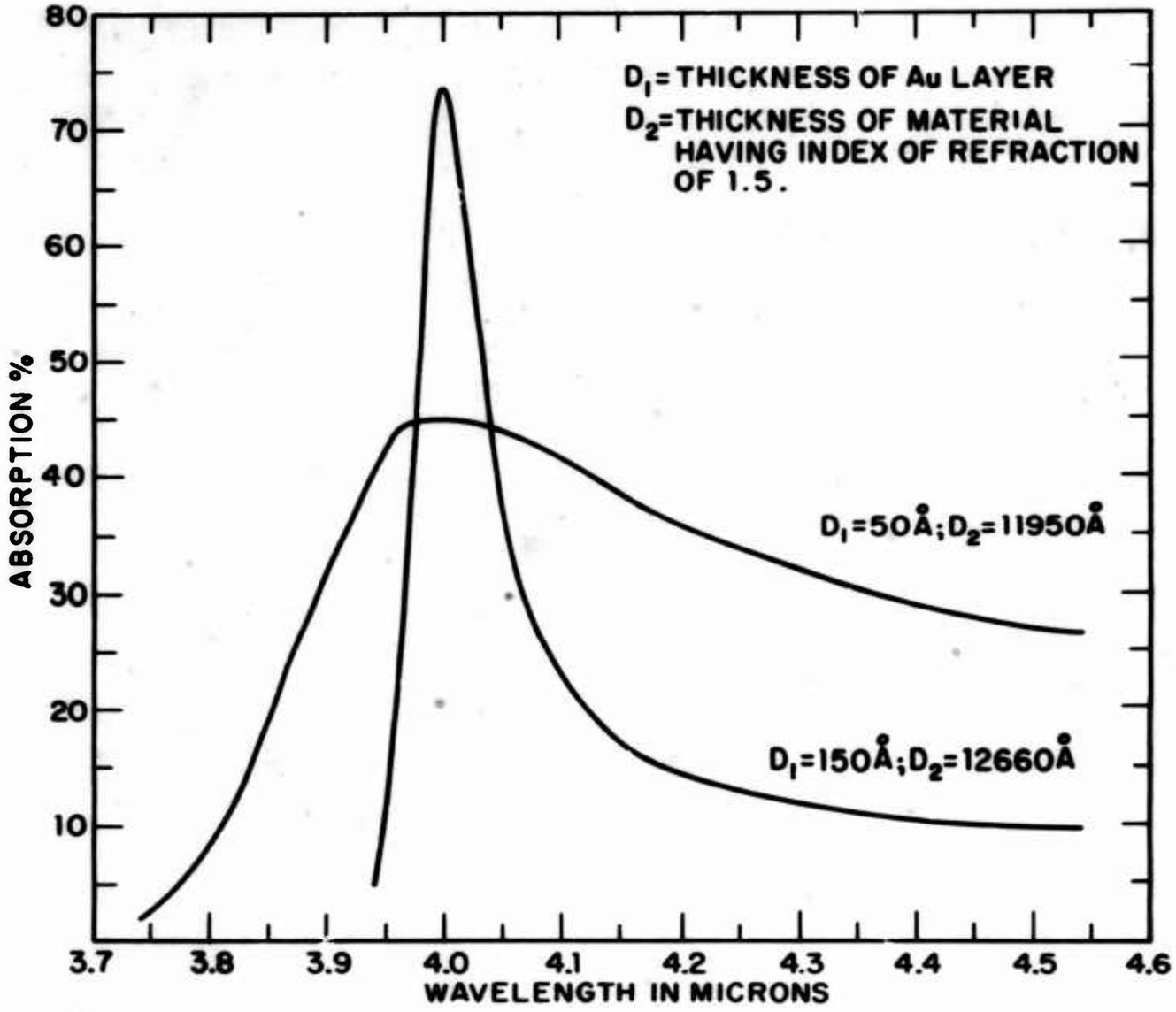

FIGURE II-30: Absorption in the thin Au layer on Si as a function of wavelength for a matching structure optimized at 4μ.

II. 5.3. Calculated Matching for Au-Ge Contacts

We have also used the same mathematical techniques employed in the Au-Si case described above to make several computations on the effect of matching on Ge at 5μ. We have computed the maximum absorption attainable in the thin Au layer of the matching structure versus the thickness of the thin Au layer and the CaF_2 thickness necessary to obtain maximum absorption in each thickness of Au film. These calculations are shown in Figure II-31. It is evident that the maximum attainable absorption maxima are fairly broad. Comparing the maximum absorption value to the absorption that occurs when the matching structure is replaced by a thick Au film, we obtain a 30-fold increase at 5μ.

We have also considered the case of matching structures optimized for maximum absorption in the thin Au layer at a specific wavelength and computed the absorption in the thin Au layer in the wavelength region around the maximum case. Each wavelength response is presented for three different matching structures characterized by the film thickness of the thin Au film for which the structure is optimized. The three film thicknesses are: (1) the optimum thickness which yields the maximum absorption; (2) a thickness less than the optimum; and (3) a thickness greater than the optimum. The results of these calculations are shown in Figure II-32. We conclude that the spectral bandwidth over which absorption and quantum efficiency are enhanced by the matching structure can be adjusted

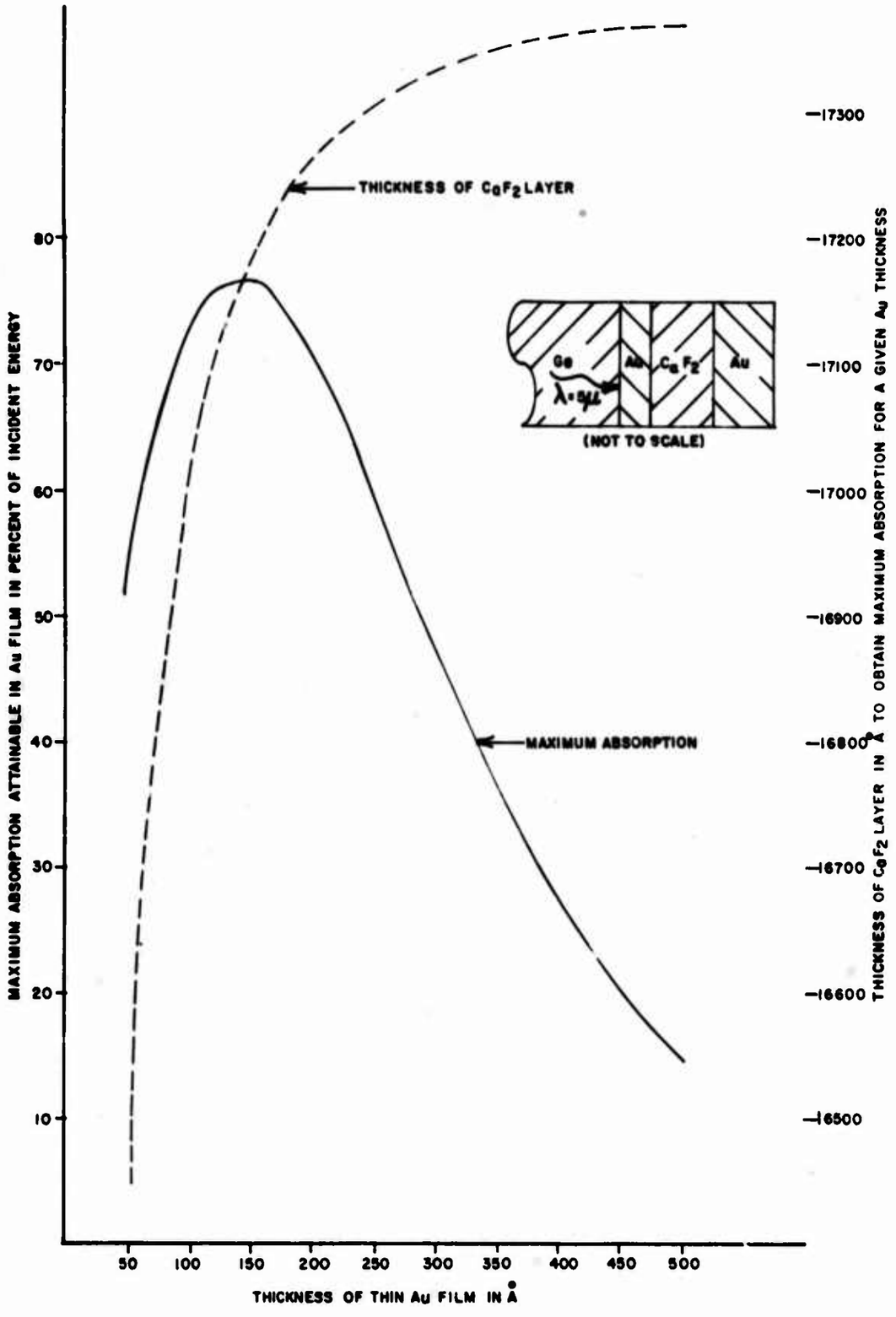

FIGURE II-31: Maximum absorption in the thin Au film at 5.0μ as a function of its thickness and the thickness of the dielectric layer required for maximum absorption.

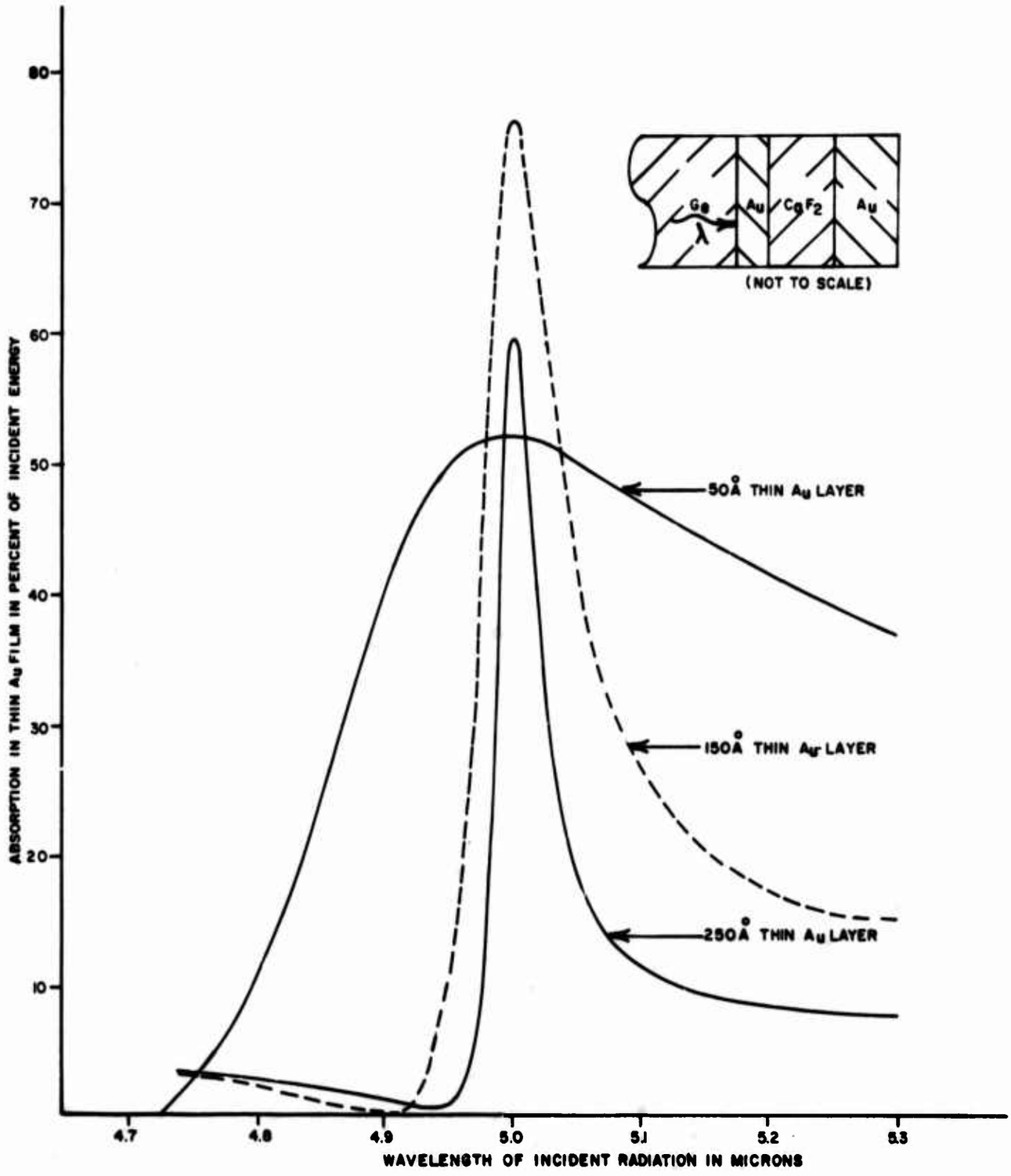

FIGURE II-32: Absorption in the thin Au film versus wavelength for three Au film thicknesses, each structure being matched at 5.0μ.

by means of the thickness of the thin metal film. Films thinner than the optimum result in increased absorption in a wider wavelength range whereas thicker films lead to a narrower range. This control of breadth is at the expense of the maximum in absorption.

Although the above calculations used the optical constants of Au, the techniques and the general features of the results are valid for other metals as well.

II. 5. 4. Experimental Photoemission from Optically Matched Au n-type Si

The matching structure was fabricated using 0.051 in. diameter diodes. The evaporations of the thin Au, CaF_2 and thick Au films proceeded sequentially, using the same mask and one vacuum system pump-down. Since the CaF_2 and Au were thrown from different boats, there was a slight misalignment between the CaF_2 and the two Au layers due to shadowing by the mask. This misalignment results in electrical contact between the Au layers and simplifies external contacting with a probe.

The experimental results are shown in Figure II-33, which compares the yield of a diode with the Au-CaF_2 matching structure with that after the removal of the top CaF_2-Au structure. The measurements were taken with a 0.036 in. diameter hole in a mask placed within the illuminating beam path so as to exclude the edge of the diode where the matching structure was not evaporated uniformly. At 0.975 eV the device with the matching

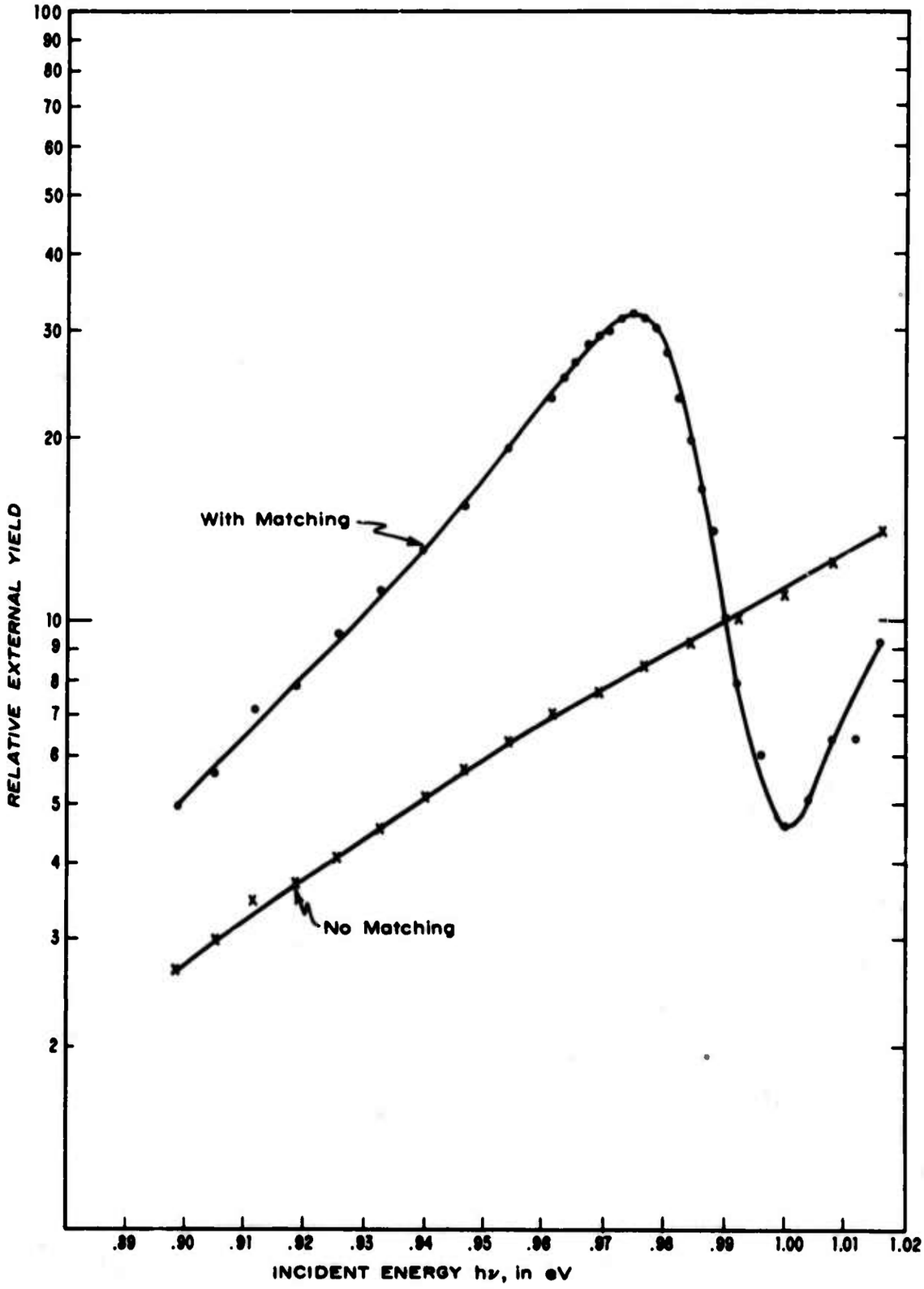

FIGURE II-33: Measured yield of a 0.051 in. diameter diode using a 0.036 in. diameter mask both with and without the CaF_2 -Au matching layers.

structure has an external yield which is about four times that of the device without it.

From Figure II-27 we expect for the matched structure about 0.7 x 58% = 41% absorption. The factor 0.7 is the transmissivity of the air-Si interface which was not matched in our structure. For the unmatched diode, we expect 1.3 x 5% = 6.5% where 5% is the value for a very thick film and the factor 1.3 is from Figure II-12. Thus, if yield is proportional to absorption, we expect a 6-fold increase for the matched relative to the unmatched diode which is in reasonable agreement with the experimental factor of 4-fold.

REFERENCES

(Chapter II)

1. R. H. Fowler, Phys. Rev., 38, 45 (1931).
2. R. J. Archer and K. Muray, quoted in M. M. Atalla, Vorträge der 2. MikroElektronik-Tagung des "Internationalen Elektronik-Arbeitkreises eV" in München, Oktober, 1966 (R. Oldenbourg Verlag, München, Germany, 1967).
3. R. S. Sennett and G. D. Scott, J. Opt. Soc. Am., 40, 203 (1950).
4. J. C. M. Garnett, Trans. Roy. Soc. (London), 203A, 385 (1904).
5. O. S. Heavens, Optical Properties of Thin Solid Films (Butterworths Scientific Publications Ltd., London, England, 1955), p. 78.
6. H. E. Bennett and J. M. Bennett, Optical Properties and Electronic Structure of Metals and Alloys (Proceedings of the International Colloquium held at Paris, 13-16 September 1965) (edited by F. Abeles) North Holland Publishing Company (1966), p. 175.
7. W. E. Forsythe, Smithsonian Physical Tables (Lord Baltimore Press, Baltimore, Md., 1951), 9th ed. p. 559.
8. F. A. Padovani and R. Stratton, Solid-State Electronics, 11, 193 (1966).
9. Fourth Quarterly Progress Letter Report, "Solid State Image Intensifier Panels, " Contract DA44-009 AMC-1250(T), April 1 - June 30, 1967; prepared by Hewlett-Packard Solid State Laboratory.
10. L. H. Hadley and D. M. Dennison, J. O. S. A., 37 (1947), 451.

11. L. H. Hadley and D. M. Dennison, J. O. S. A., 38 (1948), 483.

12. P. H. Berning in G. Hass, Physics of Thin Films (Academic Press, New York, 1963), Vol. I, p. 77.

III. METAL-SEMICONDUCTOR CATHODE

III. 1. Introduction

The aim of this part of the program is to develop a cold cathode based on cathodic emission into vacuum from metal-semiconductor barriers. In this chapter an overall description of work accomplished on this topic during all four reporting quarters will be given. The past quarter's work, not previously reported, will be treated in somewhat greater detail than the material previously described in Scientific Reports 1, 2, and 3.[1-3]

III. 2. Theory of the Cold Cathode

The mechanism of cathodic emission in the metal-semiconductor cathode is represented in Figure III-1, which depicts electron potential energy in different parts of the structure under normal operating voltages. An electron which suffers no scattering will move along a horizontal line in this diagram, and will have the same total energy everywhere in the structure. It will exchange potential energy for kinetic energy, and hence will be accelerated, wherever a spatial gradient of potential energy exists. When the diode is forward biased as shown, electrons are injected into the thin metal film. In the absence of scattering, these electrons remain at an energy corresponding to slightly above the top of the Schottky barrier, and are transported through the metal film. If the metal-vacuum work function ϕ_V is lower than ϕ_{MS}, a large fraction of the electrons are emitted into vacuum and collected at the anode.

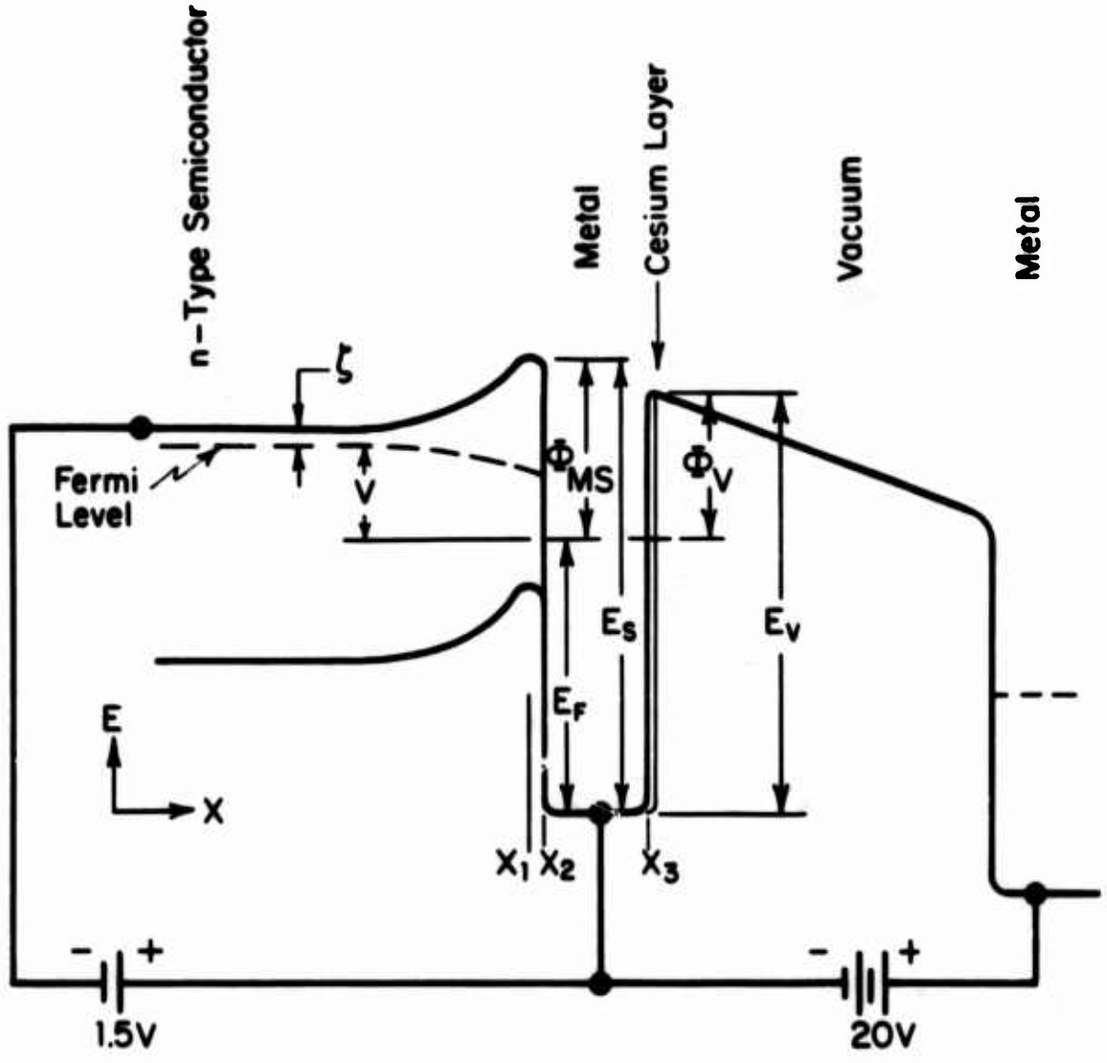

FIGURE III-1: The metal-semiconductor cathode under normal operating voltages, showing the variation of electron potential energy E as a function of distance x. Other symbols are explained in the text.

A theoretical understanding of the device on a quantitative basis was gained from a first-order calculation of the current J_A emitted into vacuum as a result of injection of electrons J_H over the barrier under forward bias. Several simplifying assumptions were incorporated into the physical model, as follows:

1. Maxwellian distribution of electron momenta at x_1 in the semiconductor.
2. Absence of electron-phonon and other scattering in the region between x_1 and x_2.
3. Isotropic elastic scattering into the positive half-sphere of momenta at the interface, at x_2.
4. A quantum-mechanical transmission coefficient of unity at x_2.
5. Absence of scattering in the metal.
6. Step-function dependence of escape probability at x_3 on the perpendicularly directed component of electron energy.
7. Sufficiently large anode voltage to ensure absence of space charge for $x > x_3$.

The combined effect of assumptions (2) and (5) in a practical structure using GaP or ZnS and Ag and with the Ag thickness less than 300Å is judged to result in less than a factor of five over-estimation of the true expected emission current, on the basis of scattering lengths reported in studies of the metal-base transistor.[4] Assumption (3) was judged to best represent

the nature of electron transport across a chemically prepared interface having a significant degree of irregularity on an atomic scale. Assumptions (1), (4), (6), and (7) do not entail any serious adverse possibilities.

The Maxwellian electron momentum distribution at x_1 is given by[5]

$$dn_1 = \frac{n_1}{(2\pi m^* kT)^{3/2}} \exp\left(-\frac{P^2}{2m^*kT}\right) d^3P, \qquad (1)$$

where n_1 is the number of electrons per cm^3 at the top of the Schottky barrier (at x_1 in Figure III-1), P is the crystal momentum of electrons at x_1, m^* is the electron effective mass, k is the Boltzmann constant, and T is the temperature.

Consider transmission of electrons from the semiconductor into the momentum-space element d^3p of the metal which is defined in spherical coordinates about the x-axis as

$$d^3p = 2\pi p^2 \sin\theta \, d\theta \, dp. \qquad (2)$$

By assumptions (2), (3), and (5), energy is conserved, as given by

$$\frac{p^2}{2m} = E_S + \frac{P^2}{2m^*}, \qquad (3)$$

where m is the effective mass and p the momentum of electrons in the metal. By assumption (3) the electrons are isotropically transferred from the momentum half-shell $2\pi P^2 dP$ into the half-shell $2\pi p^2 dp$. Hence the arrival rate dJ_{in} of electrons into d^3p is

$$dJ_{in} = \frac{2\pi q}{m^*} \frac{n_1}{(2\pi m^* kT)^{3/2}} \exp\left(-\frac{P^2}{2m^*kT}\right) P^3 dP \sin\theta \, d\theta \qquad (4)$$

where $\sin\theta \, d\theta$ is the fractional share of volume occupied by d^3p in the half-shell $2\pi p^2 dp$. The departure of electrons from d^3p occurs upon impingement on the metal-vacuum interface at x_3. At steady-state the departure and arrival rates dJ_{out} and dJ_{in} into d^3p are equal, and this defines the electron distribution function $f(p, \theta)$ in the metal:

$$\frac{2\pi q}{m^*} \frac{n_1}{(2\pi m^* kT)^{3/2}} \exp\left(-\frac{P^2}{2m^*kT}\right) P^3 dP \sin\theta \, d\theta =$$

$$\frac{qp}{m} \cos\theta \, f(p, \theta) \, 2\pi p^2 \sin\theta \, d\theta \, dp, \qquad (5)$$

where the left hand side equals dJ_{in} and the right hand side equals dJ_{out}. By assumption (6), the current J_A emitted into vacuum is given by integrating $q(p_x/m) f(p, \theta) d^3p$ over the region of momentum space defined by $p_x > \sqrt{2mE_v}$. This reduces to

$$J_A = q\bar{v}n_1 \exp(u_s) \int_{\text{Max}(u_s, u_v)}^{\infty} (u - u_s)\left(1 - \sqrt{\frac{u_v}{u}}\right) \exp(-u)\, du, \qquad (6)$$

where $\bar{v} = \sqrt{kT/2\pi m^*}$ and is seen to be the thermal velocity of electrons, u is energy measured in units of kT, $u_s = E_s/kT$, and $u_v = E_v/kT$. For large values of u_v and u_s, Eq. (6) may be evaluated approximately,

$$J_A = \begin{cases} q\bar{v}n_1 \left(\dfrac{2kT + \Delta\phi}{2E_v}\right) \exp\left(-\dfrac{\Delta\phi}{kT}\right), & \text{for } E_v > E_s \\ q\bar{v}n_1 \left(1 - \sqrt{\dfrac{E_v}{E_s}}\left(1 - \dfrac{kT}{E_s}\right)\right), & \text{for } E_v < E_s \end{cases} \qquad (7)$$

where $\Delta\phi = E_v - E_s$, the barrier height difference.

By integrating $q(P_x/m^*)\, dn_1$ over the momentum half-space, the electron current density J_H injected over the barrier is found to be

$$J_H = q\bar{v}n_1. \qquad (8)$$

The current transfer efficiency J_A/J_H may easily be obtained from Eqs. (7) and (8). In the case of $E_v > E_s$, which often described the experimental situation as will be seen later, the efficiency is a strong function of $\Delta\phi$ and T. For $E_v < E_s$, the efficiency is relatively independent of T and varies slowly as a function of $\Delta\phi$. As described by the integrand in Eq. (6), the emitted electrons have a narrow energy distribution several kT wide, centered slightly above the larger of the two energies E_s or E_v.

We note that the voltage applied to the Schottky barrier diode affects only n_1, and therefore J_A has the same voltage dependence as J_H. In an actual forward-biased Schottky barrier diode there may be other current transport processes in parallel with J_H, such as leakage at the perimeter or tunneling through the barrier. J_H is distinguished as the hot electron current due to its larger electron energy in the metal compared to that of the other currents. J_H has a voltage dependence close to exp (qV/kT), whereas the total diode current often varies as exp (qV/nkT) with $n > 1$, as will be described later in the section on barrier studies.

III. 3. Cathodic Emission Experiments

As is evident from the above theoretical discussion of the cold cathode, the requirement of $E_v < E_s$ and the avoidance of thick interfacial films and damage, which may lead to large leakage or scattering losses, are essential to a practical device. Studies concerned with lowering of the metal work function, necessary to achieve $E_v < E_s$ with available E_s values, pointed to the necessity of atomic cleanliness at the metal surface. For these reasons the last part of the device, consisting of the thin metal film and the cesium layer, was made in an ultrahigh vacuum chamber and measurements were done in situ.

III. 3. 1. Device and Holder Configuration

The choice of physical configuration of the experimental device was guided by desired simplicity of apparatus. The main design problem

here was how to electrically contact the thin metal film after its deposition in the ultrahigh vacuum chamber. The simplest and most satisfactory method and the one adopted for most of the experimental work is represented in Figures III-2 and III-3, which show the device configuration and the device holder, respectively.

Single-crystal semiconductor material having a doping level in the range of 10^{16} to 10^{18} electrons/cm^3 was used as the starting material, and was cut into dice and suitably sized by conventional sawing, lapping, and polishing methods. An ohmic contact was formed on one side and the die was attached to a Au- or Ni-plated Kovar header with an appropriate alloy preform. After suitable chemical surface preparation, the thick metal contact stripe was deposited on the other side by evaporation in vacuum. A thickness of 3000Å to 5000Å was found convenient for the contact stripe. In some cases, when possible, the ohmic contacting and die-attachment were done after the metal contact stripe was deposited. We note that the contact stripe is also a Schottky barrier diode but one which does not contribute to cathodic emission due to its great thickness; hence, its area should be small compared to that of the thin barrier. For accurate photoemission measurements near threshold, a large area was required for the thin metal film deposited later in the ultrahigh vacuum chamber. A nominal area of 8.4×10^{-3} cm^2 was employed for the thin metal film. Device fabrication details for the different materials investigated will be presented in a later section

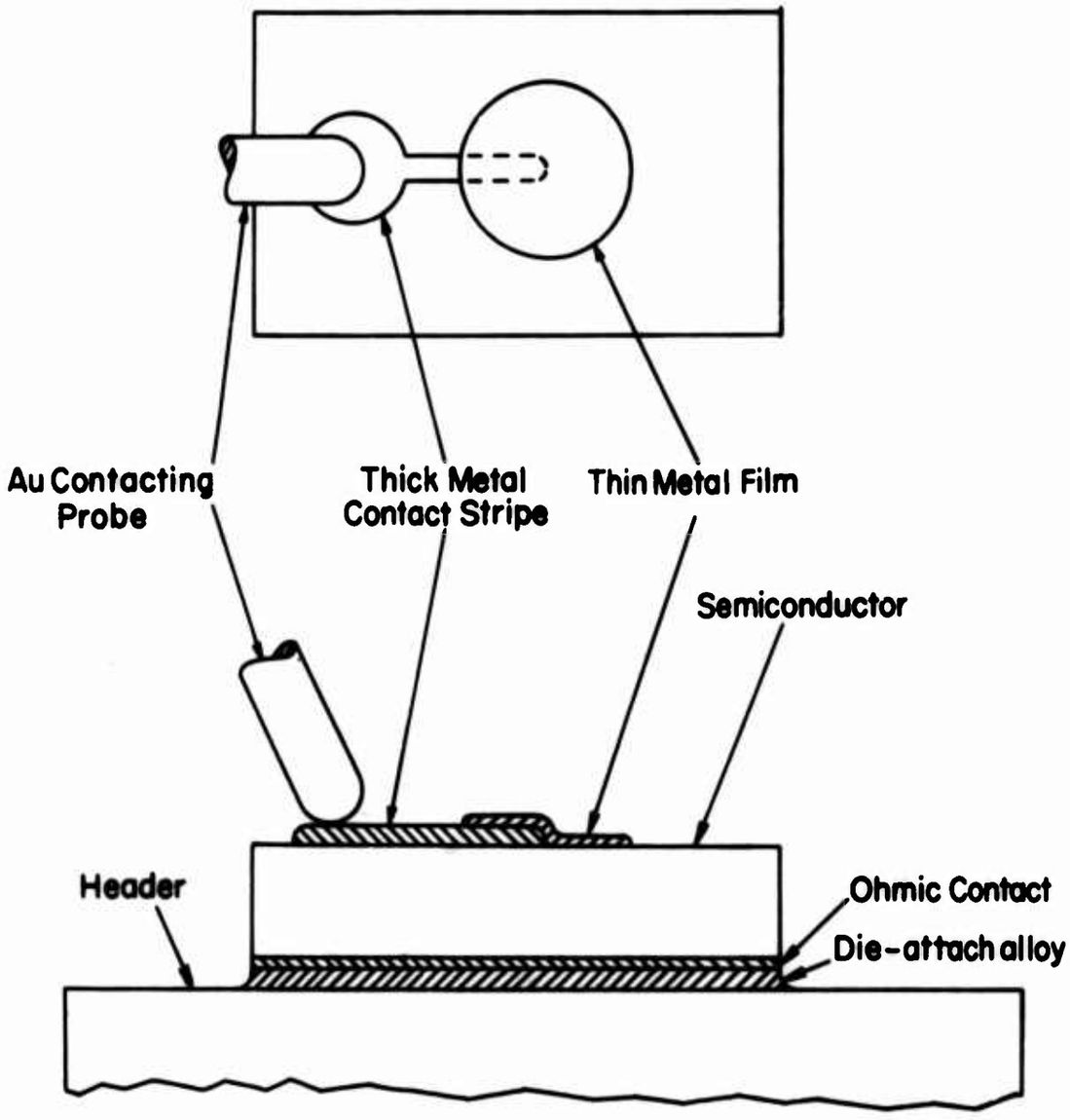

FIGURE III-2: Metal-Semiconductor diode structure employed in cathodic emission experiments.

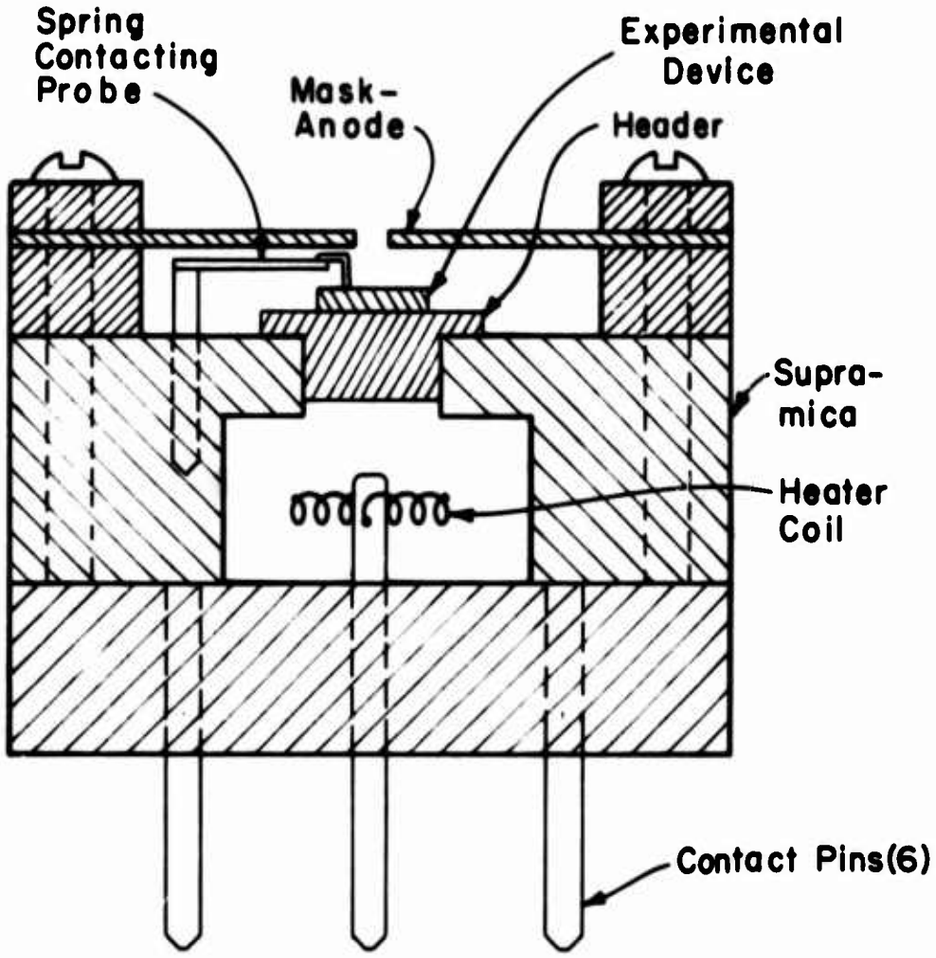

FIGURE III-3: Cold Cathode device holder.

on barrier studies. In the device holder, the mask-anode served both as an evaporation mask to form the thin metal film and as an anode to collect the cathodic emission current.

III. 3. 2. Vacuum Apparatus and Measurements

The ultrahigh vacuum chamber is depicted schematically in Figure III-4 and it was described in detail in Ref. (2). Baking at a temperature of 250°C was employed to attain a base pressure of 10^{-11} to 10^{-10} torr.

Typically the following measurements were performed to evalute a device. We used photoemission of electrons into vacuum to determine the value of the cesiated metal work function ϕ_V, and photoemission of electrons from the metal to the semiconductor to find the value of ϕ_{MS}. In this, the variation of photoemission current as a function of photon energy was analyzed according to Fowler's theory.[6] The diode characteristics including current-voltage and capacitance-voltage dependences were measured via the electrical feedthroughs, with the sample in the vacuum chamber.

The circuit of Figure III-5 was employed in determination of the cathodic emission properties including the variation of I_A as a function of I_D and V_A.

III. 3. 3. Status of Experimental Results

The experimental investigation of cathodic emission from suitable materials and the study of diode properties per se, to guide the choice of

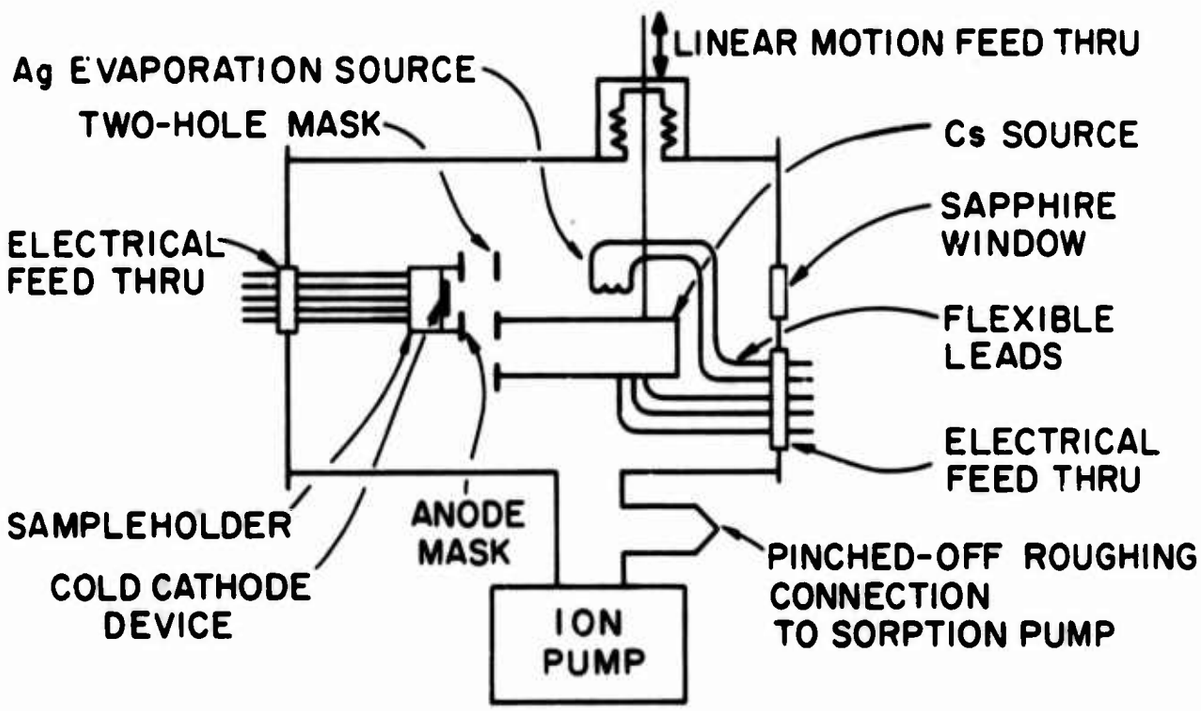

FIGURE III-4: Ultrahigh vacuum chamber.

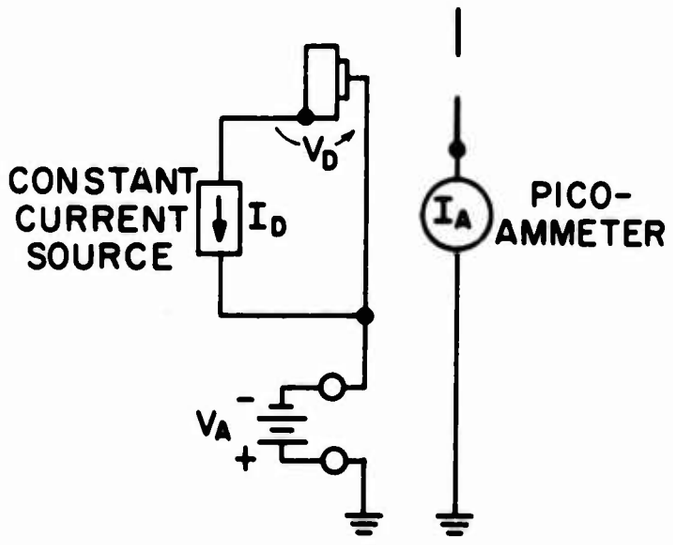

FIGURE III-5: Circuit for cathodic emission measurements

materials and processing techniques and the interpretation of cathodic emission results, were carried out in alternating chronological sequence during the course of the program. In this section the knowledge gained regarding cathodic emission is abstracted and presented separately from the diode studies.

Cathodic emission was observed from Ag barriers on GaP, ZnSe, and ZnS, using cesiation to lower the vacuum work function of Ag and chemical surface preparation of the semiconductor. These experiments were not ideal in the degree of control achieved over several variables, both in the vacuum conditions during Ag deposition and cesiation and in the interfacial cleanliness. Also, in most cases a time degradation of the cesiated Ag work function was observed. As a result, the experimental devices had a distribution of $\Delta\phi$ values, which was detrimental for evaluation of materials but which proved useful as a test of agreement with theory. Unadjusted values of current transfer efficiency I_A/I_D measured at a diode current of 10 mA to 50 mA (corresponding to a current density of 0.1 to 0.50 A/cm^2) for ten devices are presented in Figure III-6 as a function of $\Delta\phi$, together with the theoretical relationship. As the presence of non-hot-electron current was indicated in these devices, the hot electron current I_H was smaller than the total diode current I_D, and the values of I_A/I_H are higher than the indicated I_A/I_D values. For ZnSe-Ag device #9, the value of I_A/I_H was estimated to be 1.2×10^{-3} or larger, as described in Ref. (3). This

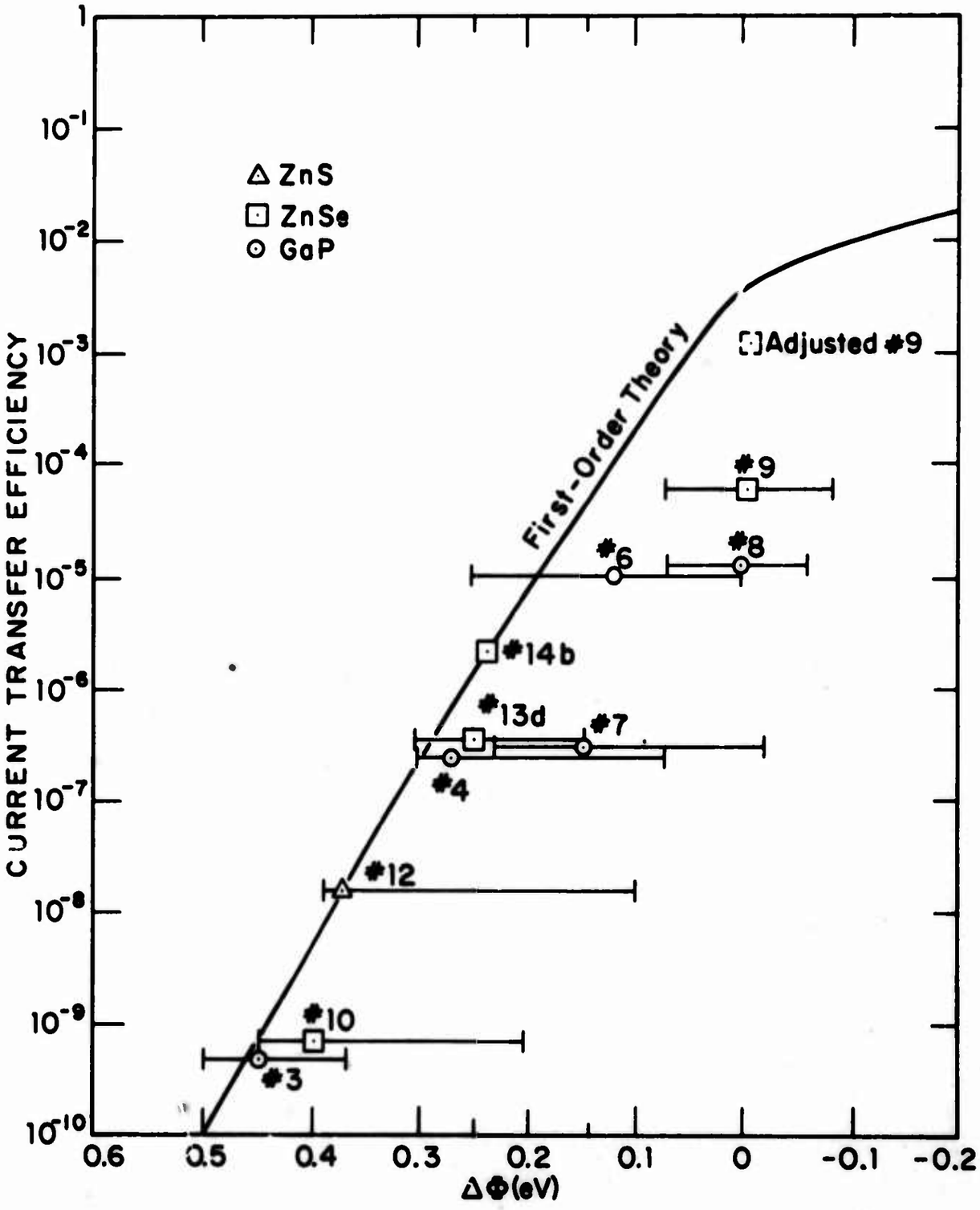

FIGURE III-6: Experimental and theoretical variation of current transfer efficiency as a function of barrier height difference $\Delta\phi$. Experimental points are for cesiated Ag-GaP, -ZnSe, and -ZnS devices. Solid curve is first-order theory, Eq. (7), for $E_v = 7.1$ eV, $E_s = 5.5 + \phi_{MS}$, and variable ϕ_{MS}.

device also had the largest unadjusted value of efficiency I_A/I_D observed in the course of this program, 6.2×10^{-5}. The wide error limits of $\Delta\phi$ shown in Figure III-6 were caused both by the time degradation of ϕ_V, occurring on a scale of minutes in the worst cases, and by the presence of two different apparent thresholds in the metal-semiconductor photoemission data of many devices, leading to an ambiguity in the value of ϕ_{MS}. The theoretical curve in Figure III-6 is a plot of Eq. (7) for variable E_s and constant E_v, the latter comprised of $\phi_V = 1.6$ eV and $E_F = 5.5$ eV.[7]

The I_A-V_D characteristics of all devices were close to exp (qV/kT) in agreement with theory, identifying I_A to be hot electron emission into vacuum as described in the theoretical section. Accurate barrier theory predicts J_H to vary as exp (qV/nkT) with n close to but slightly larger than 1. The observed values of n were between 1.05 and 1.10 with an accuracy of ±.05 for GaP-Ag, ZnSe-Ag, and ZnS-Ag devices. The I_A-V_D and I_D-V_D characteristics of ZnS-Ag device #12 are shown in Figure III-7, where the correction for the diode IR drop was obtained from a straight-line extrapolation of the semilogarithmic voltage dependence of I_D. Similar curves for GaP-Ag and ZnSe-Ag devices were presented in SR's Nos. 2 and 3. The noted agreement with theory is especially significant in that the value of n for I_D was substantially larger than 1 in more cases.

The dependence of I_A on V_A was well understood and did not exhibit any unusual features. Typical I_A-V_A characteristics for device #9,

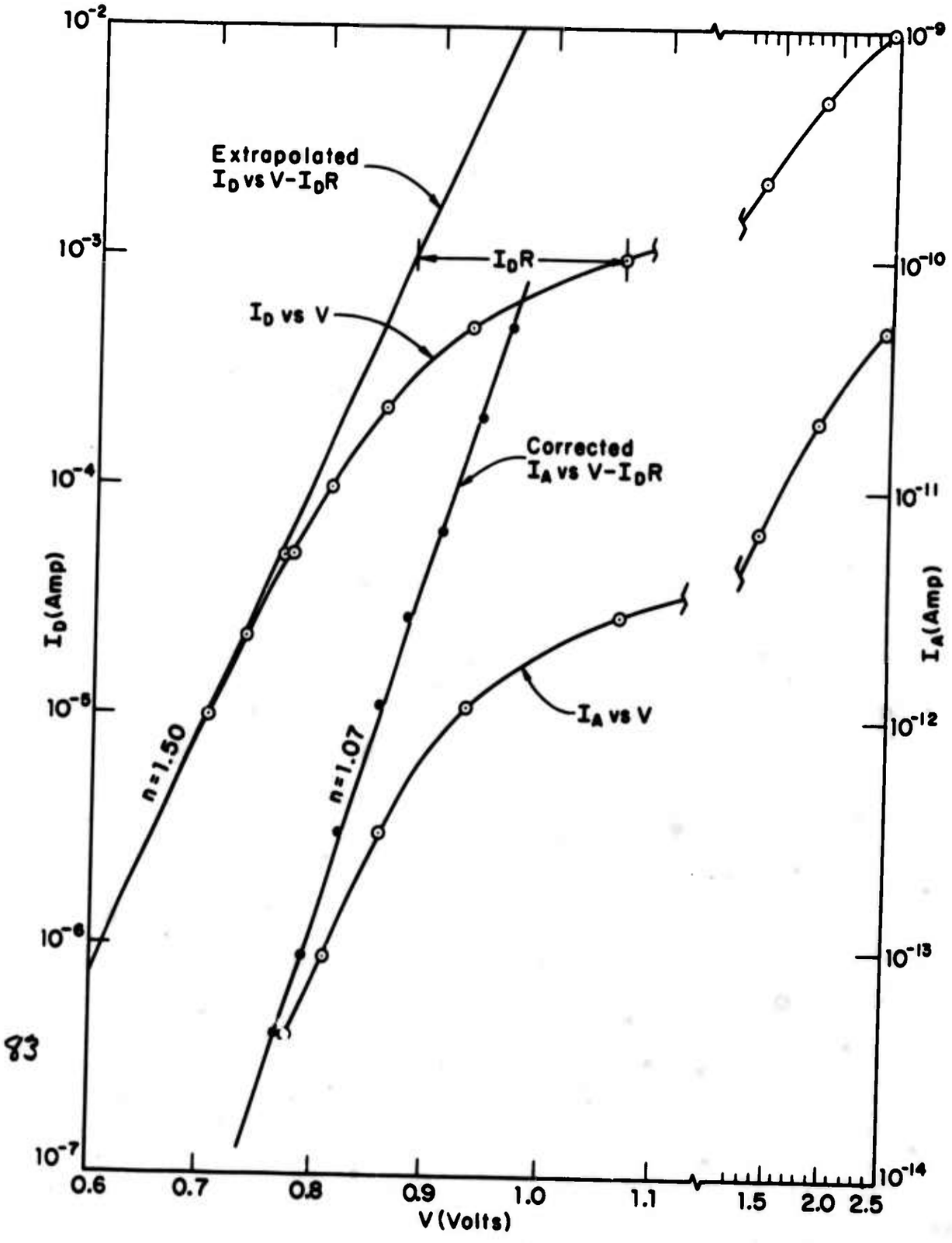

FIGURE III-7: Variation of anode current I_A and diode current I_D as a function of diode voltage V, before and after correction for diode IR drop. Ag-ZnS device #12.

for two different values of I_D, are shown in Figure III-8. The anode current cutoff at an anode voltage of about +10V was caused by a difference in the vacuum potentials of the cesiated Ag dot and the surrounding semiconductor surface in conjunction with our cathode-anode geometry (see Figures III-2 and III-3).

In summary, the experimentally observed efficiency - $\Delta\phi$ and I_A-V_D characteristics of cathodic emission from cesiated Ag barriers on GaP, ZnSe, and ZnS agree with theory and in our opinion prove the correctness of our cold cathode model, in its main features.

The barrier heights of all experimental devices were marginal and cathodic emission could not be observed in the high efficiency range where effects other than $\Delta\phi$ are significant. Hence, another important question, that of the ultimate efficiency achievable with presently known materials, was not conclusively answered yet. This question is related to the choice of materials for large ϕ_{MS} and to barrier preparation techniques, as described later.

Some conclusions regarding both the ultimate efficiency and the choice of materials nevertheless emerged from the emission results and the barrier work. The ϕ_{MS} values of ZnSe- and GaP-Ag barriers were judged fundamentally too low and marginal to be useful, but the data for ZnS barriers indicated no such limitation. ZnS appears clearly the most promising semiconductor for the cold cathode and superior to ZnSe, GaP, and probably also to SiC in view of recent literature results.[9] The one

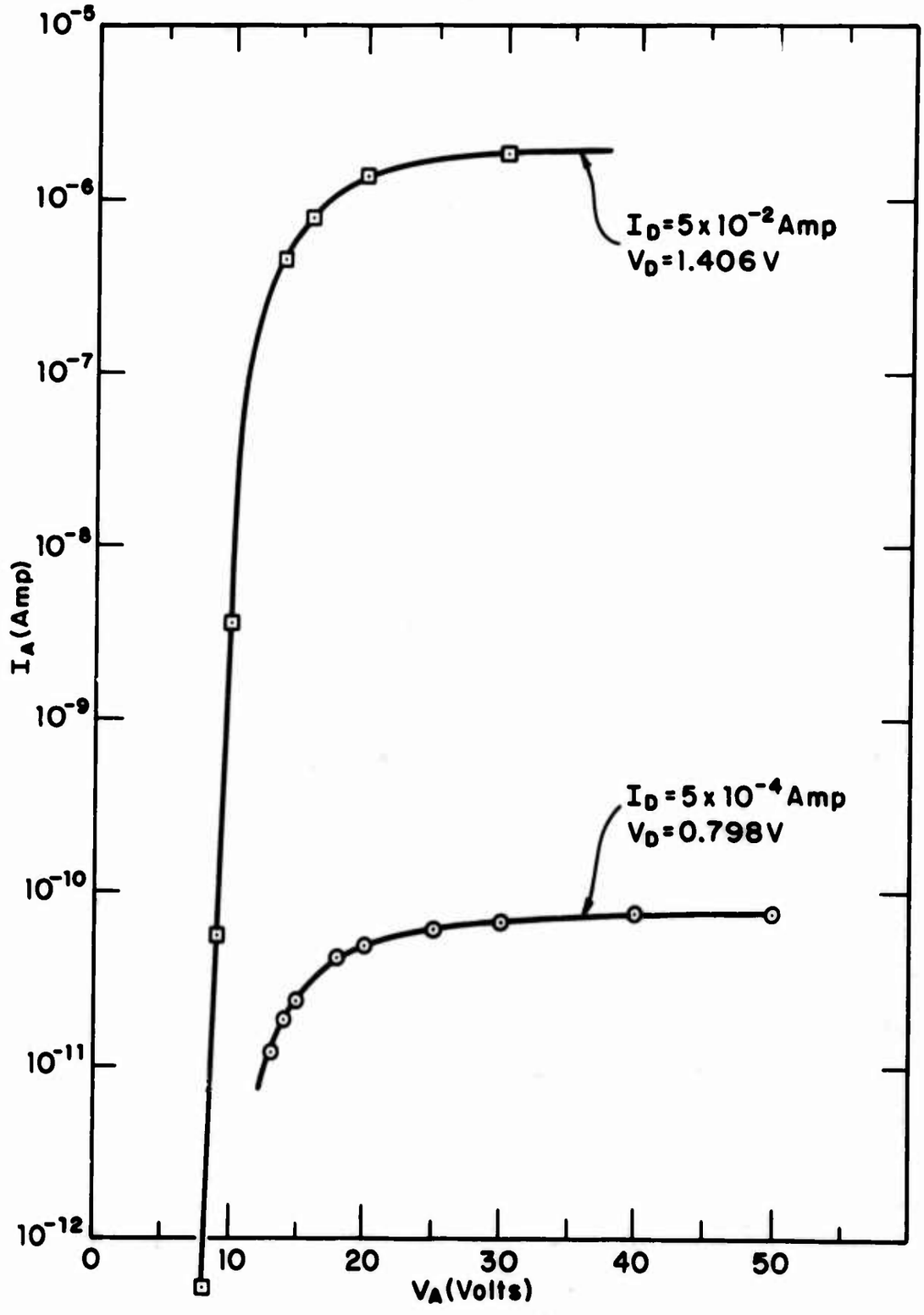

FIGURE III-8: Variation of anode current as a function of anode voltage, for two different diode driving conditions specified by the indicated values of I_D and V_D. Ag-ZnSe device #9.

measurement of cesiated ZnS-Ag, device #12 in Figure III-6, was not representative as ϕ_{MS} equaled 1.2 eV instead of 1.9 eV due to substantial processing and contamination problems unsolved at the time of measurement. In view of both theory and later barrier results, we estimated an achievable current transfer efficiency of over 2% for the cesiated Ag-ZnS cathode.

III.4. Barrier Studies

The investigation of the characteristics of metal-semiconductor diodes under this program had a three-fold purpose. The first of these was to survey and select a limited number of the most promising semiconductor and metal combinations; the second purpose was to find and optimize for each material combination the ohmic contacting and surface preparation procedures suitable for a practical experimental device, and the third, to determine the resulting barrier properties, for prediction and evaluation of cathodic emission performance.

According to previous discussion, the requirements for a satisfactory diode included a sufficiently large ϕ_{MS} to satisfy the inequality $\phi_{MS} < \phi_V$ (see Figure III-1) and a practically feasible technique to form the barrier, in a manner minimizing interfacial films, non-uniformity, and contamination. As cesiation of Cu or Ag gives a minimum ϕ_V value of about 1.5 eV, a value of ϕ_{MS} greater than 1.5 eV is needed.

Under a previous, related contract the selection of promising materials was narrowed to GaP, ZnSe, ZnS, and SiC, and preliminary

processing methods and barrier properties of GaP and ZnSe were tested.[8] The choice of the metal was limited to Au, Ag, and Cu in view of their long electron scattering lengths, Ag being the best in this respect.[4]

In the first three quarters of the present program, preliminary work on ZnS barriers was done and development and detailed characterization of GaP-Ag, ZnSe-Ag, and ZnS-Ag barrier diodes, of a practical configuration compatible with the cathodic emission apparatus and its vacuum bake-out procedure, were performed. (See Refs. 1, 2, and 3.) ZnS-Pt and -Ni diodes were also studied. SiC was not studied as planned and efforts were instead concentrated on ZnS. The reason for excluding SiC was that the recent results of Hagen[9] gave a value of ϕ_{MS} = 1.45 (±0.10) eV for Au, Ag, and Al barriers on 6H and 15R SiC for both vacuum cleaved and etched surfaces, and this value offered no advantage over GaP or ZnSe, which had already been judged to have unsatisfactorily low values of ϕ_{MS}.

In the last quarter, extensive investigation of ohmic contacts and metal barriers on ZnS was made to solve some of the problems encountered with this material.

III.4.1. Measurement Techniques and Theory

Electrical and optical measurements were employed to evaluate the physical and electronic properties of the diodes. All of these techniques have been amply discussed in literature, with the exception of the use of ellipsometry in the application described below, which we believe to be original in this laboratory.

Ellipsometry was used to monitor residual surface film thickness in the 10Å - 100Å range of values, as a guide in developing the best chemical surface preparation process for each semiconductor studied. The absolute value of film thickness measured by ellipsometry depends on a knowledge of the index of refraction of the film, and for films thinner than 100Å the index of refraction cannot be determined very accurately.[10] Hence, the absolute thickness values were uncertain by a factor of two, but the relative values were accurate to within ±0.2Å. The properties of the barriers thus developed were close to those of idealized, interfacial-film-free Schottky barriers.

The structure of a thin 300Å Ag film, deposited by evaporation in ultra-high vacuum on chemically prepared GaP, was examined by electron microscopy and found to be continuous and smooth at least to a scale of 100Å. This was believed to be representative of the morphology of all of our thin Ag films, including the ones deposited on ZnSe and ZnS.

The diodes were characterized by the three standard measurements of I vs. V, C vs. V, and I_p vs. $h\nu$, where I and V refer to the barrier diode d.c. current and voltage; C refers to the differential capacitance of the diode, usually determined using a frequency of 10^6 Hz, and sometimes checked also at 10^3 Hz and 10^4 Hz; and I_p refers to the electron emission current from the metal to the semiconductor under excitation by monochromatic light of photon energy $h\nu$.

For interpretation of the measurements, the Schottky barrier was assumed to be described by emission theory,[11, 12] which is valid if the electron mean free path l_s exceeds the distance Δx in which the potential changes by one kT/q near the top of the potential energy maximum. The presence of an interfacial film having a thickness on the order of 10Å is allowed in this model. The current density J under a forward applied voltage V is given by

$$J = q\bar{v}N_c \exp\left(-\frac{q\phi_I}{kT}\right)\left(\exp\left(\frac{qV}{nkT}\right) - 1\right), \qquad (9)$$

where $\bar{v}$ is the thermal velocity as defined before, N_c is the conduction-band density of states, ϕ_I is the barrier height, and n is a parameter having a value somewhat greater than 1. In the emission theory, the value of n is dependent upon the interfacial layer thickness d and equals 1 if d approaches zero. We note that the diffusion theory of the Schottky barrier also gives a parameter n having a value typically between 1 and 1.2, even without the presence of an interfacial layer.[13, 14] The diffusion theory is appropriate if $l_s < \Delta x$, which is realized if the semiconductor doping density is small. Eq. (9) was employed to determine the value of ϕ_I, and $q\bar{v}N_c$ was taken equal to 10^7 A/cm^2 for GaP, ZnSe and ZnS. We note that a change in $q\bar{v}N_c$ of a factor of 10 leads to a change of only 0.060 eV in the deduced value of ϕ_I.

The differential capacitance at a d.c. bias V is given by

$$\frac{1}{C^2} = \frac{2}{\varepsilon A^2 qN} \left(\phi_C - \frac{kT}{q} - \zeta + \varkappa + V\right), \tag{10}$$

where A is the diode area; ζ is the semiconductor Fermi level measured from the conduction band edge positive in the bandgap; and $\varkappa$ is a small correction term due to the interfacial layer and equals zero in its absence.[15, 16] Here again the diffusion theory with no interfacial layer leads to the same result if $\varkappa$ is taken equal to zero.

The short circuit photoemission current under monochromatic excitation is given according to Fowler[6] and Dubridge[17] by

$$I_p = cI_{exc} KT^2 \frac{f\left(\frac{h\nu - \phi_p}{kT}\right)}{\sqrt{E_s - h\nu}}, \tag{11}$$

where c is the fraction of incident light absorbed in the metal within about a scattering length of the interface, I_{exc}/q is the excitation flux in photons/sec, K is a constant independent of T and $h\nu$, T is the temperature, E_s was defined in Figure III-1, ϕ_p is the barrier height, and the Fowler function f(z) is given by

$$f(z) = \begin{cases} e^z - \frac{e^{2z}}{2^2} + \frac{e^{3z}}{3^2} - \ldots, & z \leq 0 \\ \frac{z^2}{2} + \frac{\pi^2}{6} - \left(e^{-z} - \frac{e^{-2z}}{2^2} + \frac{e^{-3z}}{3^2} - \ldots\right), & z \geq 0. \end{cases} \tag{12}$$

We note that c depends on the excitation and barrier geometry, and its value could be usually estimated to a 50% accuracy. The small $h\nu$ dependence of c was ignored here.

We note that space-charge recombination and tunneling currents were neglected and a uniform barrier was assumed in deriving these equations. In actual barriers, the interface is non-uniform in its physical properties and recombination currents, low-barrier height regions, and tunneling are known to occur either at the perimeter or at physical or chemical defects elsewhere in the interface.[13, 18] Thick interfacial layers partially or completely covering the barrier area also invalidate the equations. In the better experimental barriers, these non-idealities appeared as low level leakage currents having $n > 1.10$, as a value of ϕ_C slightly larger than ϕ_I and ϕ_p, and as an excess response "tail" at low $h\nu$ values in the photoresponse curve. In determining ϕ_I from the I-V curves having a large n-value, an excess leakage current was assumed present, and a fictitious I-V curve having $n = 1.10$ and equaling the measured current at a certain voltage was used to find ϕ_I. The value of this voltage was chosen to correspond to a current density on the order of 0.1 A/cm^2. In interpreting the C-V data, we did not estimate $\varkappa$ but arbitrarily let $kT/q + \zeta - \varkappa = 0$.

III.4.2. GaP-Ag Diode

Single-crystal vapor-grown GaP having a doping density of 10^{17} cm^{-3} and melt-grown GaP having 10^{17} to 3×10^{18} cm^{-3} doping were

used. An ohmic contact containing Sn as the n^+ dopant was deposited by evaporation, alloyed at a temperature of about 450°C, and attached to a header with Au-Sn or Au-Ge (see Figure III-2). The chemical surface preparation sequence consisted of immersion for 30 sec. in an etching solution of composition $3H_2SO_4:1H_2O:1H_2O_2$ (designated as Etch A) at 100°C, followed by evaporation of a 500Å thick protective Ag layer, and subsequent removal of this layer and some GaP by a 10 sec. rinse with Etch A at 25°C, followed by a thorough rinse with doubly distilled H_2O. This procedure gave an ellipsometrically determined surface film thickness in the range of 14 - 19Å. Typical diodes using the vapor grown GaP were characterized by n-value of 1.10 and ϕ_I, ϕ_C, and ϕ_p values of 1.48 eV in close agreement. The photoresponse had a lower-hν tail which could be fitted by $\phi_p = 1.37$. Diodes on the melt grown material exhibited a variation of n values in the range 1.10 to 1.7 and barrier heights in the range 1.21 - 1.45 eV, indicating defects or material non-uniformity.

III.4.3. ZnSe-Ag Diode

Al-doped melt grown ZnSe was used and converted to low resistivity by firing in liquid Zn at 900°C for 3 to 7 days. Typically the electron concentration was 3×10^{16} cm^{-3} and the mobility, 400 cm^2/volt-sec for this material. To form an ohmic contact to a ZnSe die, it was etched in a solution of composition $1K_2Cr_2O_7:10H_2O:6H_2SO_4$ (designated as DCS etch) at 80°C for 45 seconds, rinsed in water, soaked in a warm solution of KCN

in water for 10 minutes, and rinsed profusely in water. A 50% Ga-In alloy was applied to one face of the die and heated at 420°C for 5 minutes in an H_2 atmosphere. After removal of excess Ga-In from the die, it was then placed on an indium preform on a Ni plated Kovar header and attached by heating again at 420°C for 5 minutes in H_2. Prior to this, the indium preform had been wetted to the header surface by heating at 420°C for 5 minutes, in H_2. This technique was satisfactory but contained some deficiencies, notably the low mechanical strength of the die-header bond and the somewhat large contact resistance value. Contact resistances on the order of 0.1Ω -cm^2 were obtained.

The chemical surface preparation procedure consisted of immersion in DCS etch at 80°C for 45 sec, rinsing in water, soaking in a warm KCN solution for 10 min, and rinsing again profusely with doubly distilled water. Typical d-values of 15Å as measured by ellipsometry were achieved.

Several ZnSe-Ag diodes formed by evaporation of Ag on the ZnSe surface prepared in the above manner were characterized by n values of 1.18 and barrier heights of 1.38 - 1.67 eV, with ϕ_I, ϕ_C and ϕ_p agreeing within about 0.10 eV. Where a low-$h\nu$ photoresponse tail was significant, the value of ϕ_I agreed better with the lower ϕ_p value, and ϕ_C, with the larger. The ZnSe-Ag diodes were observed to degrade when heated for several hours at a temperature of 250°C or higher, the degradation consisting of a large increase of leakage current and a decrease of the value

of ϕ_I. This degradation phenomenon was found to be similar to that encountered in ZnS as elaborated later.

III. 4. 4. Barrier Heights and Ohmic Contacting Studies on ZnS

Greater surface preparation and ohmic contacting problems were encountered with ZnS than with the other semiconductors studied. A variable barrier height degradation phenomenon associated with heating at a temperature of 250°C was seen for ZnS-metal barriers, as well as for ZnSe-metal barriers, which tended to confuse the results of the initial experimental work. The ZnS-Ag barrier diode employed as cathodic emission device #12, described in the cathodic emission section, belonged among the earlier devices and was not representative of the best latest results of ZnS-metal barrier studies.

III. 4. 4. 1. ZnS-Metal Diodes

ZnS-metal diodes were made using Al-doped melt-grown ZnS, rendered conducting by firing in liquid Zn at 900°C for 3 to 7 days, after which the material had a carrier concentration in the range 0.3 - 2 x 10^{17} cm^{-3} and a mobility of 60 - 100 cm^2/volt-sec. Ohmic contacts were formed using a Ga-In alloy as described later. The metals were deposited by evaporation in vacuum on a chemically prepared ZnS surface.

The chemical surface preparation procedure consisted of manual etch-polishing in a 0.5% Br-methanol solution on a fiber pad, with the

sample held by a teflon fixture. This was followed by rinsing first in methanol, then in water, and drying in a N_2 gas stream. By ellipsometry, a value of d of 18 - 24Å was initially obtained. With development of an operator "feel" and optimum timing of the rinses, a d-value of 10Å or smaller was later achieved.

The n-values of the I-V characteristics of ZnS-Ag diodes having the initial type of chemically prepared interface were generally in the range 1.2 - 1.6 and the barrier height values of diodes having an area of 0.2 - 1 x 10^{-2} cm^2 were in the range 1.7 - 1.9 eV. Diodes made at this time were also subject to a degradation of varied severity upon heating, as described in detail later.

Using the improved chemically prepared surface characterized by d = 10Å, an Al or Au overlay type of ohmic contact described later, and a small diode area of 10^{-4} cm^2, ZnS-Ag, -Au, and -Cu barriers were made that have almost ideal n-values and are almost unaffected by heating. The I-V and C-V characteristics of these diodes are presented in Figures III-9 through III-14. Relevant parameters extracted from the curves are shown in Table III-1. In interpreting the data, Eqs. (9) and (10) were employed, an n-value of 1.10 was assumed after correction for the leakage current, and $kT/q + \zeta - \chi$ was assumed equal to zero. The alternative assumption of $\chi = 0$ would give ϕ_C values larger by 0.12 eV than those shown in Table III-1 for these ZnS samples. The I-V and C-V curves typify an average diode on at least two different ZnS samples. Among different diodes on the same

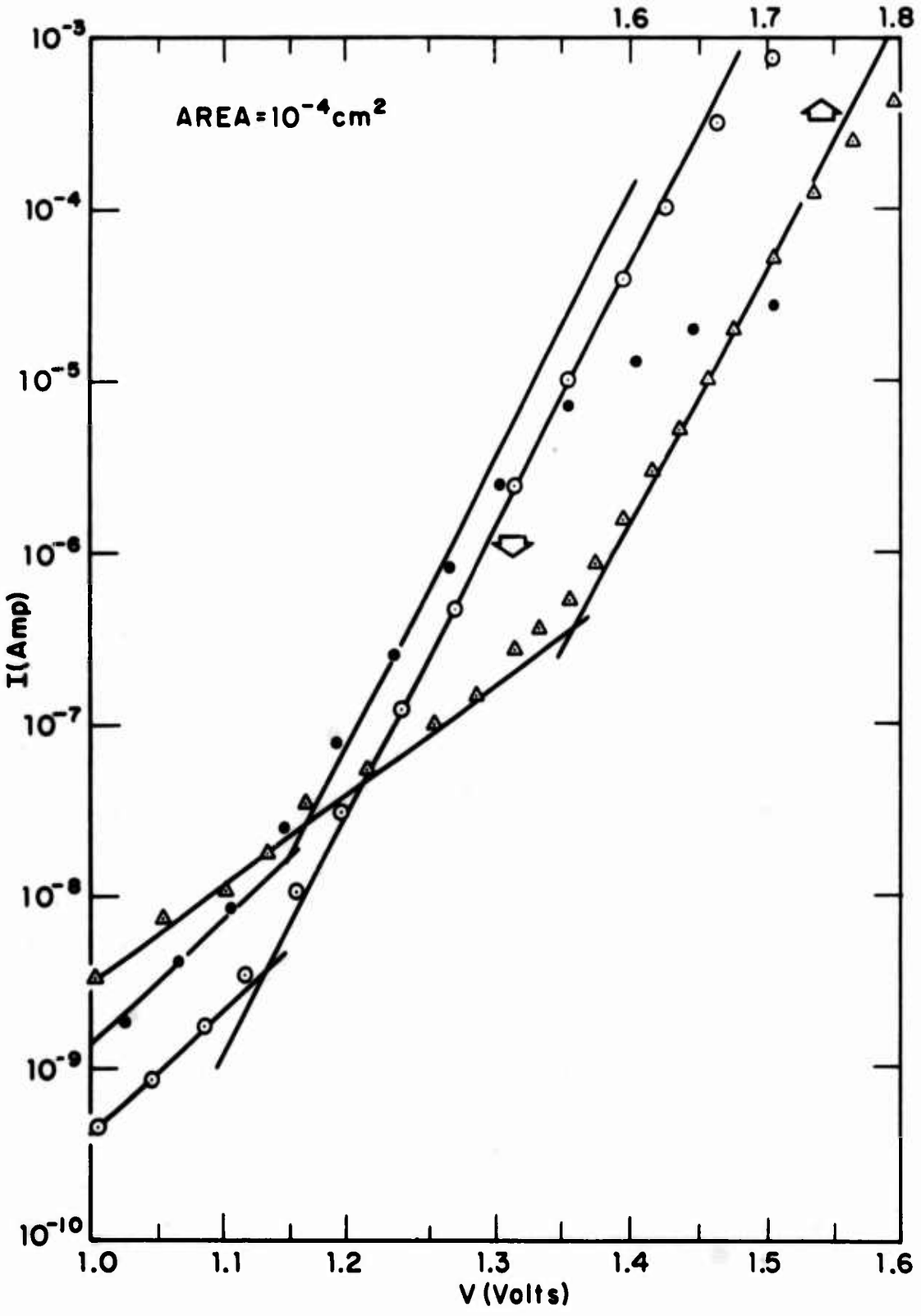

FIGURE III-9: I-V characteristic of ZnS-Ag diodes. △ - diode a, ⊙ - diode b, ● - diode b after heating 23.5 hrs. at 251°C. Use upper margin voltage scale for diode a, lower for diode b.

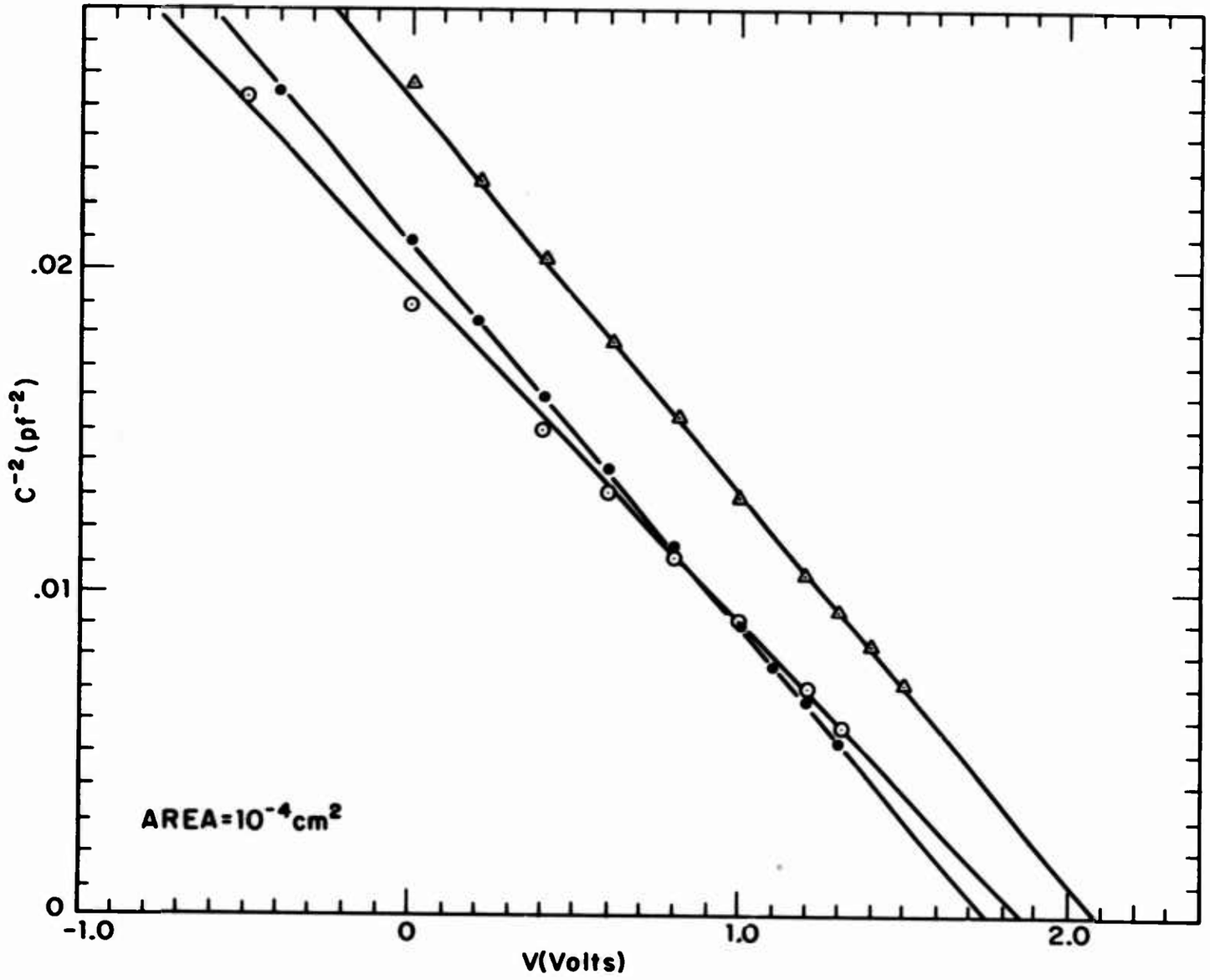

FIGURE III-10: C^{-2}-V characteristic of ZnS-Ag diodes. △ - diode a, ⊙ - diode b, ● - diode b after heating.

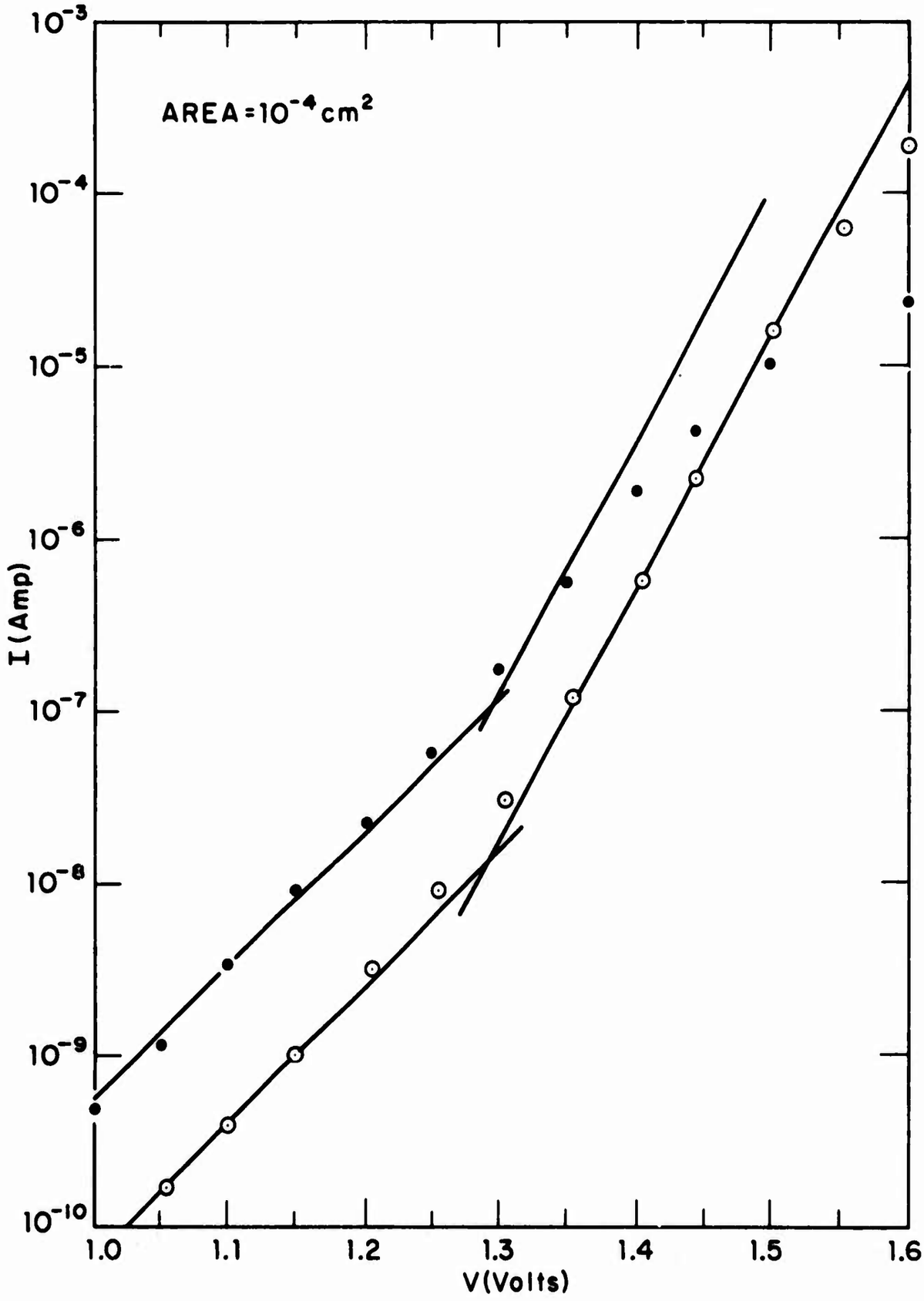

FIGURE III-11: I-V characteristics of ZnS-Au diode. ⊙ - before, ● - after heating 15.5 hrs. at 264°C.

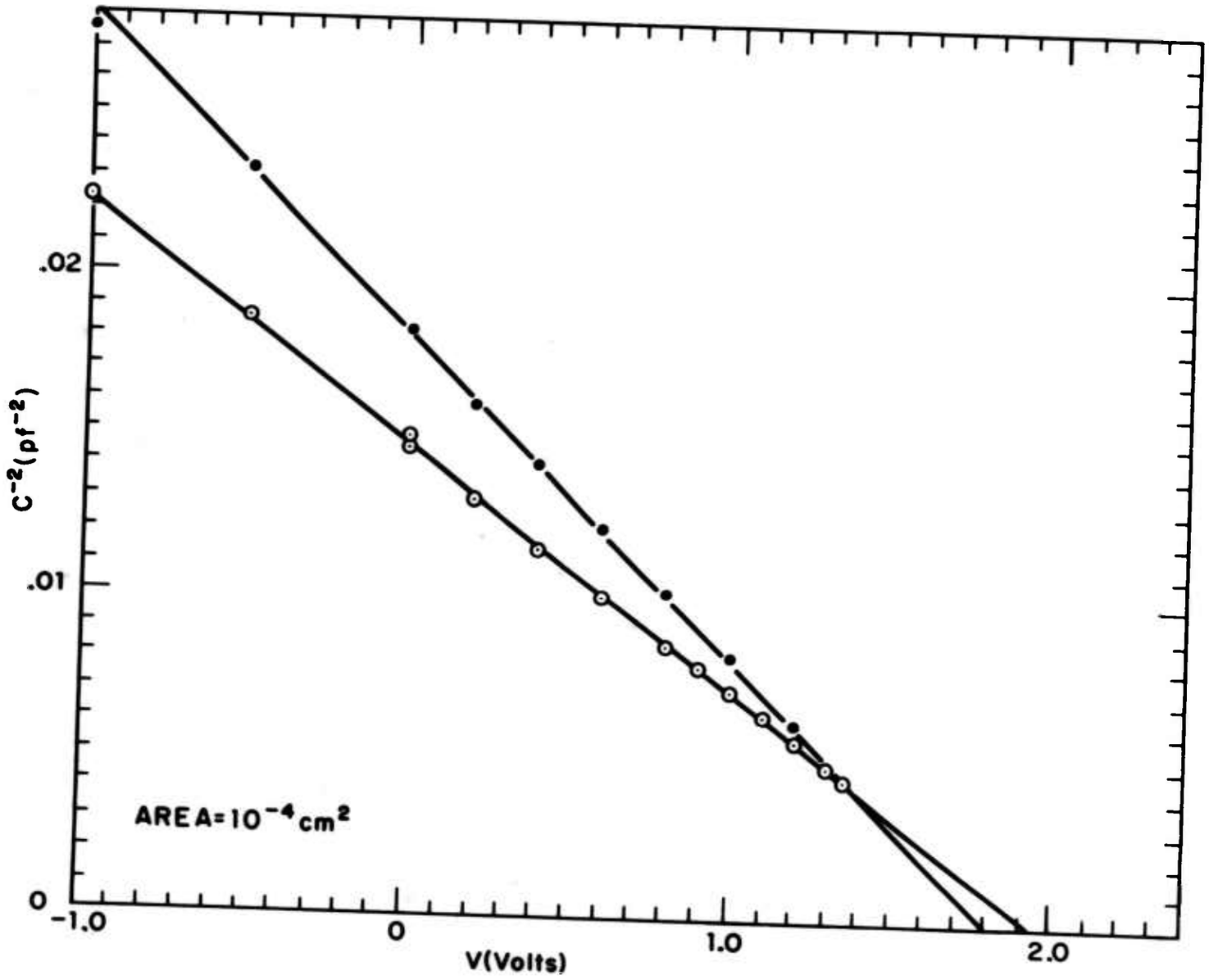

FIGURE III-12: C^{-2}-V characteristics of ZnS-Au diode. ⊙ - before, ● - after heating.

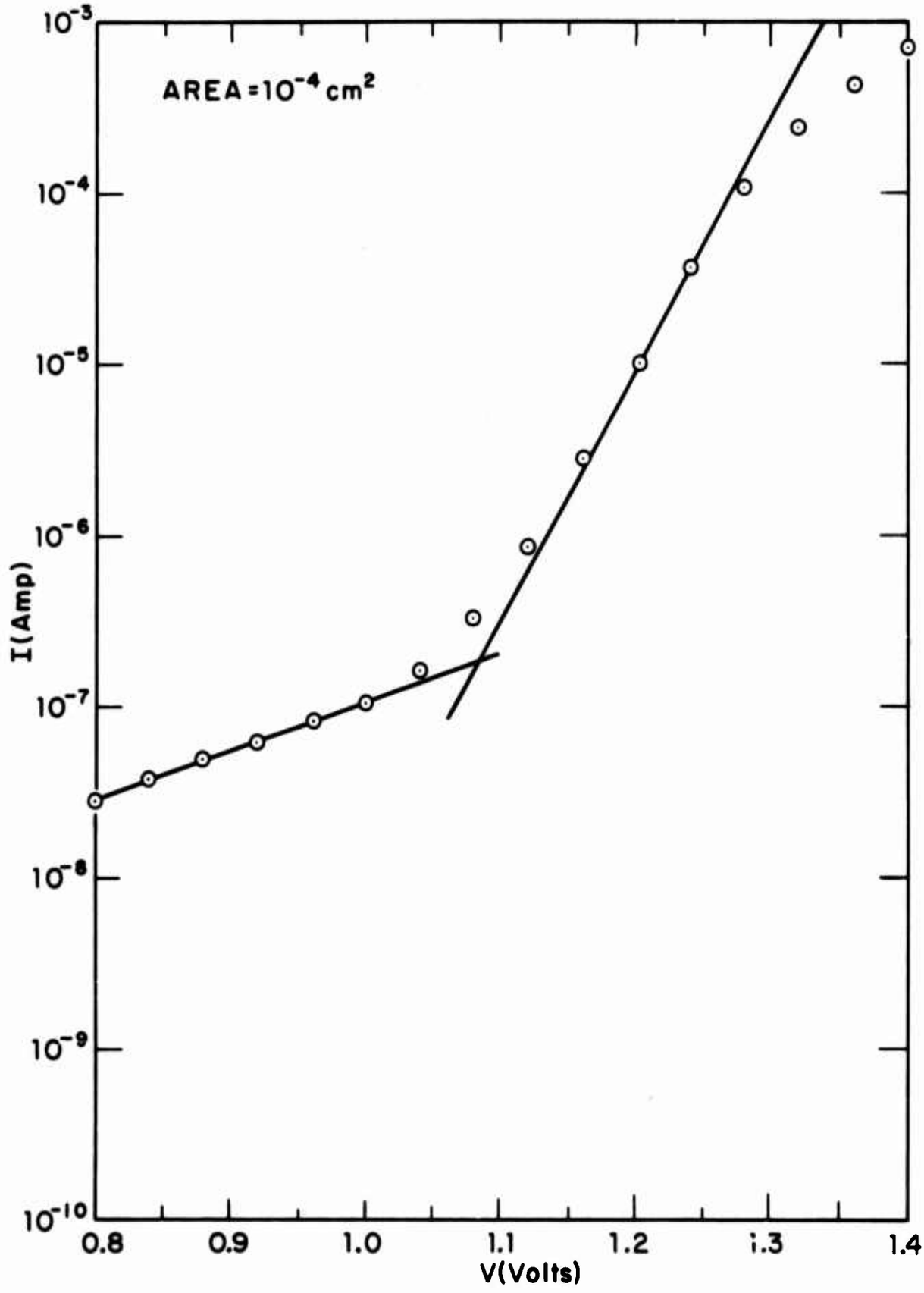

FIGURE III-13: I-V characteristic of ZnS-Cu diode.

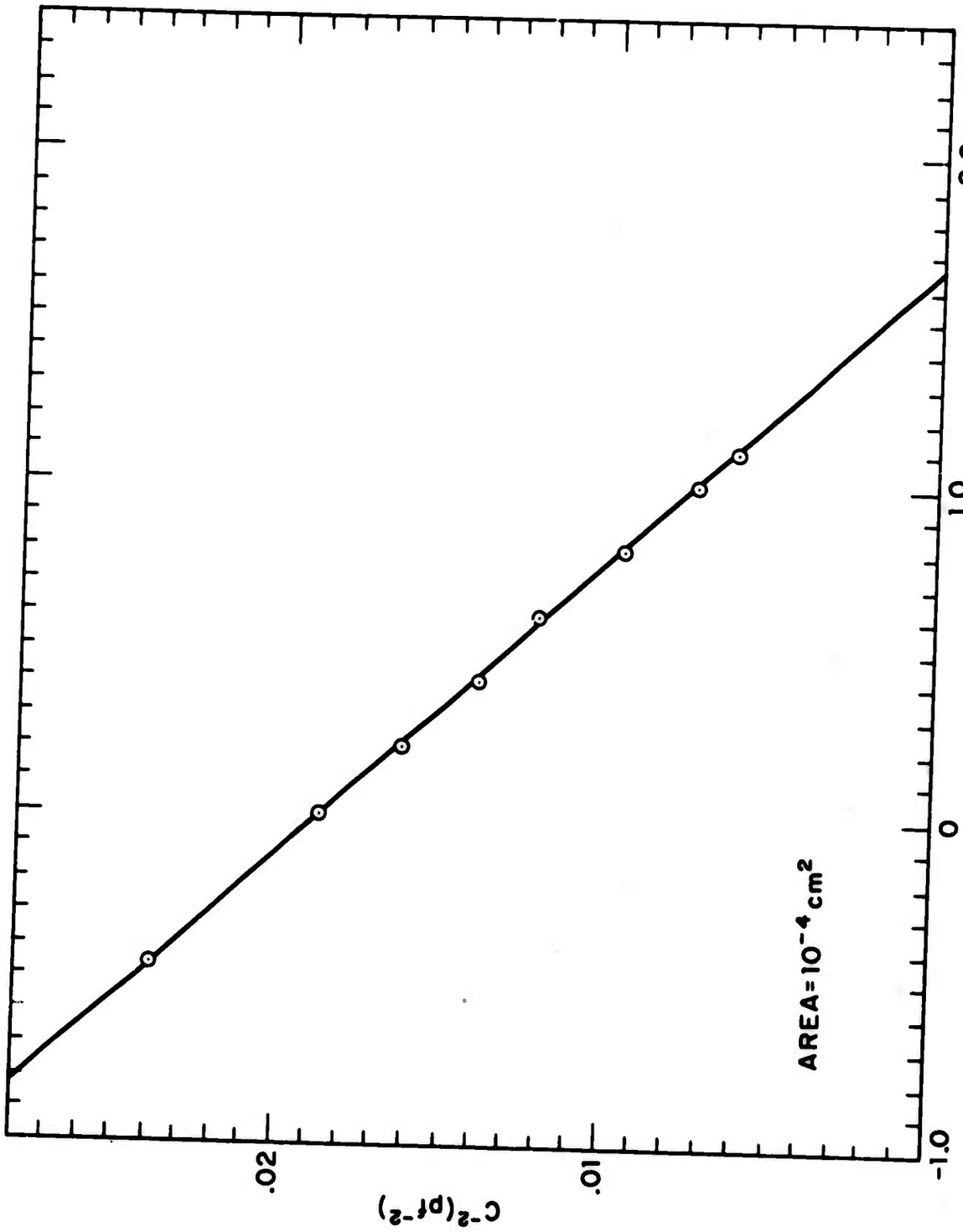

FIGURE III-14: C^{-2} -V characteristic of ZnS-Cu diode.

TABLE III-1

Properties of ZnS-Metal Schottky Barrier Diodes
(Chemically Prepared ZnS Surface)

Barrier	n	R(Ω)	ϕ_I (eV)	ϕ_C (eV)
Ag-ZnS-a	1.14	58	1.980	2.07
Ag-ZnS-b	1.10	36	1.701	1.85
Ag-ZnS-b after heating		7000	1.689	1.75
Au-ZnS	1.16	125	1.728	1.93
Au-ZnS after heating		5500	1.678	1.80
Cu-ZnS	1.14	82	1.562	1.66

sample, the variation of the voltage value for a constant current in the small n region was 60 - 70 mV. A larger number of ZnS-Ag than ZnS-Au and -Cu samples were made and some variation of barrier properties was found among the ZnS-Ag samples, but not among diodes on one sample. The two sets of curves shown in Figures III-9 and III-10 typify the extremes observed. All the C^{-2}-V curves showed a slight curvature concave downwards, the average value of $|d(C^{-2})/dV|$ being about 25% smaller at -10V than at +0.5V. Photoresponse was not measured for any diode. The Au and Ag diodes were heated at about 250°C for 15.5 and 23.5 hours, respectively, and were not markedly affected by the heating.

The barrier height value of ZnS-Ag diodes employing the best preparation technique is seen to be 1.7 - 2.0 eV. The ultimate capability of ZnS-Ag barriers in the cold cathode application appears good and superior to that of the other material combinations studied. On the basis of these results, we predict an efficiency of over 2% for the cesiated Ag-ZnS cold cathode.

III.4.4.2. Degradation Problem

The diodes need to withstand heating at a temperature of about 250°C to allow vacuum chamber baking in the cathodic emission experiment. A lowering of the barrier height value and an increase of leakage current was observed for ZnS-metal diodes upon heating at temperatures as low as 250°C. This degradation did not occur for all barriers nor always to the same degree.

Pt barriers seemed unaffected, Ni barriers responded inconsistently, and Ag barriers seemed consistently degraded at initial stages of ZnS-metal barrier studies but very little later.

Several experiments were performed in which the chemically prepared ZnS surface was heated in vacuum prior to metal barrier deposition. A sample having an ohmic contact and a Pt control diode was heated at 250°C for 4 hours under a vacuum of 2×10^{-7} torr in an oil diffusion-pumped system with a good liquid-N_2 cold trap. An Ag dot of 10^{-2} cm area was deposited by evaporation after cooling to room temperature. The I-V and C-V characteristics were measured in air immediately after removal from the vacuum chamber. The results, presented in Table III-2, show a lower-than-normal value of barrier height for the ZnS-Ag diode. Data on two other samples having Ni control diodes were ambiguous due to large initial values of series resistance ($1 - 2 \times 10^3$ ohms) but approximately confirmed the first result. Another ZnS device having a Pt diode as a contact stripe and serving as cathodic emission device #12 was heated in ultrahigh vacuum for 6 hours at 250°C and a 300Å thick Ag diode was deposited contacting the Pt stripe. This barrier was also lower than normal as seen in Table III-3 and degraded further during the cathodic emission experiment. The influences of time alone, of barrier heating due to current conduction, or possibly of cesium, were not separately distinguishable in this experiment. The barrier characteristics were anomalous in that the ϕ_C values deduced from measurements at 10^3 Hz and 10^6 Hz did not agree.

TABLE III-2

Heating of Chemically Prepared ZnS Surface in Vacuum
Followed by Formation of ZnS-Ag Barrier Diode

	Before Heating	After Heating	
	Pt	Pt	Ag
n	1.31	-------	(1.4)
$R_s(\Omega)$	8	150	140
$N(cm^{-3})$	1.6×10^{-7}	1.4×10^{17}	1.4×10^{17}
ϕ_I(eV) @ 1.3 V	1.63	(1.63)	
ϕ_I(eV) @ 1.1 V			1.53
ϕ_C(eV) @ 10^6 Hz	1.76	1.76	1.64

TABLE III-3

Heating of Chemically Prepared ZnS Surface
Followed by Formation of ZnS-Ag Barrier Diode
(Device #12)

	Before	After Heating		At Conclusion of Experiment
	Pt	Pt	Pt & Ag	Pt & Ag
n	(1.22)	-------	(1.18)	(1.17)
$R_S(\Omega)$	120	170	192	250
$N(cm^{-3})$	1.9×10^{17}	1.9×10^{17}	1.6×10^{17}	1.6×10^{17}
ϕ_I(eV)	1.64	1.64	1.48	1.27
ϕ_C(eV) @ 10^6 Hz	1.80	1.80	2.35	2.03
ϕ_C(eV) @ 10^3 Hz				1.30
ϕ_p(eV)				1.20

Whether Ga-In from the ohmic contact was responsible as a contaminant was tested by photoemission measurements on a series of samples, having a varying heating and likelihood of Ga-In contamination. Diodes Nos. 1 - 4 had standard heat-treated Ga-In ohmic contacts following the formation of which Ag was evaporated after briefly rinsing the top surface in 1% Br in methanol; for Nos. 5 and 6 the Ag barriers were deposited first and a very poor electrical contact was provided by unheated Ga-In on the back side; and the ohmic contact of No. 7, made in the standard manner, was covered by a glass disc secured with black wax and the front surface was cleaned by removing a layer of material by etch-polishing. The sample was soaked in trichloroethylene to remove the wax, rinsed in methanol, attached with indium to a header by heating for a few seconds in air, and then the Ag pads were evaporated. The area of these barriers was 10^{-2} cm^2. All photoemission curves were well described as the sum response of two emission processes, each following Eq. (11), one having a ϕ_p value of 1.8 - 2.0 eV and a K value typical of Ag-ZnS diodes, and the other having lower values of ϕ_p and K and the appearance of a low $h\nu$ "tail." As an example, the curve for sample No. 1 is given in Figure III-15. These data are presented in Table III-4. Diodes Nos. 1 and 4 were much poorer than the rest as they exhibited the greatest low-$h\nu$ response, below 1.7 eV, and diode No. 2 was almost as good. Diodes Nos. 5 and 6 were the best in having the least low-$h\nu$ response. Under microscopic observation at 450X magnification, GaIn

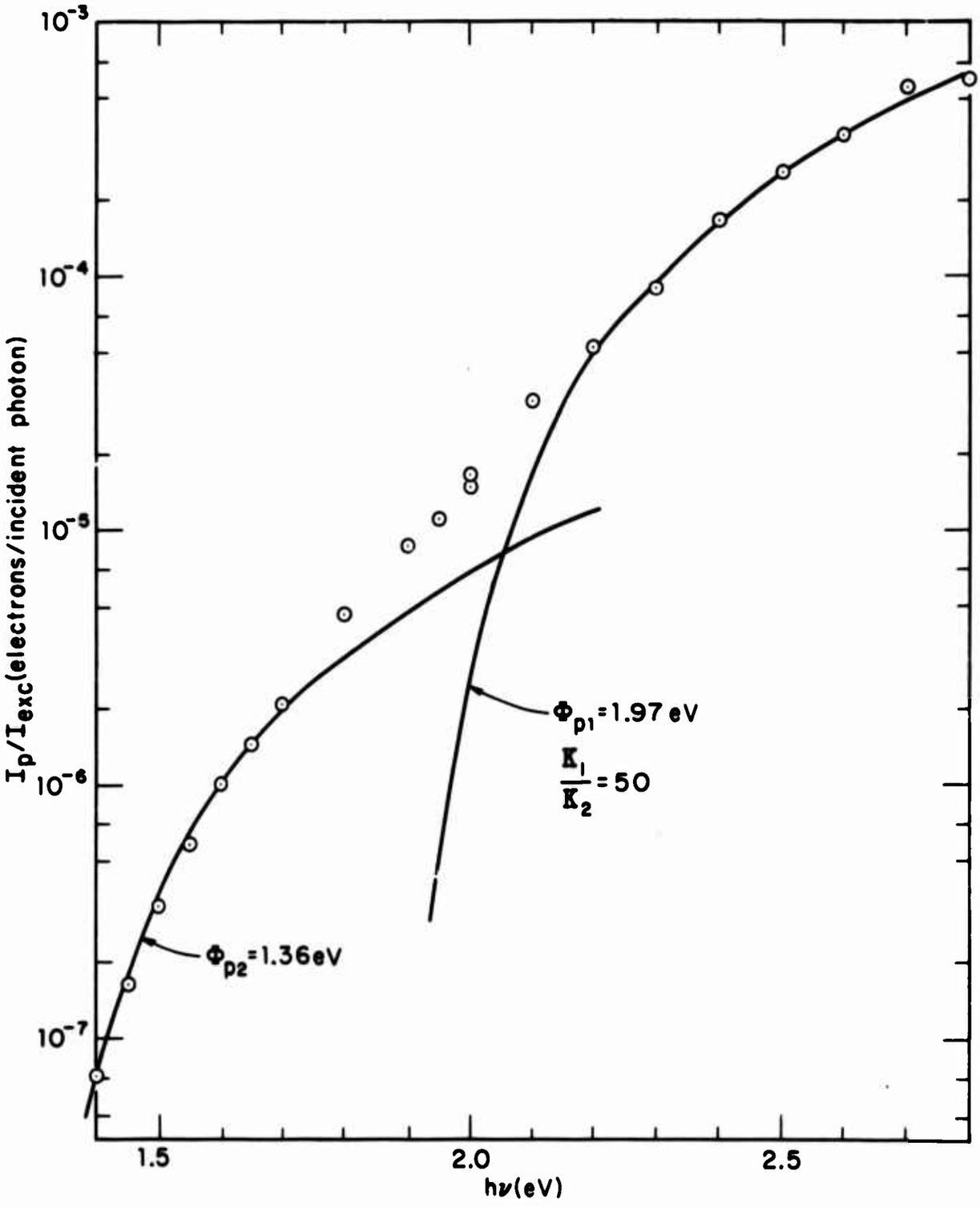

FIGURE III-15: Photoemission data for Ag-ZnS diode No. 1 of Table III-4.

TABLE III-4

Photoemission Data for Various ZnS-Ag Diodes
Differing in Exposure to Ga-In

Sample	ϕ_{p1} (eV)	ϕ_{p2} (eV)	K_1/K_2	Comment
1	1.97	1.36	50	
2	1.90	1.60	40	
3	1.80	1.55	14	
4	1.88	1.25	12	
5	2.01	1.77	10	No heating.
6	1.92	1.68	28	No heating.
7	1.99	1.40	1000	Covered ohmic contact.

globules were noted on the front surface of some diodes, including No. 5 but not Nos. 6 and 7. During the course of this experiment the chemical surface preparation procedure was improved as previously mentioned, so that the surface film thickness d of these samples was not a constant. The value of d was 20 - 35Å for samples Nos. 1 - 3 and 10Å for No. 6.

The heating experiments on the ZnS-Ag and -Au diodes mentioned in the previous section are also relevant to the degradation phenomenon. As seen from Figures III-9 - III-12 and Table III-1, these barrier heights were lowered only by 130 meV or less and the leakage currents did not increase much more than the current at the low n region of the I-V curve.

The results of these experiments concerning the degradation associated with heating were not straight-forward and several likely causative factors were not isolated. Nevertheless, some conclusions and conjectures can be made. Since the ZnS-Ag barrier height value in the ZnS surface heating experiments varied, the varying presence of some type of surface contamination was likely. Heated Ga-In or the film due to chemical surface preparation may have been responsible, especially as these diodes were made early in the ZnS studies. The similarity of the photoresponses of diode No. 4 of Table III-4 and cathodic emission device #12 of Table III-3 suggested that Cs was not necessarily a contaminant in the latter. Since unheated diode No. 5 was good and had Ga-In globules, contamination by unheated Ga-In was proved not to lead to a low barrier height, at least within

24 hours. In view of the minor effect of heating on the latest ZnS-metal barrier diodes, it is likely that avoidance of all Ga-In contamination of the barrier interface and extreme care in surface preparation would ensure a ZnS-Ag barrier height of 1.7 eV or higher after vacuum bake-out.

III.4.4.3. Ohmic Contact Studies

To form an ohmic contact to a ZnS sample, a 50% Ga-In alloy was applied to one face of the sample and heated at 400°C for 15 to 20 minutes in an H_2 atmosphere; the excess Ga-In was removed, new Ga-In was applied, and the heating was repeated for 5 minutes. After removal of excess Ga-In again, the sample was placed on an In preform on a Ni-plated Kovar header and attached by heating at 400°C for 5 minutes, in H_2. This technique yielded contact resistances on the order of $1\Omega\text{-cm}^2$ but suffered from a low mechanical strength of the die-header bond, from a lack of reproducibility, and possibly from providing Ga-In contamination in the M-S barriers.

A better ohmic contact than the Ga-In one was sought along two different lines of approach--n^+ doping by Al diffusion, and complete removal of the usual Ga-In contact followed by covering by a solid metal layer.

Several experiments were performed with the objective of obtaining an n^+ surface layer in ZnS by Al diffusion at a high temperature. The diffusions were done at 1000°C for times of 4 to 16 hours, using both pure Al and Al-Zn alloy sources containing 10 - 30 atomic % Al, in physical contact with the sample. A high resistance layer was observed at the

surface in all cases, as determined by capacitance and I-V measurements on Ag dots evaporated on the original surface and on several other surfaces etch-polished incrementally down from the original surface. Intense blue-green photoluminescence was observed from the edge region of surfaces cut perpendicularly to the diffused surface, under UV excitation ($\lambda < 4000\text{Å}$). The thickness of the high resistance layer corresponded closely to that of the luminescent layer, and represented a diffusion coefficient value of $1.9\ (\pm 0.5) \times 10^{-9}\ \text{cm}^2/\text{sec}$. These findings were in approximate agreement with published results[19, 20, 21] and suggested that Zn vacancy-Al interstitial associates form, at least in equal numbers to free substitutional Al atoms, and hence compensate the Al-diffused layer. Hints of a very thin ($< 1\mu\text{m}$) conductive layer were obtained on some sample surfaces by I-V probing.

It was concluded that Al diffusion in the presence of Zn does not give a high net donor concentration at the sample surface but produces a compensated layer despite the high Zn activity, and that this approach was unsuccessful for ohmic contacts.

Almost complete removal of the excess Ga-In after forming the standard contact was obtained using a water jet and wiping with a cotton swab. A few small metallic specks presumed to be In remained on the surface. If In was omitted as a contact constituent, the excess material could be totally removed, although the contact resistance in that case was slightly

higher. Under microscopic observation the resulting ZnS surface appeared polished but slightly darkened and contained a distribution of small rounded pits on the order of 1μm in diameter as the only evidence of the contact, excepting the above-mentioned specks of In. Overlays of Pt, Au, Al, In, Ga, and Ga-In were applied to that surface, the first four materials by evaporation in vacuum and the last two by contact with the liquid, in air. The resistance of these overlay contacts was measured employing both split contact areas formed by masking and etching, and also metal-semiconductor diodes evaporated on the opposite surface. A contact resistance value close to the original one was found in all cases as shown in Table III-5. The stability of the overlay contacts with heating was studied to ascertain their ability to withstand vacuum-chamber bake-out, and was found to be poor as shown in Table III-5. Heating was in vacuum except in one case in H_2, as noted. Al overlay seemed best but was not completely reproducible as formation of a gray insulating layer, associated with In specks remaining after contact removal, presented a problem in some cases.

The nature of the Ga-In contact was not understood completely, but these results suggested a high degree of n^+ doping of a very thin surface layer as the likely ohmic contact formation mechanism. The deterioration upon heating, even with Ga and Ga-In overlays, and at a lower temperature than that at which the original contact was formed, indicated that the

TABLE III-5

Properties of Overlay Type Ohmic Contacts to ZnS
Before and After Vacuum Heating

Overlay Material	Original R (Ω)	After Removal and Overlay R (Ω)	T (°C)	Time (hrs.)	Final R (Ω)
Al		120	264	15.5	6×10^3
Al		37 - 60	251	23.5	7×10^3
Al	30	35	320	2	1.25×10^6
Au	28 - 100	330	320	15.5	$>10^6$
Pt	20	32	320	4	3.1×10^6
In	50 - 100	95 - 170	260	15	5×10^5 - 3.3×10^6
In	340		230	17	$>10^6$
Ga	37		250 (in H_2)	2	3×10^4 - 10^6
Ga-In	20 - 50	110 - 150	230	6	10^4

deterioration mechanism was not a simple dispersion of the n^+ layer by diffusion.[22] This investigation contributed to the available knowledge concerning the Ga-In ohmic contact for ZnS and resulted in a major practical improvement in eliminating the exposed excess Ga-In which served as a possible source of contamination during chemical processing of devices. The improved cleanliness was offset, however, by a poor bakeability of the overlay contact.

REFERENCES

(Chapter III)

1. R. J. Archer, J. Cohen and J. Vilms, "Investigation of Semiconductor Schottky Barriers for Optical Detection and Cathodic Emission," Scientific Report No. 1 (Contract No. F19628-68-C-0090), March, 1968.
2. Ibid., Scientific Report No. 2 (Contract No. F19628-68-C-0090), June, 1968.
3. Ibid., Scientific Report No. 3 (Contract No. F19628-68-C-0090) September, 1968.
4. S. M. Sze, C. R. Crowell, G. P. Carey, and E. E. LaBate, Jour. Appl. Phys, 37 (7), 2690-2695 (June, 1966).
5. J. L. Moll, Physics of Semiconductors, McGraw-Hill Book Company, New York, 1964, 62.
6. R. H. Fowler, Phys. Rev., 38, 45 (1931).
7. C. Kittel, Introduction to Solid State Physics, 2nd ed. John Wiley and Sons, Inc., New York (1956), 250.
8. T. O. Yep and R. J. Archer, "Investigation and Development of Semiconductor-Metal Cathodes," Final Report, AFCRL-67-0530, August, 1967 (Contract No. AF 19(628)-5946).
9. S. H. Hagen, J. Appl. Phys., 39, 1458 (February, 1968).
10. R. J. Archer, J. Opt. Soc. Am., 52 (9), 970 (September, 1962).

11. A. M. Cowley, "Surface States and Barrier Height in Metal-Semiconductor Surface Barrier Diode," Stanford Electronics Laboratories, TR No. 0410-1 (Contract Nonr-225 (83), NR 373 360), May, 1965.

12. C. R. Crowell, Solid-State Electronics, 8, 395-399 (1965).

13. M. M. Atalla, "Metal Semiconductor Schottky Barrier Devices and Applications," Vorträge der 2. Mikroelektronik-Tagung des "Internationalen Elektronik-Arbeitkreises eV" in München, Oktober 1966, R. Oldenbourg Verlag, München, Germany (1967), 138-145.

14. J. R. MacDonald, Solid-State Electronics, 5, 11-37 (1962).

15. A. M. Goodman, J. Appl. Phys., 34, 329 (1963).

16. A. M. Cowley and S. M. Sze, J. Appl. Phys., 36, 3212 (October, 1965).

17. L. A. Dubridge, Phys. Rev., 39, 108 (1932).

18. F. A. Padovani and R. Stratton, Solid-State Electronics, 9 (7), 695-707 (July, 1966).

19. W. Van Gool, "Fluorescence Centres in ZnS," Philips Research Reports Suppl, No. 3, 1961.

20. M. Aven and R. E. Halsted, Phys. Rev., 137, A228 (January, 1965).

21. R. M. Swank, M. Aven, J. Z. Devine, to be published (September, 1968).

22. G. H. Blount, M. W. Fisher, R. G. Morrison, R. H. Bube, J. Electrochem. Soc., 113 (7), 690 (July, 1966).

IV. SUMMARY, CONCLUSIONS, FUTURE WORK

IV. 1. Photoemission

Our results for the photoemissive yield of either electrons or holes from Au into Si, for thick Au films, in the absence of an edge effect approximately obey

$$y = \frac{(h\nu - h\nu_o)^2}{h\nu} \%. \qquad (1)$$

The threshold, $h\nu_o$, is 0.8 eV for n-type Si and 0.3 eV for p-type Si.

The yield can be increased by about an order of magnitude over narrow wavelength ranges by optical impedance matching with a thin film multilayer structure. The yield can also be increased by at least a factor of six by using Au films that are thinner than 100Å. The maximum possible increase is of the order of a factor of 20 - 40, depending upon wavelength, which corresponds to the absorption of all of the incident radiation in the Au.

The increase of yield for very thin films (< 100Å) results in an "edge effect" for diodes with thick Au films when there is shadowing and a decrease in thickness at the edge of the metal pad such as can result from a loosely fitting evaporation mask. This effect is manifest as an order of magnitude greater efficiency at the edge than at the center of the pad and as a strong increase in yield with the perimeter to area ratio of the pad.

Contacts with very low barrier heights were discovered for p-type Ge. Au contacts have barrier heights less than 0.03 eV; for Ag contacts the barrier height is 0.11 eV, and for Ni contacts the value is about 0.09 eV to 0.10 eV. Yields have not been measured for these diodes.

The yield at any photon energy for any barrier height, assuming the general validity of Eq. (1) is given by the plot of Figure IV-1. For example, for detecting 10μ radiation a diode with a barrier height of 0.07 eV would have a yield of 0.02% for thick Au films of uniform thickness, and impedance matching or the use of very thin films would give yields of about 0.2%.

For future work, we recommend that the yields for the very low Ge barriers be determined and that a detailed theoretical analysis be made to determine whether or not the yields of Figure IV-1 (enhanced 10-fold) offer special promise for optical detection in any wavelength range. If an affirmative conclusion is reached, such devices should be developed and evaluated. This development would begin by determining the maximum yields that can be obtained in the very thin film range or by use of impedance matching or by a combination of the two methods.

IV.2. Cathodic Emission

There is good agreement between a theoretical model for cathodic emission from metal-semiconductor diodes and experimental results for cesiated Ag contacts on GaP, ZnSe and ZnS. The critical feature of the model is the assumption of isotropic scattering of electrons on transmission

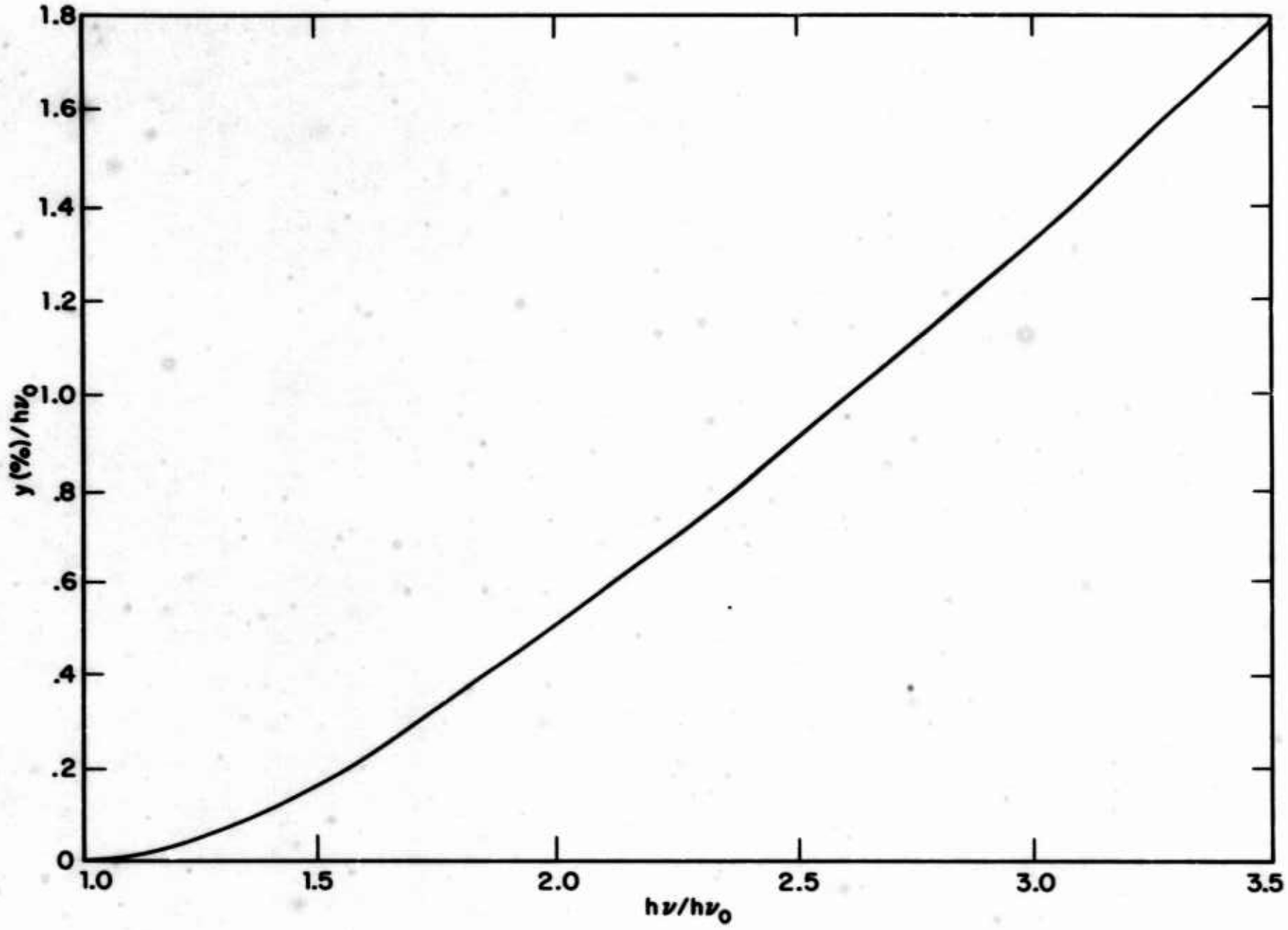

FIGURE IV-1: A plot of Eq. (1) for the photoemission of either electrons or holes from Au into Si.

through the metal-semiconductor interface, and the agreement with experiment is judged to substantiate that this phenomenon is an inherent feature of metal contacts on etch-polished semiconductors. Such interfaces are not flat and smooth on the scale of electron wavelengths and have the further complication of interfacial films (e.g., oxides) of the order of 10Å - 20Å thick and of unknown composition and structure. Both factors should contribute to non-specular reflection and transmission of electrons.

Contacts with nearly ideal I-V characteristics for all three of the semiconductors have been developed. But there are two problems. The first is that the ideality is difficult, so far impossible, to maintain or achieve under the cathodic emission conditions. The second is that there is a serious, unsolved problem in making ohmic contact to ZnSe and ZnS that withstands the high temperature treatment required in vacuum bake-out.

The highest cathodic emission efficiency measured is about 0.01%. This value was obtained for cesiated Ag-ZnSe.

The most promising device for a practical cold cathode is the Ag-ZnS diode which is expected to have an emission efficiency of about 2% or more. At the conclusion of the present project, we had not yet determined the emission from a ZnS diode with the standard 1.7 eV to 1.9 eV Schottky barrier height. This determination should have first priority in future work.

Two other future undertakings on diode development are also indicated. First, further work on developing a practical, inert ohmic

contact to ZnS is required. And, second, diodes with film-free interfaces that are flat and smooth should be fabricated in order to determine whether or not specular electronic transmission occurs in such a structure. If so, at least an order of magnitude increase in emission efficiency would result.

Unclassified
Security Classification

DOCUMENT CONTROL DATA - R & D

(Security classification of title, body of abstract and indexing annotation must be entered when the overall report is classified)

1. ORIGINATING ACTIVITY (Corporate author)
Hewlett-Packard Company
1501 Page Mill Road
Palo Alto, California 94304

2a. REPORT SECURITY CLASSIFICATION
Unclassified

2b. GROUP

3. REPORT TITLE

INVESTIGATION OF SEMICONDUCTOR SCHOTTKY BARRIERS FOR OPTICAL DETECTION AND CATHODIC EMISSION

4. DESCRIPTIVE NOTES (Type of report and inclusive dates)
Scientific. Final. Period covered: 11/15/67 - 11/14/68 approved: 10 Jan. '69

5. AUTHOR(S) (First name, middle initial, last name)
Jerome Cohen
Jüri Vilms
Robert J. Archer

6. REPORT DATE	7a. TOTAL NO. OF PAGES	7b. NO. OF REFS
19 December, 1968	122	34

8a. CONTRACT OR GRANT NO.
F19628-68-C-0090

b. PROJECT NO., Task, Work Unit Nos.
5621-07-01, 5638-01-01

c. DoD Element
6144501F

d. DoD Subelement 681301, 681305

9a. ORIGINATOR'S REPORT NUMBER(S)

9b. OTHER REPORT NO(S) (Any other numbers that may be assigned this report)
AFCRL-68-0651

10. DISTRIBUTION STATEMENT
1- Distribution of this document is unlimited. It may be released to the Clearinghouse, Department of Commerce, for sale to the general public.

11. SUPPLEMENTARY NOTES
TECH, OTHER

12. SPONSORING MILITARY ACTIVITY
Air Force Cambridge Research Laboratories, L. G. Hanscom Field (CRW)
Bedford, Massachusetts 01730

13. ABSTRACT

The yield in percent for photoemission of either electrons or holes into Si from Au contacts approximately obeys

$$y = \frac{(h\nu - h\nu_o)^2}{h\nu}$$

for thick Au films and incidence from the Si side of the contact. For p- and n-type Si $h\nu_o$ is, respectively, 0.3 eV and 0.8 eV. By optical impedance matching the yields can be increased by at least 10-fold over narrow wavelength ranges. Au films thinner than 100Å also exhibit nearly an order of magnitude greater yield. This latter fact leads to enhanced yields at the edges of Au pads evaporated through loosely fitting masks. Very low barriers are obtained on p-type Ge. For Au, Ag and Ni, the values are < 0.03 eV, 0.11 eV and 0.9 eV - 0.1 eV, respectively.

Rectifying Ag contacts to etch-polished GaP, ZnSe and ZnS can be made with nearly ideal I-V characteristics. The Schottky barrier heights are about 1.5 eV for the former two contacts and 1.8 eV for the latter. The efficiency of cathodic emission into vacuum for diodes with barrier heights equal to or less than 1.5 eV and with cesiated Ag films 300Å thick having work functions of about 1.5 eV obeys a

(Continued)

DD FORM 1 NOV 68 1473 REPLACES DD FORM 1473, 1 JAN 64, WHICH IS OBSOLETE FOR ARMY USE.

Unclassified
Security Classification

14. KEY WORDS	LINK A		LINK B		LINK C	
	ROLE	WT	ROLE	WT	ROLE	WT
Schottky Barriers						
Schottky Barrier Optical Detectors						
Cold Cathode						
Cold Cathodic Theory						
Photoemission						
Metal-Semiconductor Contacts						

ABSTRACT (Continued)

theory which assumes isotropic scattering of electrons on transmission through the interface. The maximum measured efficiency is nearly 10^{-4} for Ag-ZnSe. At least 0.02 is expected for Ag-ZnS but has not yet been measured. Under the cathodic emission conditions, the diodes have so far not had ideal electrical properties and there is a serious problem in achieving stable, chemically inert contacts to the II-VI materials.